An analysis of the uptake mechanism of nanoparticles, its temporal effect on autophagy and organelle dynamics in breast cancer cells

THESIS

Submitted in partial fulfillment

of the requirements for the degree of

DOCTOR OF PHILOSOPHY
by

Ms. Leena Fageria

2014PHXF0425P

Under the Supervision of

Prof. Rajdeep Chowdhury

&

Co-Supervision of

Prof. Surojit Pande

BITS Pilani
Pilani | Dubai | Goa | Hyderabad
BIRLA INSTITUTE OF TECHNOLOGY AND SCIENCE

PILANI

2020

BIRLA INSTITUTE OF TECHNOLOGY AND SCIENCE, PILANI

CERTIFICATE

This is to certify that the thesis entitled **"An analysis of the uptake mechanism of nanoparticles, its temporal effect on autophagy and organelle dynamics in breast cancer cells"** submitted by **Ms. Leena Fageria** ID No**. 2014PHXF0425P** for award of Ph.D. of the institute embodies original work done by her under my supervision.

Signature of the Supervisor:

Dr. Rajdeep Chowdhury

Associate Professor

Department of Biological Sciences

Birla Institute of Technology and Science,

Pilani

Pilani campus, Rajasthan

Signature of the Co-Supervisor:

Dr. Surojit Pande

Associate Professor

Department of Chemistry

Birla Institute of Technology and Science,

Pilani

Pilani campus, Rajasthan

Date:

Acknowledgment

This thesis represents not only the work I did in the lab but also my journey from being a layman to growing as a researcher. My experience at BITS has been nothing short of amazing, since my first day, I have felt like home at BITS. Throughout these years, I have learned many aspects of research and techniques. Today, along with my thesis, I wish to acknowledge dozens of remarkable individuals who have directly or indirectly contributed to the accomplishment of this dream.

First and foremost, I wholeheartedly thank my Ph.D. research supervisor, Prof. Rajdeep Chowdhury, Department of Biological Sciences and co-supervisor, Prof. Surojit Pande, Department of Chemistry for providing me an excellent platform to follow my passion. I am grateful for getting an opportunity to work under their expert guidance. Their constant efforts oblige me from the beginning to the completion of my research work. Their supervision has improved my research and teaching aptitude and, their "Never Give Up" approach has always kept me motivated. I would like to express sincere gratitude to my DAC members, Prof. Jitendra Panwar and Dr. Sudeshna Mukherjee, Department of Biological Sciences, for their constructive evaluation of the research work. I owe special thanks to Prof. Jitendra Panwar for providing us with fungal derived-silver nanoparticles, and allowing me to work in collaboration with their research group.

This work would not have been possible without the infrastructural and administrative support from the institute, for which I thank Prof. Souvik Bhattacharyya, Vice-Chancellor, BITS Pilani, Prof. Sudhirkumar Barai, Director, BITS Pilani, Pilani campus. I also thank Prof. Jitendra Panwar, Associate Dean, AGSRD, and Prof. Shibasish Chowdhury BITS Pilani, Convener, Departmental Research Committee, Prof. Prabhat Nath Jha, HOD, Department of Biological Sciences for their timely guidance and support regarding the academic formalities throughout the thesis work. I am thankful to UGC for helping me with financial assistance.

I would also like to thank all the faculty members and research scholars, Department of Biological Sciences, for extending their help and support during my research and teaching practices. A special

thanks to the non-teaching staff, especially Mukesh Ji, for providing with the pre-requisites for my experiments.

As a learner, I received immense support, care, and guidance from my seniors Miss. Jyothi Nagraj, Dr. Zarna Pala, and Dr. Gagandeep Singh Saggu, which is unforgettable. I would like to thank my loving friends and inspiring lab mates Dr. Subhra Dash and Mrs. Heena Saini, for always being my pillar of support in any situation and sharing an undefined relationship of understanding and caring. I will forever cherish the warmth shown by my lab members, Ms. Abhilasha, Ms. Ankita Daiya, Mr. Anirudh, Ms. Mahima, Ms. Propanna, Mr. Lohitesh, Ms. Ifrah, Ms. Shivangi, Ms. Vishakha, Ms. Angel, Ms. Swetha, Ms. Swati, Ms. Neelam, Ms. Aastha, Mr. Sumukh, Ms. Ashima, Ms. Niyati, Ms. Smita, Ms. Srinidhi, Ms. Sanhita, Ms. Tejaswini, Ms. Prachi, Mr. Santonu and Ms. Parichita. I thank you all for the cooperation and assistance given during my experiments. A Special thanks to Mr. Shobham for helping me in the conductance of ICP analysis on such short notice.

Heartfelt thanks to my enthusiastic friends, Dr. Anuradha, Dr. Vajir, Mr. Sandeep, Ms. Shraddha, Ms. Nisha, Mr. Vikram, Mr. Vikas, Ms. Tripti, and Ms. Vishalakshi for the memorable and beautiful time spent together and for always being so compassionate and motivating throughout my tough times.

My unique words of thanks should also go to my amazing friends, even counselors, Ms. Ankita Sharma, and Mr. Himanshu, for providing continuous support and cooperation, going out of their ways. I express my indebtedness to them for always being there for me. My beloved friends have still boosted me by showing their never-ending spirit of positivity.

I owe my deepest gratitude to my family for their constant support and understanding of my goals and aspirations. The unfailing love and blessings of my parents Mrs. Krishna and Mr. Dharampal Fageria, have always been my strength; their patience and efforts will keep me inspiring throughout life. I am eternally grateful to my brother Ajay and sister in law Manisha, who not only supported me throughout my journey but also are the ones who made me realize my potential. I will never forget

the constructive and fun-filled advice of my sister Tinki and brother in law Dr. Anil, without their motivational help I would not have been able to complete much of what I have done. I also thank my little nieces, Taani, and Medhanshi for their innocent smiles and affection, which always kept me motivated while completing this journey.

Leena

Abstract

Nanoparticles (NPs), in recent years, have emerged as a unique class of materials with the potential for a wide array of biomedical applications. The intrinsic properties of NPs, like their potential to act as a vector, and their cell/tissue penetrative property, have made them valuable as a prospective therapeutic arsenal. Amongst the various nanomaterials, metal NPs are often considered as the next generation of therapeutics as they owe versatile physicochemical properties. In this context, the silver nanoparticles (AgNPs) have been much explored for their exceptional therapeutic potentials, such as anti-inflammatory, antimicrobial, and anticancerous activities as well. They are known to possess unique properties such as conductivity, chemical stability, relatively lower toxicity, which have further fueled their extensive use in various biological applications. However, despite a remarkable boost in the use of these nanomaterials in the field of diagnostics, therapy, or healthcare, the major obstacle has been the transition forward from the bench to the bedside. A better understanding of AgNP and its crosstalk with the human cellular system might hold the key and facilitate this switch. In this regard, this research was designed to find answers to a series of fundamental questions associated with AgNP and its cellular effect. Before we embarked upon the actual experimental study, the following are some of the questions, the answer to which was explored through this research- does a minute variation in size of AgNPs affect their internalization and intracellular function? Does the route of entry vary with the size of NPs? Does the internalization and therapeutic potential of AgNPs amplify or reduce when transitioned from a mono-metallic to a bi-metallic state? AgNPs are known to induce cytotoxicity in tumor cells; however, what is the temporal effect of AgNPs on cellular homeostatic processes, like autophagy that is reported to have both pro-survival or pro-apoptotic effect? How AgNPs shape the intracellular organelle dynamics? To experimentally explore answers to the above questions, we selected breast cancer cells as our model for study. AgNPs were synthesized in the mono-metallic state or in bi-metallic/dual (combined Ag/Au, core@shell type) state using beta-cyclodextrin (β-CD), an oligosaccharide which

acts as both reducing and stabilizing agent. Further, AgNPs of two different sizes- small-sized (ss-AgNPs; ~9 nm) and large-sized (ls-AgNPs; ~19 nm) were also synthesized to understand how alterations in physical dimensions of the AgNPs impact their intracellular entry, mechanism of entry and their subsequent cellular function. Interestingly, we observed that the β-CD coated NPs, both mono-metallic and bi-metallic, are primarily internalized by the cultured tumor cells by an energy-driven process. The mechanism of internalization was strictly dependent on the size of NPs. A significant observation was that there was enhanced internalization potential of ss-AgNPs compared to the ls-AgNPs. We thus prove that a small variation in the size of NPs (approximately around 10 nm) can have an impact on the internalization potential of the NPs. Furthermore, upon pharmacological inhibition of the different endocytic pathways, we observed that the endocytic route of ss-AgNPs was predominantly different than ls-AgNPs. The ss-AgNPs showed more cytotoxicity then other synthesized NPs. Further analysis proved that the intracellular release of Ag ions was considerably less in bi-metallic NP treated cells. Probably resulting in their reduced cytotoxicity. We, thereafter, characterized the dynamic crosstalk that exists between internalized AgNPs and the cellular homeostatic process- autophagy. Interestingly, we observed that inhibition of autophagic flux (fusion of autophagic vesicles with lysosomes) by the drug chloroquine (CQ) significantly reduced the internalization of the AgNPs, irrespective of their route of entry; functional autophagy thus augmented successful internalization of the NPs. Also, autophagy induction after AgNP exposure was mediated through an upstream activation of Janus Kinase (JNK) signaling. Importantly, the cellular homeostatic process autophagy also significantly contributed to the mitigation of intracellular ROS levels after AgNP exposure, thus playing a protective role in the tumor cells. However, prolonged exposure to AgNPs resulted in lysosomal dysfunction leading to inhibition of autophagic flux. Therefore, inhibition of flux after extended exposure to AgNPs resulted in increased ROS and ubiquitinated protein accumulation alongside pronounced cytotoxicity. Hence, from the above study, we conclude that AgNPs exert a temporal effect on

autophagy, which dynamically changes over time in the tumor cells; functional autophagy initially imparts a protective function and but its eventual impairment leads to irreversible cytotoxic damage. Since autophagy is not only involved in regulating cellular redox or protein homeostasis but also actively controls cellular organelle dynamicity, we thereafter explored changes in mitochondria and ER function coupled to autophagy after AgNP exposure. Strikingly, a loss of autophagic function after prolonged exposure to AgNPs was associated with massive mitochondrial depolarization, enhanced fragmentation or fission of mitochondria, and recruitment of Parkin that marks mitochondrial disposal. An autophagy inducer, rapamycin partially rescued this effect, while CQ promoted it. Furthermore, an inhibition of flux and disruption of mitochondrial homeostasis were coupled to AgNP induced ER stress as well. A further induction of ER stress with Tunicamycin, enhanced AgNP induced cell death indicating that ER stress positively contributes towards AgNP-mediated cytotoxicity. Overall, this study provides key information on how alteration in physic-chemical property of NPs impacts its biological function; furthermore, it also provides insights into how the internalized NPs temporally modulate key intracellular events like autophagy and organelle dynamics. Our research provides critical information on the development of NP-based therapy, especially, AgNPs and their prospective use in cancer treatment.

Table of contents

List of figures

List of tables

List of abbreviations

AgNPs- Silver nanoparticles

AO- Acridine Orange

ATF6- Activating transcription factor 6

ATG- Autophagy related genes

AuNPs- Gold nanoparticles

β-CD- Beta cyclodextrin

C6- Coumarin 6

CCIE- Clathrin caveolae independent endocytic mechanism

CDK- Cyclin-dependent kinases

CME- Clathrin-mediated endocytosis

CPZ- Chlorpromazine

CQ- Chloroquine diphosphate

CST- Cell Signaling Technology

CVE- Caveole-mediated endocytosis

Drp1- Dynamin related protein 1

DWNTs- Double-walled nanotubes

Dyn- Dynasore

EEA1- Early endosome antigen 1

EPR- Enhanced permeability retention

ER- Endoplasmic reticulum

ER^+ - Estrogen receptor-positive

ERBB2- Erb-B2 receptor tyrosine kinase2

Gen- Genistein

HER2- Human epidermal growth factor 2

HR^+ - Hormone receptor-positive

HRTEM- High-resolution transmission electron microscopy

ICP-OES- Inductively coupled plasma optical emission spectrum

IMM- Inner mitochondrial membrane

IRE1- Ionisitol-requiring Kinase 1

JNK- Jun-N-terminal kinase

LAMP1- Lysosomal associated membrane protein 1

LMP- Lysosomal membrane permeabilization

ls-AgNPs- large-sized silver nanoparticles

LT- Lysotracker

Mfn1/2- Mitofusin 1 or 2

MMP- Mitochondrial membrane potential

MT- Mitotracker

mTOR- mammalian Target of Rapamycin

MTT- 3-(4,5-dimethylthiazol-2-yl)-2,5-di-phenyltetrazolium bromide

MWNTs- Mono-walled nanotubes

NAC- N-acetyl cysteine

Noc- Nocodazole

NPs – Nanoparticles

OMM- Outer mitochondrial membrane

OPA1- Optic atrophy 1

PARP- Poly (ADP-ribose) polymerase

PERK- Protein kinase R-ER like kinase

PINK- PTEN-induced putative kinase

PR^+ - Progesterone receptor-positive

Rapa- Rapamycin

ROS- Reactive oxygen species

SERS- Surface-enhanced Raman spectroscopy

ss-AgNPs- small-sized silver nanoparticles

SWNTs- Single-walled nanotubes

TFEB- Transcription factor EB

Tuni- Tunicamycin

UPR- Unfolded protein response

WHO- World Health Organization

Chapter-1

Introduction

Chapter-1

Introduction

1.1 Cancer:

Cancer is the name given to a disease caused by uncontrolled division and proliferation of cells. Unlike healthy cells of our body, the cancer cells acquire distinct hallmarks depicted in **figure 1.1.1**, which makes these abnormal cells grow out of control and spread to other parts of the body as well. Cancer is reported as the second prime cause of global death by the World Health Organization (WHO). In the year 2018, about 18.1 million people around the world were diagnosed with cancer, and nearly 9.6 million were accounted for deaths from cancer [1].

Figure 1.1.1. Different hallmarks of a cancer cell. *A cancer cell is characterized by features like immune evasion, genomic instability, escaping death pathways, metastasis, immortalized replication, and sustained angiogenesis causing its poor prognosis.*

Amongst various cancers, breast cancer is the most common cancer type among women worldwide. It is now on the verge of becoming the top cause of morbidity and mortality across the globe, second only to lung cancer. In India, too, breast cancer has surpassed cervical cancer as per recent statistics, with incident rates around 25.8 per 100,000 women [2]. According to a recent report on the Indian cancer burden by WHO, incidences of breast cancer will drastically increase by the year 2040 **(Fig 1.1.2**) [3]. Approximately 80% of the early-stage patients who have not metastasized can be cured. However, advanced-stage breast cancer, which has metastasized to other organs, is considered incurable.

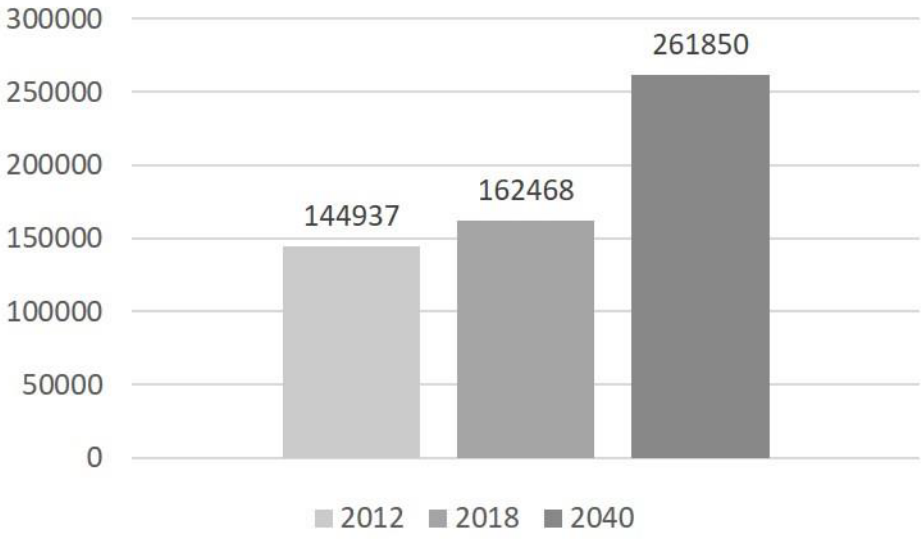

Figure 1.1.2. Trends of breast cancer cases in India [3].

1.1.1 Classification of breast cancer

Breast cancer is a complex disease which can be classified in the following ways [4] (**Fig 1.1.3**):

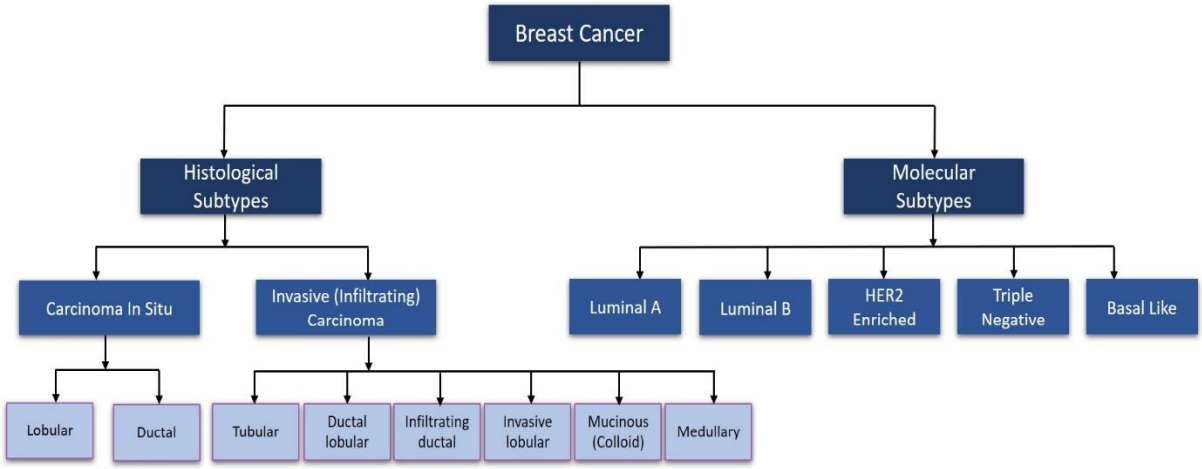

Figure 1.1.3. Classification of breast cancer. *Breast cancer is classified broadly into histological and molecular subtypes, which are further divided into carcinoma in situ, invasive carcinoma, luminal A and B, HER2, triple-negative, and Basal-like* [4].

1. Histological subtypes: It is the primary method of breast cancer classification.
    - Carcinoma in Situ: It spreads via ducts and damages the ductal architecture and can metastasize.
    - Invasive Carcinoma: It does not distort the ductal architecture and is more of a risk factor than a precursor.

2. Molecular subtypes: Molecular subtypes were developed using microarray-based on the resemblance in the profile of gene expression.

- Luminal A: It consists of estrogen receptor (ER^+)/progesterone receptor (PR^+) positive or human epidermal growth factor receptor-2 (HER2) negative and consists of almost 60-70% of the cases of invasive breast cancer. It is characterized by a low proliferation rate and a good prognosis.
- Luminal B: In this type, ER^+/ PR^+ is positive but lower ER^+ and PR^+ expression when compared to Luminal A-type. It can be HER2 positive or HER2 negative and forms 10-20% of invasive breast cancer cases.

- HER2 enriched: High expression of HER2 gene and absence of ER^+/ PR^+ is the characteristic of this type and accounts for approximately 15% cases.
- Triple-negative: ER^+/ PR^+ and HER2 negative, high grade with poor prognosis, and is present in 10-15% of the cases.
- Basal-like: It is characterized by TP53 and BRCA mutations and genetic instability.

1.1.2 Risk Factors

The pathogenesis of breast cancer is multifactorial and is not well understood [5]. However, there are certain risk factors which are known to play a role in the development and progression of breast cancer are described below (**Fig 1.1.4**):

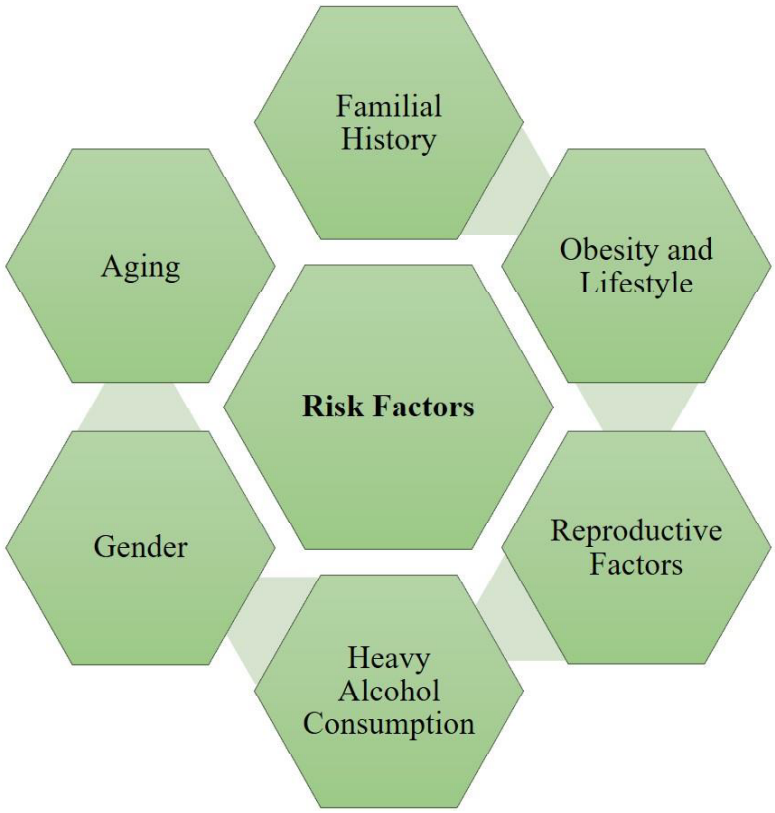

***Figure 1.1.4. Risk Factors leading to breast cancer pathogenesis* [5].**

1. Age: is found to be the most critical risk factor with reports suggesting that majority of the breast cancer-associated deaths (~70%) in women above 40 years of age.
2. Familial history: Data suggests that almost $1/4^{th}$ of breast cancer patients have a family background of breast cancer. As per a study including 113,000 women, the risk for contracting breast cancer was increased by 1.75-fold in women with one first degree relative and almost 2.5-fold with more than two first degree relatives having breast cancer.
3. Reproductive factors: Several factors related to the reproductive life of women such as delayed menopause, menarche at an early age, number of childbirths, age at the time of the first childbirth can be decisive in the occurrence of breast cancer.
4. Obesity and Lifestyle: Excessive weight, along with the consumption of alcohol and fatty foods, have been reported to increase the risk of breast cancer. It is found that alcohol consumption alters the level of estrogen-related hormones and may initiate the estrogen pathway to breast cancer. Early age smokers are more susceptible to the development of breast cancer [5].

1.1.3 Available treatment options for breast cancer

Non-metastatic breast tumors are removed by surgical resection along with radiation and systemic therapy, depending on the subtype of cancer. For hormone receptor positive (HR^+) subtype, endocrine therapy includes oral anti-estrogens, tamoxifen; it inhibits the binding of estrogen to ER^+. Anastrozole, letrozole, is aromatase inhibitors that inhibit the conversion of androgens to estrogen [6]. Chemotherapy is essential to avoid the risk of recurrence of tumor, anthracyclines, and taxane such as methotrexate, adriamycin, cyclophosphamide are the appropriate choices. For Erb-B2 receptor tyrosine kinase-2 (*ERBB2+)* tumors, trastuzumab-based ERBB2 directed antibody with chemotherapy. If concurrent HR positivity exists, then endocrine therapy is also given. For triple-negative breast cancers, chemotherapy alone is given.

In the case of metastatic breast cancer, medicines are given to prolong the lifespan and ease the severity of the disease. This type of cancer is still incurable. Early treatment includes endocrine therapy with CDK 4/6 inhibitors like abemaciclib, ribocicilib in HR^+ type. PARP inhibitors like olaparib and talazoparib are approved for triple-negative metastatic subtypes. First-line treatment for *ERBB2+* tumors, taxane with trastuzumab is used, followed by using trastuzumab emtansine, an antibody-drug conjugate as second-line therapy [7].

Although available treatments have reduced the chance of tumor recurrence, but the side-effects of the current therapies have limited the success of treatment so far. Acquisition of drug resistance, lack of specificity towards cancer cells, inhibiting the growth of healthy cells, etc. are few of the drawbacks of cancer therapies, which demands a more effective and better alternative.

1.2 Nanotechnology:

Nanotechnology is an allied branch of science viz. physics, chemistry, biology, and engineering. In the past few decades, the research on nanoparticles (NPs) in drug development has grown leap and bounds. NPs are materials which have a size ranging from 1 nm to 100 nm. Owing to the extremely small size and the large surface area, they are known to possess novel physicochemical and biological properties, which are enhanced as compared to their usual size counterparts [8]. These unique properties of nanoparticles provide them with the capacity to communicate at the level of biomolecules, thus impacting intricate biological functions [9]. Therefore, they have emerged as an excellent candidate for biomedical applications. Researchers from different disciplines are using this opportunity to devise and develop NPs that can be used for diagnosis and treatment of diseases including but not limited to cancer.

1.2.1 Classification of NPs

There are multiple classes of NPs based on their size, surface morphology, and physicochemical

properties (**Fig1.2.1**).

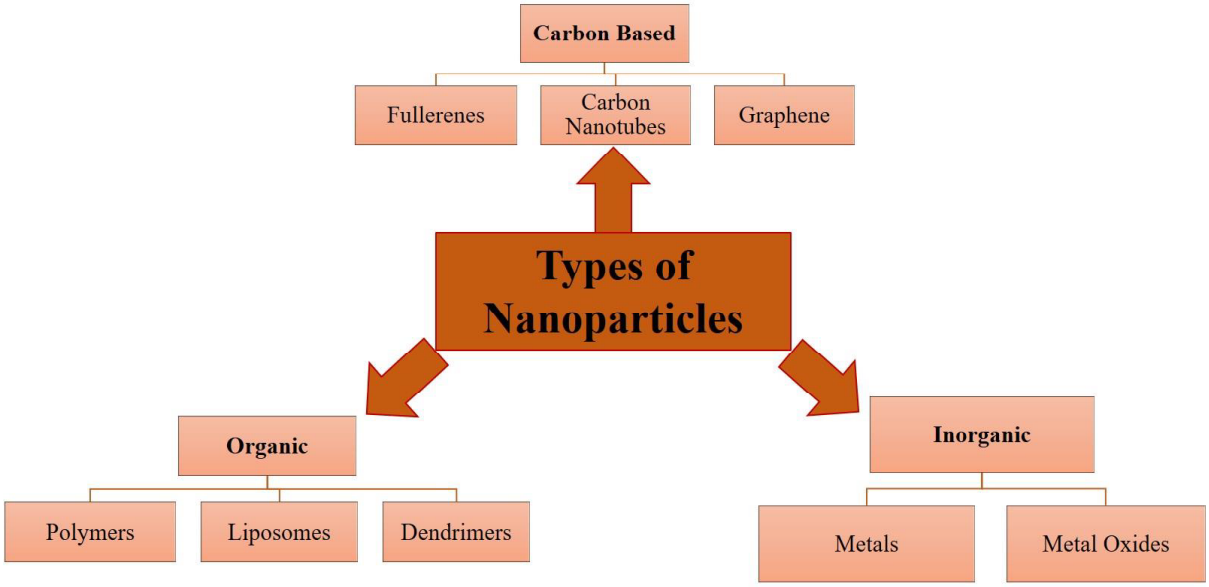

Figure 1.2.1. Classification of NPs. *Carbon-based, Organic and Inorganic are three major categories of NPs. Each of which is further divided into different sub-categories based on their properties* [10, 11].

Carbon-based NPs: Carbon nanotubes and Fullerenes are the primary types of carbon-based NPs. They are similar in appearance to the graphite sheets rolling on themselves classified as single-walled nanotubes (SWNTs), double-walled nanotubes (DWNTs), and multiple walled nanotubes (MWNTs). Carbon-based NPs and Fullerenes have been reported to show antioxidant and antimicrobial activities and have been successfully utilized in different cancers such as leukemia, lymphoma, bladder cancer.

Organic NPs: consist of polymers, liposomes, dendrimers, etc. Polymeric NPs are constituted of either nanosphere (matrix systems), or nanocapsules (vesicular system). Lipid nanoparticles are promoted as an alternative to liposomes, emulsions, and polymeric NPs, particularly for the lipophilic drugs. It is structurally akin to polymeric NPs having a solid core made up of lipid and a matrix which houses the lipophilic molecules. Different emulsifiers and surfactants are used to stabilize the core. Application wise they are employed in drug delivery via different routes, non-viral transfection, RNA release, etc.

Inorganic NPs: Metal and their oxides lie under this category. These NPs are composed of the metal antecedents. This is considered to be a multifaceted class of substance, including quantum dots, metallic oxide NPs (copper/cuprous, zinc, titanium), metal NPs and magnetic NPs (nickel, iron, cobalt, manganese). Literature suggests the use of a variety of metals such as silver, gold, platinum, titanium, zinc, iron, etc. Besides, different types of ligands, proteins, DNA, aptamers, drugs, etc. can be attached to the metallic NPs providing surface functionalization. These potential attributes of metallic NPs make them useful in the biomedical field, including targeted drug delivery, cancer therapeutics, gene therapeutics, anti-microbial activity, diagnostic techniques (magnetic resonance imaging, computed tomography, and positron emission tomography) [10, 11].

However, plasmonic metal NPs like silver (Ag) and gold (Au) are gaining attention in the field of nanomedicine. These NPs possess a unique property called localized surface plasmon resonances (LSPRs), which offers better ways of diagnosis. Also, conjugation of two metals for the formation of bi-metallic NPs makes them multifunctional and, even more, better diagnostic agents because of enhanced surface plasmon resonance.

1.2.2 Synthesis of NPs

The selection criteria to develop an NP based therapeutic entity should consider the following points:

- Starting materials should be biocompatible and non-toxic.
- It should have the ability to encapsulate a higher percentage of the active moiety to attain therapeutic dose and also protect it from degradation and clearance.
- The stability of the nanoparticulate vehicle as well as the surface functionalization in physiological conditions towards changing pH values, temperature, etc.
- Specific cell or tissue targeting, which facilitates the highest concentration in the required tissue and minimal side effects in adjacent healthy tissues. It could be active targeting by attaching receptor molecules on the surface or passive targeting.

- Clearance of the NPs is required once it is done with its task of delivering the active drug; otherwise may cause cumulative side effects.

To obtain NPs of intended size, shape, and function, various methods have been explored. However, the techniques have been divided into two major categories, namely, Top-down approach and Bottom-up approach (**Fig 1.2.2**). Top-down synthesis involves larger initial structures that are further reduced in a controlled manner using techniques such as lithography, chemical etching, sputtering, ball milling, laser ablation, etc. Bottom-up synthesis or the building up approach as per the name employs simple and smaller molecules to build up the nanoparticles via techniques such as spray and laser pyrolysis, green synthesis, sol-gel processes, and atomic/molecular condensations. The synthesis of NPs is broadly classified into a physical, chemical, and biological synthesis, which could either fall into Bottom-up or Top-down strategy [12].

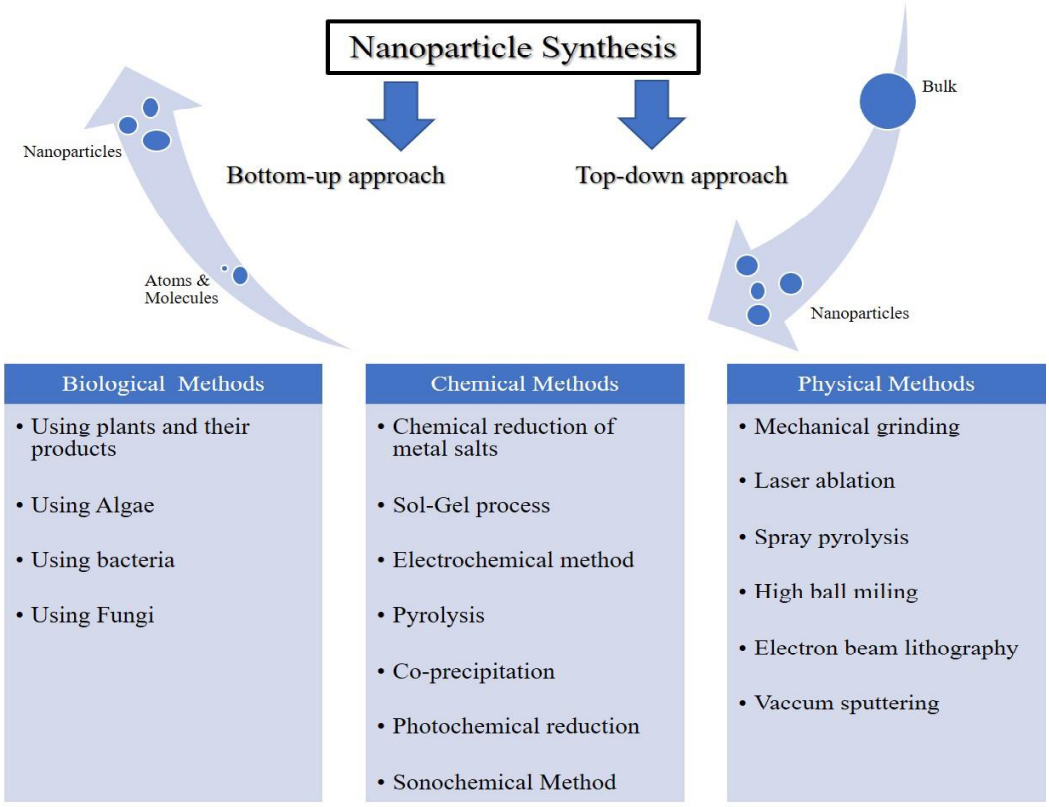

Figure 1.2.2. Different methods of NP synthesis. *The synthesis procedure of NPs occurs by chemical, biological, or physical processes that can fall either in the Top-down or Bottom-up approach* [12, 13].

Chemical methods: Chemical reduction using organic and inorganic reducing agents is one of the most common procedures of NPs production since it can be performed in aqueous as well as inorganic solvents. Chemical reductant such as sodium borohydride ($NaBH_4$), Sodium hypophosphite (NaH_2PO_2), Hydrazine (N_2H_4), Hydroxylamine (NH_2OH) has been successfully used in the formation of different metallic NPs via reduction [12]. $NaBH_4$ is reported to reduce cations of different metals like silver, gold, tin, nickel, rhodium, cobalt, lead, palladium to their nano-sized counterparts.

Biological method/Green synthesis method: The biological process of NP synthesis is a promising course of nanotechnology. Green synthesis involves the usage of several biological precursors such as microorganisms (bacteria, fungus, and algae), plant derivatives (leaves, root, flower, fruit, etc.). It has the edge over various physical and chemical methods of NPs synthesis, which use several toxic reductants, radiations, and extreme reaction conditions, which is harmful to the environment and the individual. This method is further divided into bio-reduction in which stable metallic NPs are formed by chemical reduction from microbes and their enzymes [13].

Physical Methods: In this method, NPs are produced by either material evaporation/condensation, abrasion, or melting using mechanical pressure, electrical energy, thermal energy, radiations. This method generally falls into the top-down approach and offers advantages such as no risk of solvent contamination and the true nature of produced NPs [13].

Each of these methods has its pros and cons, like physical synthesis procedures used, are energy and capital intensive, thus hindering their biomedical applications. Biological or green synthesis of NPs using bacteria, fungi, algae, yeast, or plant extracts is considered eco-friendlier and more sustainable [14], however, this method has disadvantages like the formation of non-homogenous NPs, occasional pathogenicity, etc. The chemical process is although less time consuming, but it employs toxic chemicals and often yields particles in non-polar organic solutions. To overcome these drawbacks, an alternative chemical method that replaces toxic chemicals by using bio-compatible molecules like

sugars, proteins, etc. as reducing and stabilizing agents would be an advantage.

1.2.3 Characterization of NPs

There has been a surge in the synthesis of different types of NPs in the past decade, creating a requirement to develop different characterization techniques for precise and reproducible characterization. We already have numerous methods at our disposal for the characterization such as X-ray diffraction (XRD); Absorbance, emission and excitation spectroscopy; surface-enhanced Raman scattering (SERS) spectroscopy; ultraviolet laser stimulated surface Raman scattering (UV-SERS) spectroscopy; scanning electron microscopy (SEM); transmission electron microscopy (TEM); high-resolution transmission electron microscopy (HRTEM), etc. [12, 15]. Characterization could be completed using a combination of optical, structural, and gravimetric techniques (**Fig 1.2.3**).

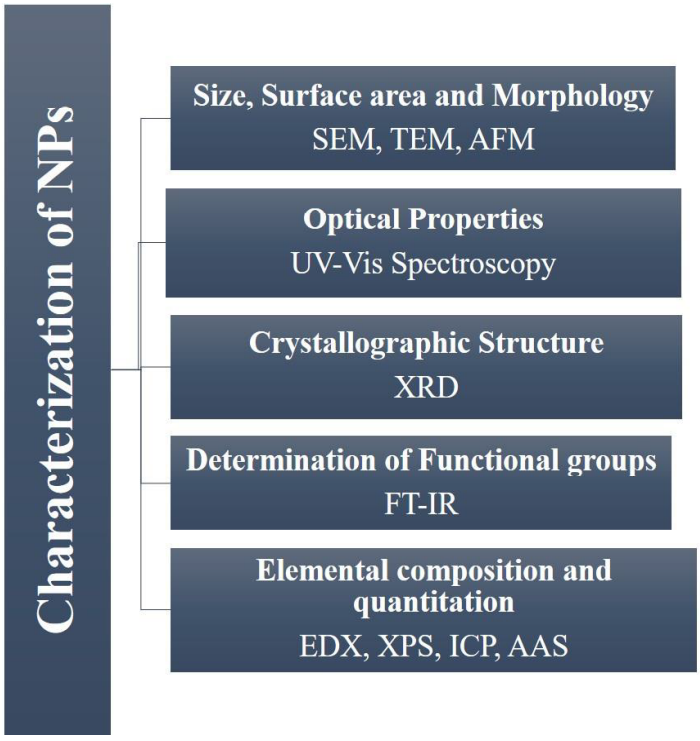

Figure 1.2.3. Characterization of NPs. *The synthesized NPs can be characterized by different techniques like UV-Visible spectroscopy, SEM, TEM, AFM, XRD, FT-IR, EDX, XPS, ICP, AAS, etc. for their features* [12, 15].

1.2.4 NPs in cancer

Primary treatment options available for breast cancer include Chemotherapy, Radiotherapy, Hormonal therapy, and Mastectomy. However, currently available options are neither successfully preventing its progression and recurrence, nor they specifically target the breast cancer cells. This is the reason behind the various side effects related to the therapy. Researchers across the globe are focusing on developing methods that will not only enhance the efficiency of the treatments but also reduce their toxicity in order to improve the quality of life of breast cancer patients [16]. Nanotechnology has emerged as one of the ways which could help scientist achieve the aforementioned targets. It provides tools not only for treatment but also for the identification and diagnosis of cancer. During the last decade, several NPs have been unearthed and synthesized, which are selective towards the tumor cells without causing much harm to the adjacent healthy cells. Besides, they possess distinctive properties such as high compatibility, minimal toxicity, easy preparation, enhanced photoluminescence, facilitates bioimaging *in vivo,* etc. which gives them an edge in cancer therapeutics (**Fig 1.2.4)** [17].

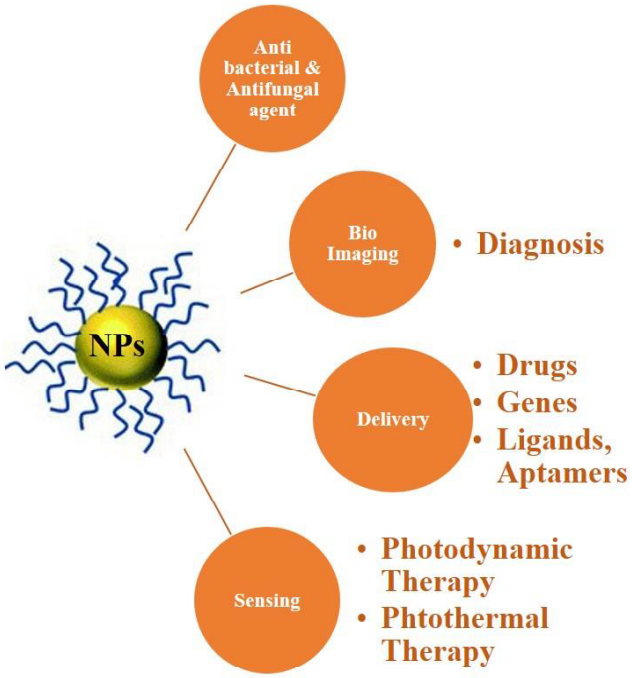

Figure 1.2.4. Various biomedical applications of NPs. *NPs can be used for diagnosis, targeted delivery of drugs by conjugation with ligands or aptamers, delivering genes, or ligands into the*

tumor. The metal NPs are also utilized for photothermal and photodynamic therapies [17].

Studies suggest that numerous anticancer drugs can be encapsulated in the nanocarrier, which leads to improved anticancer efficacy and reduced systemic effects [18]. Moreover, few NPs may induce autophagy, which is a usual result of material toxicity. Gold (Au) and Silver (Ag) NPs, Quantum dots, Zinc oxide, Carbon nanotubes, etc. are the nanoparticles that have the ability to induce autophagy [10]. Besides, nanoparticles have also been reported to overcome the problem of multidrug resistance, which is commonly associated with chemotherapy [19]. Several nanoparticulate based therapies have received approval from the FDA and are under clinical trials (**Table 1.1**) [20].

Table 1.1: FDA approved nano-drugs against different cancers.

Product Name	Nano-Drug	Cancer type	Status
Doxil	Pegylated doxorubicin	Ovarian/breast cancer	FDA Approved
Abraxane	Albumin-bound Paclitaxel	Pancreatic cancer	FDA Approved
Myocet	Liposome encapsulated Doxorubicin	Breast cancer	FDA Approved
LEP-ETU	Liposomal Paclitaxel	Breast/lung/Ovarian	Clinical phase I/II

Aroplatin	Analog of Cisplatin encapsulated in a liposome	Colorectal cancer	Clinical phase I/II
SPI-77	Liposomal Cisplatin	Lung/ Head and neck cancer	Clinical phase III

1.3 Interaction of NPs with a cell:

Understanding the interaction of NPs with a cell and their intracellular fate is very critical to facilitate their clinical application. The interaction of NPs with the cell is affected by various factors like physicochemical properties of NPs, the type of cell, a response in multiple cellular organelles, and their intracellular fate.

1.3.1 Cellular uptake of NPs

Internalization of nanomaterials inside a cell can be through various mechanisms including simple diffusion, phagocytosis, micropinocytosis, endocytosis with or without the help of receptors, or through adhesive interactions [21]. The trafficking of foreign materials in cells is performed through the formation of membrane-bound vesicles, while endocytosis is a predominant active transport process of internalization. The internalization mechanism involves multiple ways, including clathrin-mediated endocytosis (CME), caveolae-mediated, macro- and micro-pinocytic endocytosis (**Fig 1.3.1).**

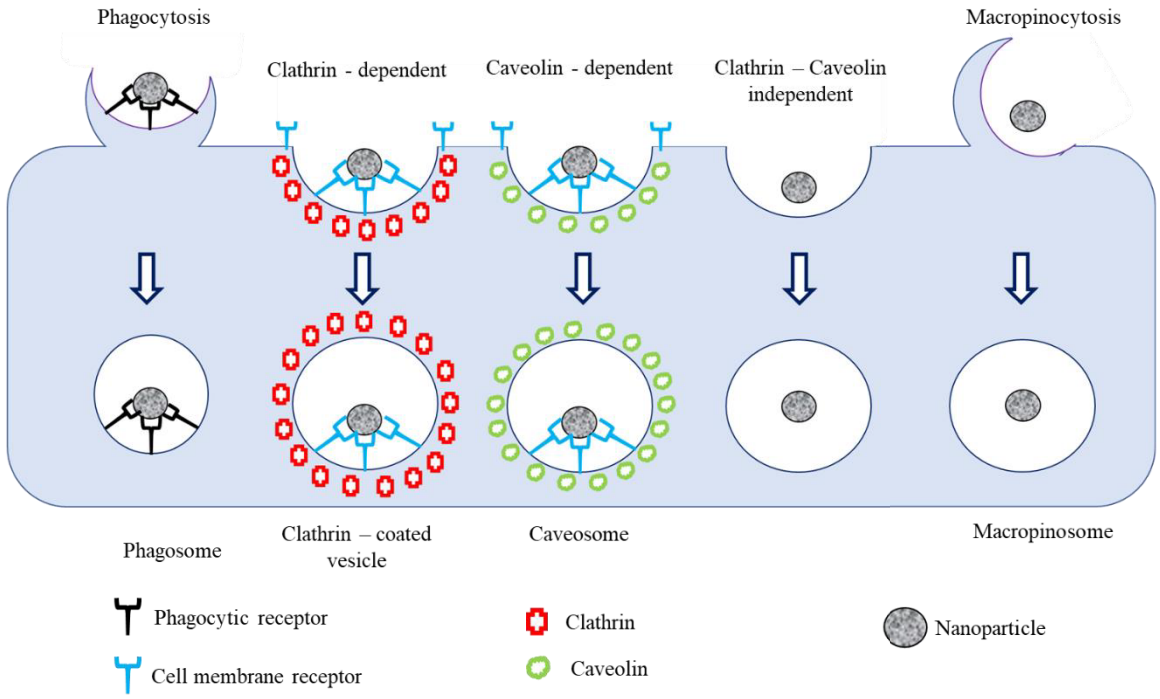

Figure 1.3.1. Different endocytic routes of NP internalization. *The cellular uptake of NPs can occur by various endocytic pathways like phagocytosis, clathrin, and caveolin dependent or independent mechanism, and micropinocytosis* [21].

The uptake of NPs is reported to depend on their size, shape, charge, surface coating, and rigidity [22]. Some studies suggest, for NPs smaller than 100 nm, sphere morphology is better than rod shape; in contrast, a report suggests better uptake of rod-shaped NPs in Hela cells than spherical and cylindrical [23]. Surface charge is another essential factor, positively charged NPs are preferred over negative or neutrally charged [24], however, literature also suggests that negatively charged NPs can enhance the cellular uptake [25, 26]. In the clathrin-mediated endocytic process, the vesicles formed are of around 100-150 nm, the NPs are directed towards lysosome followed by their degradation [27], positively charged NPs were reported to follow only CME, whereas negatively charged NPs follow CME and caveolae-mediated endocytosis in Hela and cervical cancer cells [27, 28]. Caveolae dependent endocytosis is involved in processes like cell signaling, regulation of lipids, fatty acids, and membrane proteins; also, its role has been investigated in viral infections [29]. Caveolae are

vesicles of 50-80 nm surrounded by caveolin protein, and these vesicles escape lysosomes [27, 29]. Clathrin and caveolin independent endocytosis involve cargoes like growth hormones, interleukin 2, and cellular fluids, and folate bound NPs are reported to internalize by this route [27, 30]. Macropinocytosis does not involve lipid rafts or pit formation; particles are taken up directly into endocytic vesicles, formed by cytoskeleton rearrangement [31]. This pathway is known for the uptake of large-sized or bulk NPs [32].

1.3.2 Trafficking of NPs inside a cell

The intracellular trafficking of NPs is very crucial in determining the fate of NPs. Upon entry of NPs in the cell via endocytic vesicles, cellular endosomes determine their fate. The endocytic vesicles fuse with early endosomes after pinching from the membrane, which then differentiates into late endosomes, which can again fuse with the plasma membrane to exocytose the NPs, or they can merge with lysosomes for their degradation (**Fig 1.3.2**) [26, 33]. The ones which escape lysosomes either remain intact in the cytoplasm or intracellular organelle [27]. When cells uptake nanoparticles, they are considered as foreign bodies; as a result, clearance mechanisms, including autophagy, is triggered. Autophagy, a process involved in the trafficking of cellular constituents affects the NP trafficking, by targeting them to lysosomes. NPs are known to induce autophagy and can also cause its dysfunction. Many nanomaterials, including gold nanoparticles (AuNPs), silver nanoparticles (AgNPs), silica, iron oxide, carbon nanotubes, graphene, fullerene, and their derivatives, are reported to alter autophagy upon cellular entry. The cellular mechanisms lying behind the regulation of autophagy, cellular stress induced by the nanomaterials, and its effect in triggering various facets of signaling cascade are investigated for understanding its therapeutic purpose [34].

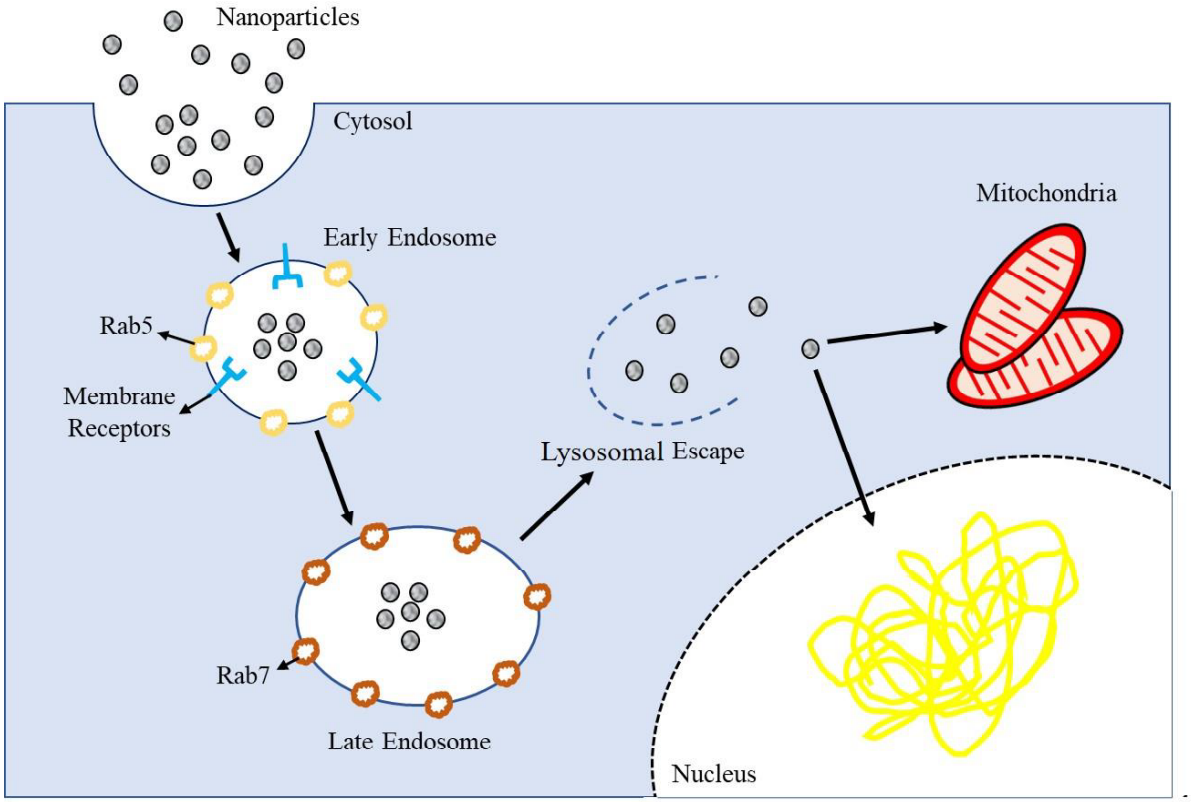

Figure 1.3.2. Probable intracellular trafficking routes of endocytosed NPs. *The endocytosed NPs are enclosed in early endosomes, which matures into a late endosome marked by Rab proteins. The late endosome fuses with lysosomes, or if they escape lysosomes, they target other cellular organelles like mitochondria, ER, nucleus, etc* [26, 33].

1.3.3 Intracellular signaling induced upon entry of NPs

Generation of Reactive oxygen species (ROS), is known to be the primary cause of toxicity influenced by various types of NPs. Increased levels of ROS, hampers different biological processes causing oxidative stress. The extent of oxidative stress activates distinct signaling pathways, like Nrf2 activation by mild oxidative stress causes transcription of phase II antioxidant enzymes, intermediate levels cause induction MAPK and NF-κB signaling [35]. Whereas, excess of oxidative stress causes mitochondrial membrane depolarization (MMP) that marks the initial step of intrinsic apoptosis [36]. MMP triggers cytosolic/mitochondrial calcium accumulation or ROS or both,

eventually leading to the formation of mitochondrial permeability transition pore (MPTP) [37], causing the release of apoptotic factors and ultimately cell death. ROS regulates mTOR (mammalian target of Rapamycin) signaling, which in turn, is very crucial in regulating autophagy. Also, endocytosis of various metal NPs like AgNPs have been reported to directly interact with the mTOR signaling pathway by regulating the activators (PI3K, Akt) and inhibitors (AMPK, TSC) of mTORC1, a subunit of mTOR [38]. NPs that are endocytosed forms endosomes and fuse with autophagosome, which can interact with lysosomes and upon prolonged exposure is reported to cause lysosomal damage by lysosomal membrane permeabilization (LMP). While partial LMP can induce intrinsic apoptosis, an immense LMP can cause necrosis by acidifying cytosol [39, 40]. All these reports suggest NP-induced toxicity by induction of oxidative stress is a cumulative effect of different intracellular organelles (**Fig 1.3.3)**.

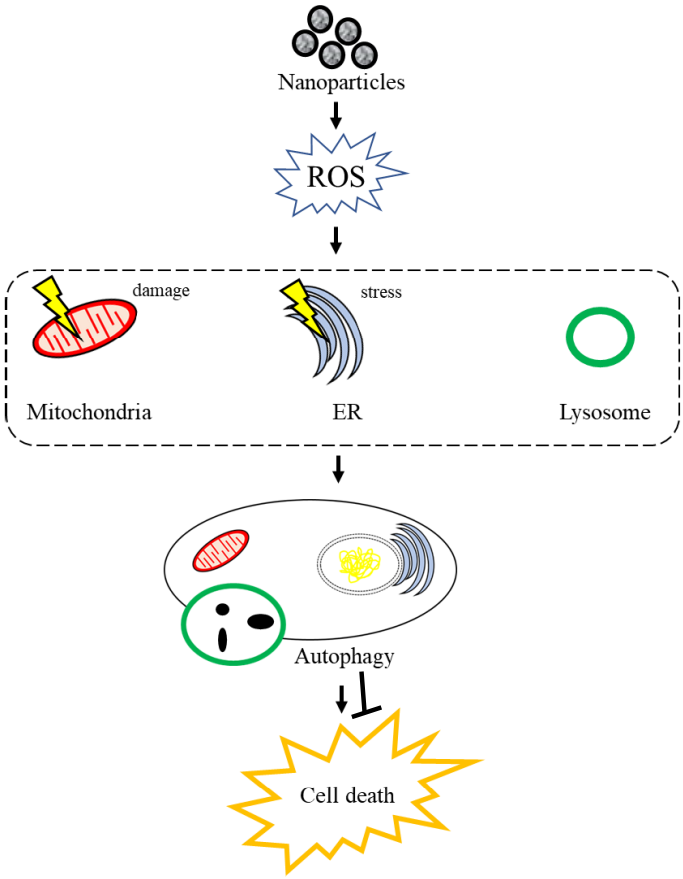

Figure 1.3.3. Image displaying plausible intracellular effects of NPs. *Upon entry, NPs increase the ROS level, which can affect organelles like, mitochondria, ER and lysosomes triggering autophagy,*

which can determine cell fate [36, 40].

As these nanomaterials are reported to induce cellular stress by regulating autophagy and other signaling pathways, which are discussed below, there is a growing interest in exploring their potential as therapeutics in diseases like cancer.

1.3.4 Autophagy: a self-digestion process

During the 1960's, Christian de Duve coined the term autophagy, which means self-eating. Very less was known about this process until, in the 1990s, scientists unveiled the molecular mechanism and conditions responsible for the autophagic process. In 2016, Yoshinori Ohsumi was awarded Noble Prize for discoveries in understanding the mechanisms involved in recycling cellular contents through autophagy [41]. Autophagy is a process that maintains cellular homeostasis through continuous degradation and recycling of proteins and organelles in nutrient-deprived conditions. Nutrient deprivation, immune system responses, organelle quality control, and cellular stress condition like hypoxia, oxidative stress, etc. are the main reasons responsible for autophagic induction [42]. Autophagy can be divided into four major intracellular categories **(Fig 1.3.4.1)**:

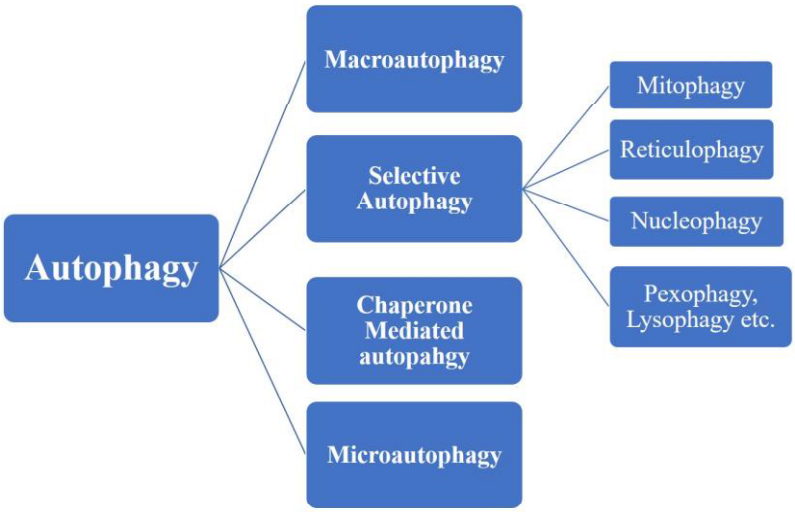

Figure 1.3.4.1. Flowchart showing classification of autophagy. *Autophagy is can be classified into*

four types: Macroautophagy, selective autophagy, chaperon mediated autophagy, and microautophagy. Selective autophagy is further classified based on the type of organelle, for example, mitophagy for mitochondria, nucleophagy for the nucleus, etc [41, 43].

Macroautophagy: begins with the formation of the phagophore, which then elongates to form autophagosome and then fuses with lysosomes to form autolysosome, where lysosomal enzymes digest its contents (**Fig 1.3.4.2**).

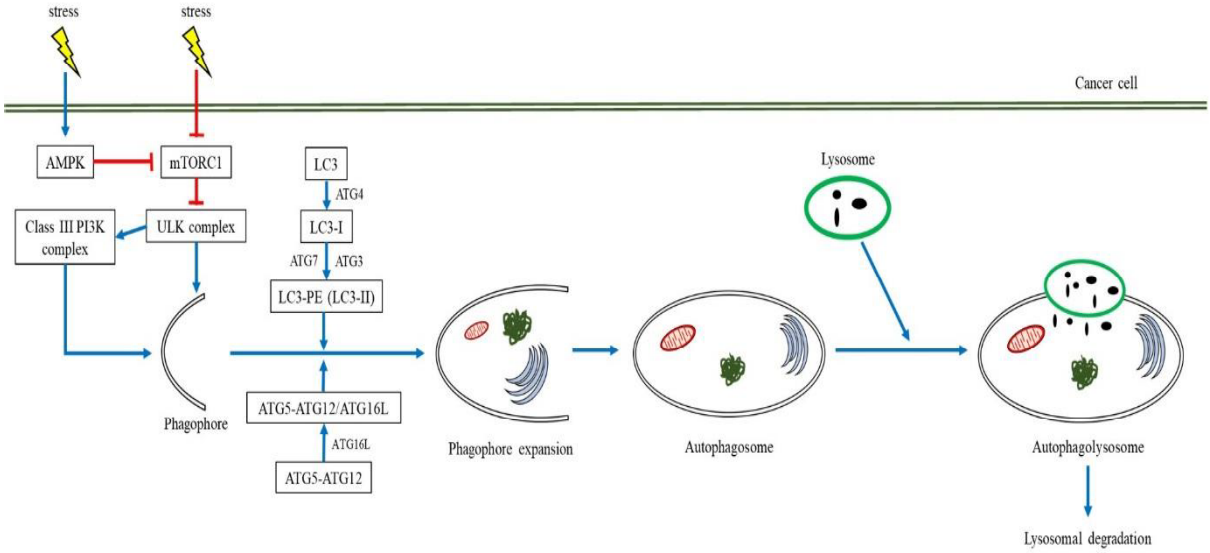

Figure 1.3.4.2. Schematic representation of machinery involved in macroautophagy. *Autophagy is necessary for maintaining cellular homeostasis. The process of autophagy is initiated by the formation of the phagophore followed by its elongation and, finally, a double-membrane structure called an autophagosome. This autophagosome fuses with the lysosome, where different enzymes degrade and recycle the components* [34, 44].

Under conditions like hypoxia and starvation, mTOR is inhibited, which activates autophagy. AMP-activated protein kinase (AMPK) inhibits the mTORC1, which dissociates the components of UNC-51 like autophagy activating kinase (ULK), thus causing inhibition of autophagy. Phosphoinositide 3-Kinase class III (PI3K-III) proteins form one of the major complexes involved in the initiation of

autophagosome formation. The second complex required for the same includes ULK1 in the presence of ULK2 and focal adhesion kinase family interacting protein of 200kDa (FIP200), ATG 13, and ATG101 [34, 45]. Beclin-1 interacts with vacuolar protein sorting kinase 34 (VPS34), which is essential for phagophore elongation and the recruitment of the ATG proteins [46]. Further, maturation of autophagosome includes protein complexes ATG12-ATG5-ATG16L and microtubule-associated protein light chain 3 (LC3)-II-phosphatidylethanolamine (LC3-II-PE). SNARE and Rab7 proteins help in the movement of autophagosomes towards lysosome [44].

Selective autophagy: Degradation of damaged organelles, e.g., mitophagy is for clearance of mitochondria, reticulophagy for ER, pexophagy for peroxisomes, nucleophagy and lysophagy for nucleus and lysosomes, respectively. Mitophagy is an essential aspect of cellular differentiation and development. PINK1 (PTEN-induced putative kinase1) and Parkin are the main proteins involved in this process. These proteins recruit SQSTM1 and OPTN (Optineurin), which binds LC3 and ultimately fuses with autophagosomes for degradation. ER stress and unfolded protein response triggers reticulophagy. RETREG1 has been reported as the cargo receptor protein, which binds to LC3, thus targeting ER for degradation [41, 43].

Chaperone mediated autophagy (CMA): Unlike other autophagic processes, CMA is specific for the KFERQ sequence containing substrates, which forms a complex with chaperon proteins followed by their degradation. Heat shock protein70 (HSC70) delivers substrates to the lysosomal membrane where it interacts with LAMP2A, which then translocate substrate inside lysosomes where proteolytic enzymes hydrolysis substrate [47].

Microautophagy: cargos are directly delivered to lysosomes for degradation without the involvement of autophagosomes. Rab7, several ATGs, and endosomal sorting complex required for transport (ESCRT) machinery proteins are reported to be involved in this type of autophagy [48].

1.3.4.1 Dual role of Autophagy

Cancer cells exploit the phenomenon of autophagy to sustain survival by supplementing metabolism in nutrient-deprived and stress conditions. Still, in some circumstances, it induces degradation of necessary cell components, which can cause cell death. Thus, autophagy plays a dual role; it can either promote or suppress tumor (**Fig 1.3.4.3**).

Autophagy as a tumor suppressor: Around 50-70% of human breast, prostate, and ovarian tumors are reported to have an allelic deletion in beclin-1 (BECN1) gene. Liang et al. have observed decreased expression of BECN1 in breast tumor cells as compared to healthy tissue, which confirms the tumor suppressor role of autophagy [49]. BECN1 associating proteins like UV radiation-resistance associated gene (UVRAG) and BAX interacting factor-1(Bif-1) functions as a tumor suppressor and is known to regulate autophagy positively. Autophagy regulating genes like ATG3, ATG5, and ATG9 are also reported to inhibit oncogenesis. Autophagy is reported to suppress tumors by regulating reactive oxygen species (ROS) [50].

Autophagy as a tumor promoter: Autophagy recycles intracellular components to provide substrates to meet the high metabolic demands of tumor cells. Various studies suggest that knockdown of ATGs or inhibition of autophagy results in cell death. ATG17 deficient mice were resistant to breast tumor, deletion of ATG7 accelerated p53 mediated cell death and mitochondrial dysfunction, impaired fatty acid oxidation, and reduced TCA cycle intermediates confirming the pro-survival role of autophagy. Also, inhibition of autophagy increases the accumulation of damaged mitochondria, which causes cell death. Cancers like colon, lung, and pancreatic, which have RAS mutations, were found to have high levels of autophagy, which is responsible for tumor survival and oncogenesis [50].

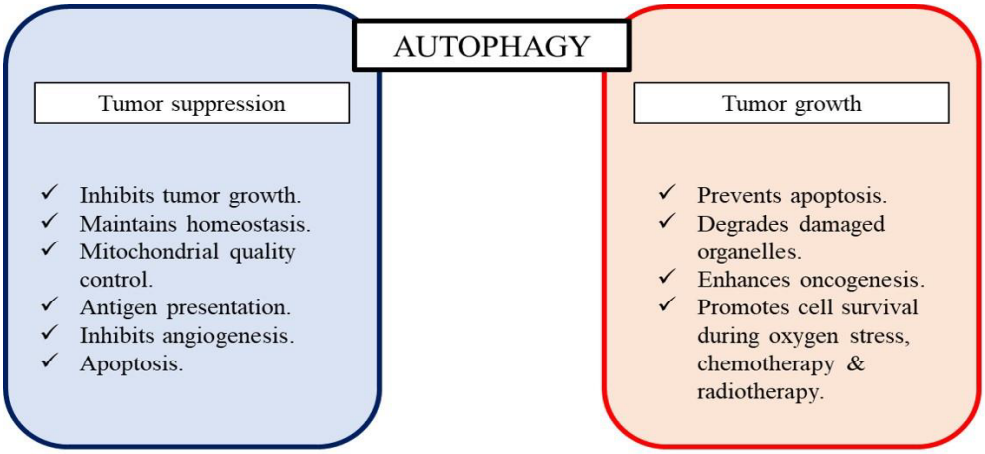

Figure 1.3.4.3. Representation of the dual role of autophagy in cancer. *The role of autophagy is context-dependent; it can play as a tumor suppressor by inhibiting the growth of the tumor by inducing apoptosis, inhibiting angiogenesis, regulating mitochondrial quality control. Contrarily, it can promote tumor by decreasing ROS levels, preventing cell death, clearing damaged organelles supporting cell survival during stress* [50].

1.3.5 Mitochondrial quality control

Mitochondria are the dynamic organelles involved in maintaining cellular homeostasis. Many evidences support an essential role of mitochondria in the regulation of cell cycle by regulating calcium ion or ROS levels. Apart from their role in maintaining cellular health and growth, they also act as executioners of cellular death pathways like apoptosis and necrosis. Therefore, it becomes necessary for a cell to control and maintain mitochondrial health. Mitochondria are involved in diligent quality control (QC) system, which is a three-step cyclic process:

(i) identification of damaged mitochondria

(ii) elimination of irreparable mitochondria by mitophagy

(iii) biogenesis of mitochondria.

If this cycle is compromised, the cell becomes susceptible to apoptosis. When a cell experiences any stress mitochondrial quality control system activates where proteolysis system of mitochondria

initiates degradation of misfolded proteins, cellular proteasome machine helps in the degradation of damaged mitochondrial membrane proteins. Mitochondria start undergoing a constant cycle of fusion and fission to repair damaged mitochondria, and finally, mitophagy comes into play where damaged mitochondria are degraded through lysosomes [34]. Below, we have discussed the reported molecular regulation of mitochondrial quality control:

Mitochondrial fission and fusion: Various functions of mitochondria depend on their morphology and the delicate balance between fusion and fission, which is a must for their proper function. Uninterrupted fission results in mitochondrial fragmentation, which is responsible for many metabolic disorders. However, constant fusion gives rise to hyper fused mitochondrial network, which forestalls metabolic insults and prevents autophagy [51]. Hence, balanced mitochondrial dynamics maintain the metabolic needs of the cell and regulates the clearance of damaged organelle (**Fig 1.3.5**.). Looking into molecular machinery, the mitochondrial dynamicity is regulated by conserved GTPases. Mitochondria are double-membrane organelles, the outer mitochondrial membrane (OMM) fuses with the help of Mfn1 and mfn2 (mitofusin1 and 2) whereas, OPA1 (Optic Atrophy 1) is known to mediate fusion of inner mitochondrial membrane (IMM). Chen et al. [52] reported lethal embryos in Mfn1 or 2 null mice. They mentioned, Mfn2-/- mice died due to abnormal placental development; however, the mechanism for Mfn1-/- is not much clear [53]. OPA1 is involved in the fusion of IMM; OPA1 undergoes proteolytic cleavage to produce isoforms, L-OPA1, and S-OPA1, which are crucial for initiating fusion and cristae remodeling. OPA1 mutation also causes embryonic lethality in mice just, reports suggest, in dominant optic atrophy OPA1 is essential in the maintenance of retinal ganglion cells [54]. Under normal conditions, fission is said to facilitate the autophagic clearance of mitochondria (mitophagy), which makes cells to adjust mitochondria to physiological demands. Dynamin-related protein 1 (DRP1) is involved in the regulation of mitochondrial fission. DRP1 binds to its receptors, fission protein 1 (FIS1), mitochondrial fission factor (MFF), mitochondrial dynamics of 49 kDa and 51 kDa protein (MiD49 and MiD51) on OMM

leading to constriction of both the membranes. Mitochondrial fission is necessary for cell growth and proliferation; however, it is also reported to cause various cellular dysfunction like cancer, cardiovascular, and neurodegenerative diseases [53].

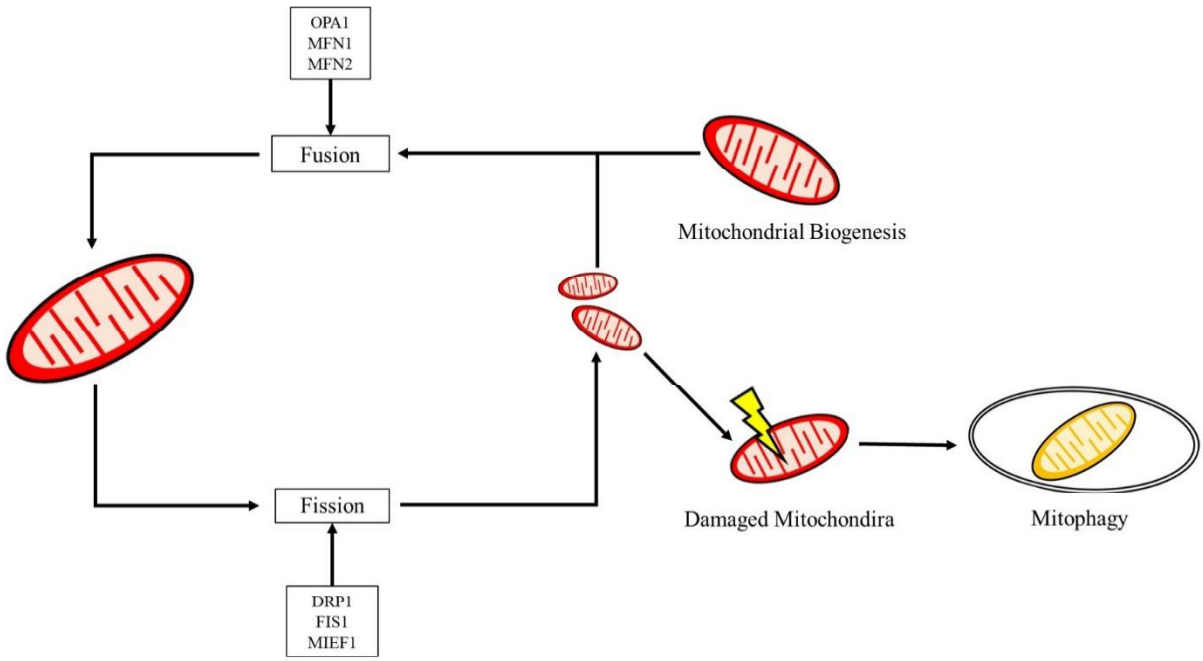

Figure 1.3.5. Schematic representation of mitochondrial dynamics. *Mitochondria repetitively undergo fusion & fission to maintain mitochondrial quality. OPA1, Mfn1, Mfn2 are proteins involved in fusion; mitochondria can get repaired by fusing with a healthy mitochondrion or Drp1, initiates fission. If mitochondria are unable to recover, they are cleared by mitophagy* [55].

1.3.5.1 Mitophagy: Mitophagy is the removal of superfluous mitochondria through lysosomes. Mitochondrial damage triggers cellular responses, continued defect marks the removal of mitochondria through mitophagy. However, impairment in mitochondrial clearance causes accumulation of damaged mitochondria causing various cellular disorders. The signaling pathways which regulate mitophagy can be ubiquitin-dependent or independent (**Fig 1.3.5.1**). Ubiquitin-dependent mitophagy is regulated by the PINK1-Parkin pathway. In healthy mitochondria, PINK1 is

cleaved by proteases upon its transportation to IMM, followed by its degradation by ubiquitin-proteasomal system (UPS) [56]. When mitochondria get depolarized, PINK1 is activated by autophosphorylation stabilizes on OMM, which translocates Parkin to damaged mitochondria. Parkin is an E3 ubiquitin ligase; it binds to poly-Ub chains to activate PINK1 to amplify the mitophagic signals further [57]. Poly-Ub of proteins by Parkin makes them visible for autophagy adaptors or by proteasomal degradation system [58]. This PINK1-parkin pathway is reported to interfere with mitochondrial dynamics as well [59]. PINK1, once recruited to OMM induces DRP1 activity, promoting fission, enabling their degradation. However, recently DRP1-independent mitophagy has also been reported [60]. PINK1 causes phosphorylation of MFN2, which then associates with parkin for its degradation, reducing the fusion of mitochondria. This degradation destroys the ER-mitochondria contact sites; these sites are known to regulate mitophagy negatively [61]. In addition to parkin, E3 ligases like, SMURF1, Gp78, SIAH1 are also reported to regulate mitophagy, they recruit OPTN, nuclear dot protein 52 and p62 which directly interacts with LC3 anchoring mitochondria to autophagosomes [62]. Various studies have suggested p62 is not essential for mitophagy [63, 64]. Ubiquitin independent mitophagy involves mitochondrial protein, which targets dysfunctional mitochondria for degradation. Proteins of OMM like NIX (NIP3-like protein X), BNIP3 (BCL2 interacting protein 3), and FUNDC1 (FUN14 domain-containing protein) acts as receptors of mitophagy [65, 66]. Prohibitins (PHB) are IMM recently reported to be involved in mitochondrial regulation, increased proteasomal activity, and depolarization triggers PHB2 to associate with LC3 [66]. Cardiolipins like PHB2 interacts with LC3 to promote mitochondria and autophagosome fusion [65].

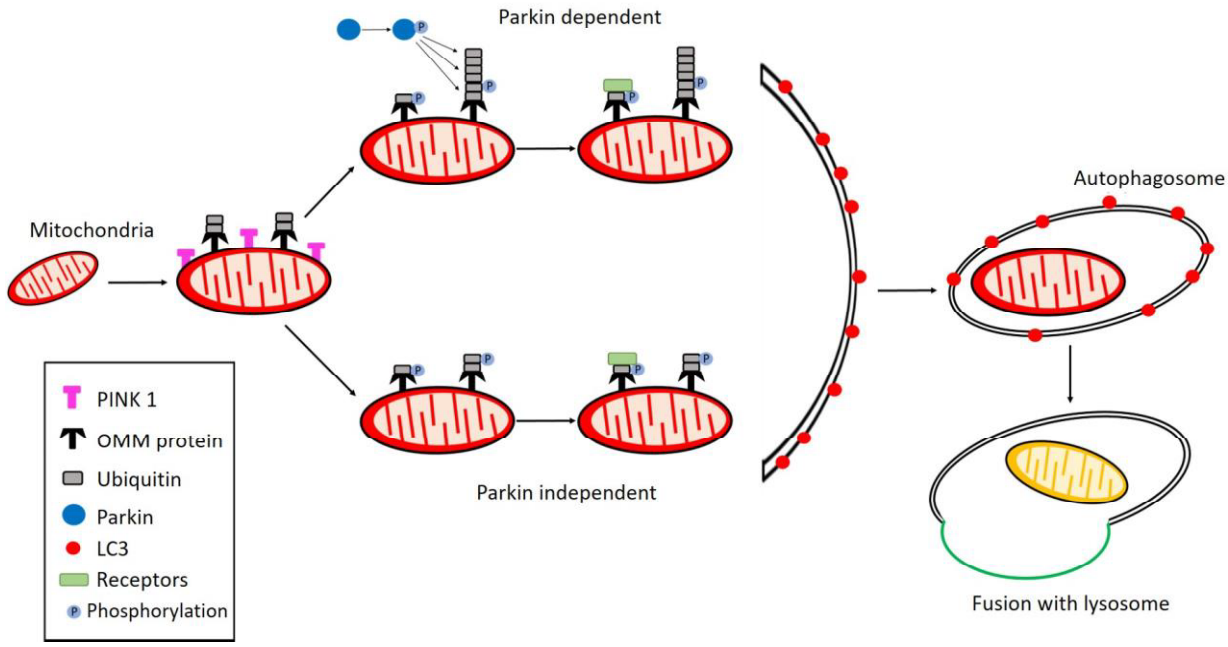

Figure 1.3.5.1. Schematic representation of molecular events leading to mitophagy. *Parkin-dependent mitophagy involves polyubiquitination, which recruits autophagy receptors like p62, OPTN. In contrast, in the Parkin-independent process, mitochondrial proteins recruit the autophagy receptors causing the formation of mitophagosome, which then fuses with lysosomes for its degradation* [62].

1.3.5.2 Mitochondrial dynamics and cancer: Mitochondrial dynamics are involved in the regulation of cell cycle and death mechanisms [53]. Recent findings suggest the co-relation of mitochondrial fusion and fission with cancer progression. Fission has been reported to support tumor progression in several cancers including, breast, colon, lung, liver, and melanoma, as DRP1 inhibition was found to inhibit the cell growth and induces apoptosis [53, 67, 68]. Silencing DRP1 or increasing the expression of MFN1/2 resulted in reduced migration and invasion in breast cancer cells [69]. Another study suggests hypoxia increases the expression of DRP1 in glioblastoma cell line upon inhibition of fission with mDIVI-1 decreases the metastasis of gliomas [70]. Contrarily, some studies suggest increased fragmentation increases the metabolic stress in cancer cells. In

prostate cancer, androgens are found to increase DRP1 expression, which facilitates apoptosis of cells in response to mitochondrial stress [71]. In another study, Cervical and ovarian cancers resistant to cisplatin were found to have a high proportion of fused mitochondria, whereas in non-resistant controls, cisplatin-induced mitochondrial fragmentation and apoptosis [53, 72]. All these reports suggest mitochondrial dynamics regulating proteins can be used as biomarkers or targets for different types of cancer. However, these studies indicate either inhibition of fusion or fission can increase the sensitivity of cancer cells to therapy depending on the type of cancer. However, a precise and deep understanding is still needed to exploit mitochondrial dynamics for cancer therapy.

1.3.6 Endoplasmic Reticulum Stress (ER stress)

When cells tend to lose their homeostasis upon prolonged oxidative stress or nutrient deficiencies, to heal themselves, a series of protection mechanisms are induced, which includes endoplasmic reticulum (ER) stress. Upon initiation of ER stress, a cascade of events including unfolded protein response (UPR), ER-associated degradation (ERAD), autophagy, mitochondrial biogenesis takes place to clear the accumulation of misfolded or unfolded proteins thereby restoring the homeostasis of ER [73]. However, the extent of ER stress will eventually determine either re-establishment of cellular homeostasis or activation of programmed cell death. ER chaperons, Grp78/BiP promotes proper folding or degradation during UPR induced by ER stress; it can also decrease the production of protein, thereby reducing the ER stress. There are three major transmembrane proteins through which UPR is executed, including protein kinase R-like endoplasmic reticulum kinase (PERK), inositol-requiring kinase 1 (IRE1), and activating transcription factor 6 (ATF6). When ER stress is absent, these transmembrane proteins bind to Grp78/BiP, thereby remaining inactive. However, under ER stress, the misfolded proteins would compete with PERK, IRE1 and ATF6 to bind with Grp78/BiP thus these transmembrane proteins are activated which induces myriad of downstream signaling cascade eventually regulating certain gene expression, chaperone production, thereby

degrading misfolded proteins or reducing the synthesis of new proteins, leading to the restoration of ER homeostasis [74].

1.3.6.1 Role of ER stress in Autophagy and Mitochondrial dynamics: ER stress can induce autophagy *via* unfolded protein response to restore protein homeostasis by clearing out the damaged or misfolded proteins. The three arms of UPR are involved in the activation of cell autophagy, depending on the cell type and its environment. ER stress-induced autophagy can have a pro-survival effect on the cell. While PERK has been reported to promote the expression of autophagy-related gene Atg12 and LC3 through the phosphorylation of eIFα, a transcription factor, interestingly growing body of evidence reveals that the real cell autophagy induced by ER stress is IRE1 rather than PERK or ATF6 [75]. *In-vivo* studies show that IRE1 is required for the aggregation of autophagosomes rather than PERK or ATF6. Also, they found that the IRE1 can form a complex with tumor necrosis factor receptor-associated factor-2 (TRAF-2), which can phosphorylate the apoptosis signal-regulating kinase 1(ASK1). Then the phosphorylated ASK1 further phosphorylates the JNK, which can promote the activation of the Bcl-2, eventually leading to cell autophagy. Induction of autophagy orchestrates regulation of organelle dynamics *via* selective autophagy, including ER-phagy and mitophagy, ensuring quality control [76]. The regulation of mitochondrial dynamicity is reported to be performed by PERK-mediated UPR during ER stress. During ER stress, the mitochondrial function can be disrupted and can promote the mitochondrial-derived apoptotic pathway through mitochondrial depolarization and fragmentation. However, the cellular fate is decided after careful evaluation of reverting the damage. The cellular stress could be reduced through protective mechanisms during ER stress if the overall cellular damage is low. These protective mechanisms again are found to happen through PERK-mediated UPR, which mediates mitochondrial remodeling where PERK activates ATF4, which leads to subsequent transcription and translation of mitochondrial chaperones such as HSP70 and proteases including LON. Also, PERK promotes inhibition of TIM23 by the degradation of TIM17A, a subunit of TIM23 to decrease the

import of proteins to mitochondria as a response to ER stress, thereby remodeling the mitochondrial quality control mechanisms. Another mechanism by which mitochondrial remodeling can happen is by alteration of its morphology as a combat mechanism of cellular stress. When cellular stress tends to damage the mitochondrial function, fragmentation of mitochondria increases, thereby leading to mitophagy. Thus, damaged mitochondria are eliminated, and cellular insults are overcome, eventually restoring the global function. Acute ER stress induces proper remodeling of mitochondrial morphology through stress-induced mitochondrial hyperfusion (SIMH). ER stress-dependent SIMH is again reported to be regulated by the PERK arm of the UPR by promoting eIF2α phosphorylation-dependent inhibition of protein expression [77]. **Figure 1.3.6.1** represents the activation of different signaling cascades upon induction of ER stress, leading to autophagy.

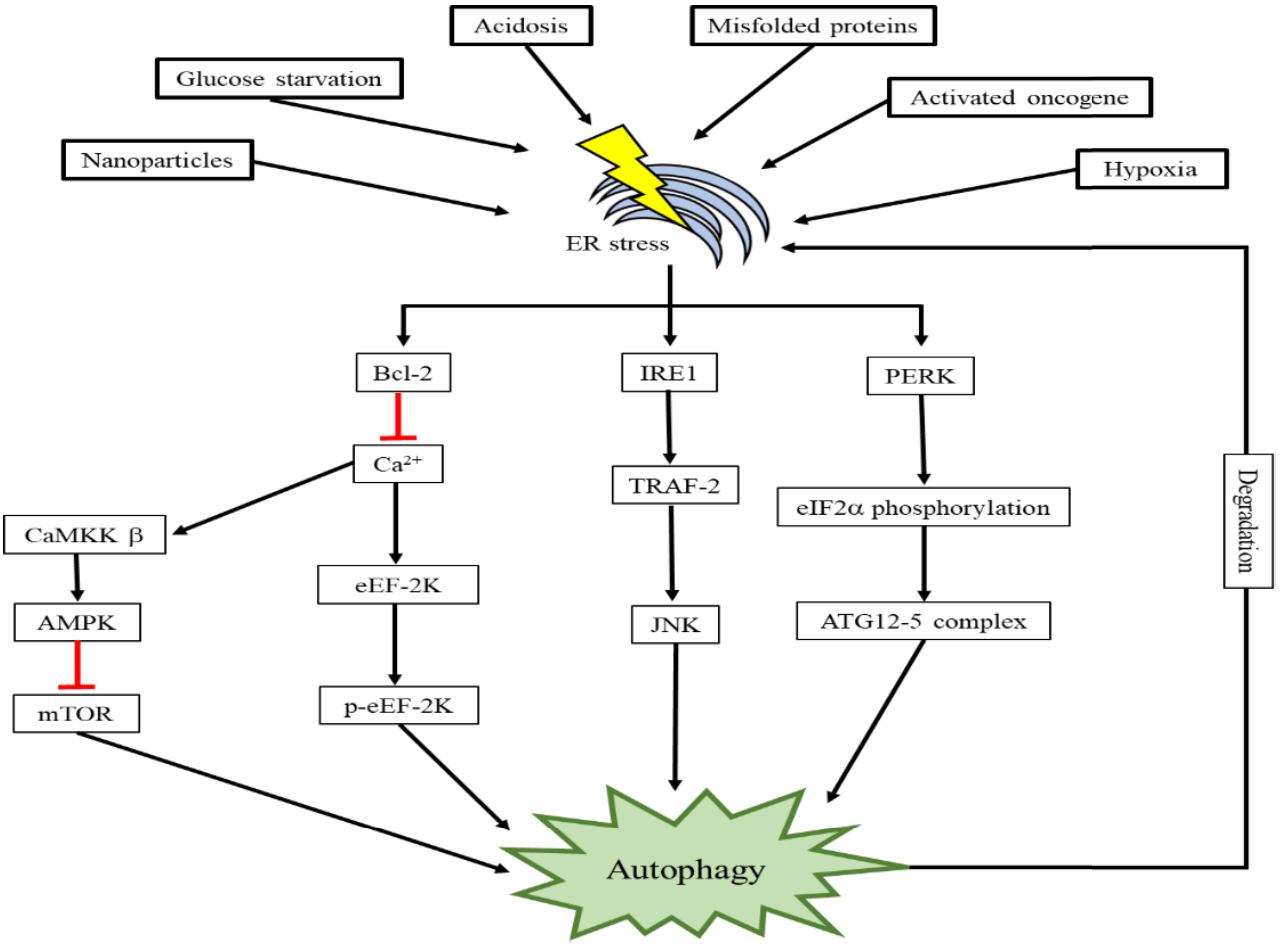

Figure 1.3.6.1. Schematic representation of different arms of ER stress. *Various factors like NP*

exposure, glucose starvation, accumulation of misfolded proteins, hypoxia, etc. induce ER stress. Activation of different signaling pathways like, IRE1 activates JNK signaling through TRAF-2; PERK causes phosphorylation of eIF2α, which activates ATG12-5 complex; Bcl-2 inhibits mTOR, which can modulate autophagy [74].

1.3.6.2 ER stress and cancer: During cancer progression, a cell experiences external conditions such as hypoxia, low glucose, oxidative stress, lack of growth factors, etc. and internal stress like the high metabolic status of tumor cell, genomic instability, mutations in protein folding and secretory pathway, together with these compromises the protein folding efficiency of ER, causing ER stress. In response to ER stress, activation of UPR (IRE1α, PERK, ATF6) is reported in several cancer studies including, glioblastoma, leukemia, breast, colon, lung, pancreas and liver [78]. UPR promotes or restricts the tumor progression is still not elusive, despite various evidence supporting existent ER stress in many cancer types. Studies suggest IRE1α is a crucial kinase which, upon mutation, is most liable to become cancer driver [79]. Several reports indicate IRE1α promotes tumor progress through XBP1, in triple-negative breast cancer, genetic ablation of IRE1α inhibited angiogenesis and tumor growth in glioma cells [80, 81]. The IRE1α/XBP1 axis is also involved in chemotherapy resistance [82]. Many studies suggest PERK promotes tumor growth, its inhibition was found to reduce breast cancer metastasis to the lung in immunocompromised mice [83] and decreases tumor growth in xenograft models of human pancreatic cancer [84]. PERK deficient cells are unable to phosphorylate eIF2α affecting the protein translation in hypoxic tumors; it is also known to modulate various signaling pathways including NRF2, regulates metabolism, lipid biosynthesis, cellular redox [85]. In HT29, colon cancer cell line, PERK signaling was involved in promoting chemoresistance [86], haploinsufficiency of PERK is also reported to promote melanoma development [87]. Few reports are the present mentioning role of ATF6 in cancer, recently, high expression of ATF6 was suggested as a marker for colorectal carcinoma [88]. Thus, most of the reports indicate the pro-oncogenic role

of UPR and the contribution of ER stress to different cancer hallmarks, showing the components of UPR is an emerging therapeutic target against cancer.

1.4 NPs targeting intracellular signaling as therapy for cancer:

The effect of nanomaterials on the modulation of several signaling pathways, including autophagy, mitochondrial dynamics, ER stress, etc. have shown the tremendous therapeutic potential of NPs against different types of cancer cells.

1.4.1 NPs modulating autophagy: Various studies have shown metal-based NPs have been successful in inducing toxicity of cancer cells either by themselves or in combination with other treatments. For example, the embedment of AgNPs in exopolysaccharide (EPS) is reported to increase ROS levels, which induces autophagic cell death in SKBR3 cells [89]. Synergistic effect of reduced graphene oxide AgNP nanocomposite with cisplatin was observed against cervical cancer. This combination resulted in an accumulation of autophagosomes, which induces ROS generation and cell death in HeLa cells [90]. According to another report, Salimycin and AgNPs also showed substantial synergism by inducing massive autophagy, which resulted in mitochondrial dysfunction and death of A2780 ovarian cancer cells [91]. Recently, AgNPs have also been reported to reduce the expression of TFEB (transcription factor EB), affecting the lysosome function and autophagic flux in A459, a lung cancer cell line [92]. AuNPs, in combination with TRAIL (TNF-related apoptosis-inducing ligand), has been suggested as a strategy to overcome the treatment in many TRAIL-resistant tumors. This combination is reported to induce Drp-1 mediated mitochondrial damage leading to autophagy and mitophagy activation, which, in turn, resulted in cell death [93]. In another recent study in MDA-MB-231 cells, autophagy was reported to induce cytotoxicity by anti-EGFR-antibody conjugated AuNPs combined with near-infrared photothermal therapy (NIR-PTT) [94]. AuNPs layered over iron core forming, Fe@Au bi-metallic NP, is also reported to induce toxicity through mitochondria-mediated autophagy in oral and colorectal cancer cells [95, 96]. Similarly, many other NPs are being used to target autophagy, some of which are summarized along with their

probable mechanism of action in the following **Table 1.2.**

Table 1.2: List of some metal NPs with autophagy modulatory functions.

S. No.	Type of NPs	Cancer Type	Probable Mechanism of Action	References
1.	Silver	Breast, Ovarian cancer	Inhibition of autophagic flux, Low MMP, Mitochondrial dysfunction	[91, 97]
2.	Gold	Liver Cancer	Modulation of MAPK/Akt/mTOR pathway and EGFR/FAAD proteins	[98]
3.	Titanium dioxide	Cervical Cancer, Leukemia	TFEB activation, Autophagic flux blockage, enhanced ROS, cell death	[99, 100]
4.	Zinc Oxide	Oral cancer	Activation of PINK1/Parkin-mediated mitophagy	[101]
5.	Iron Oxide	Breast, Gastric Cancer	Accumulation of LC3-positive autophagosomes, ↓MMP, ↓ATP production, and ↑ROS, Lysosome Impairment, Mitochondrial Damage	[102, 103]
6.	Silica	Glioblastoma	Increase in LC3-II/LC3-I ratio, the upregulation of the Atg5 gene	[104]
7.	Cuprous Oxide	Cervical Cancer	Induction of autophagy through the AKT/mTOR pathway, Mitochondrial damage, Cell Death	[19]
8.	Copper Oxide	Breast Cancer	↑ LC3B-II, ATG-5, Beclin1, Autophagy, Apoptosis	[105]

1.4.2 NPs targeting ER stress: As discussed above, cancer cells are sensitive to ER stress, modulation of ER stress using NPs is being used as another strategy for cancer treatment. Several studies have already been reported in this regard, AgNPs and AuNPs have been shown to induce

massive ER stress, ultimately leading to cell death [106, 107]. Some recent reports suggest the induction of ER stress depends on the physicochemical properties of NPs, for example, smaller sized ZnO (Zinc Oxide) NPs induces more ER stress as compared to larger ones [108]. Another report says insoluble CeO_2 NPs (Cerium oxide) are unable to activate CHOP and HSP protein, the ER stress markers. Contrarily, insoluble TiO_2 NPs are reported to induce ER stress [109]. These reports suggest ER stress induction depends on the type of NPs. Other reports indicate NPs can be used as ER stress-inducing agents, PLGA NPs loaded with LY294002, a PI3K inhibitor, are shown to localize in ER, producing induction of ER stress and causing toxicity in cancer cells [110]. Similarly, various other NPs are reported to induce ER stress some of which are summarized in **Table 1.3** below:

Table 1.3 List of some metal NPs causing modulation of ER stress

S. No.	Type of NPs	Cell Type	Mechanism of ER Stress Induction	References
1.	Silver	ZFL cells, Human Chang liver cells	↑ GRP78, ATF6, and XBP-1s protein or mRNA; ↑ ER tracker staining and protein levels of p-PERK, p-IRE1, peIF2α, XBP-1s, ATF6, GRP78, and CHOP.	[111, 112]
2.	Gold	HUVEC, Human Neutrophils	↑ XBP-1s mRNA; ↑ p-PERK, p-IRE, and ATF6 proteins	[113, 114]
3.	Titanium dioxide	Mice, 16HBE14o- lung cells	Swelling of ER; increased GRP78, CHOP and p-IRE1α protein	[115, 116]
4.	Zinc Oxide	HUVEC	↑ XBP-1s, CHOP, p-PERK, p-eIF2α, HSP proteins or mRNA	[117]

5.	Iron Oxide	MCF-7 cells, RAW 264.7 cells	Disrupted & dispersed ER; ↑ CHOP mRNA, p-IRE1α, IRE1α, CHOP proteins.	[118, 119]
6.	Silica	HUH7	↑ GRP78 and XBP-1s mRNA.	[120]
7.	Zinc Sulphide	Mice retinal pigment epithelial cells	Suppressed GRP78 and CHOP proteins.	[121]
8.	Cerium Dioxide	MCP-1 transgenic mice	Suppressed GRP78, PDI, and HSP mRNA	[122]

All these reports suggest nanomaterials can serve as a potent therapeutic against cancer because of its ability to enter the cell and initiate the cascade of signaling, which ultimately leads to cell death.

1.5 References

1 Organization, W.H. (2020) WHO report on cancer: setting priorities, investing wisely and providing care for all.

2 Manoharan, N. et al. (2017) Descriptive epidemiology of female breast cancer in Delhi, India. Asian Pacific journal of cancer prevention 18 (4), 1015

3 Organization, W.H. (2020) Cancer (Vol. 2020)

4 Makki, J. (2015) Diversity of breast carcinoma: histological subtypes and clinical relevance. Clinical medicine insights: pathology 21;8:23-31.

5 Sun, Y.-S. et al. (2017) Risk factors and preventions of breast cancer. International journal of biological sciences 13 (11), 1387

6 Fabian, C. (2007) The what, why and how of aromatase inhibitors: hormonal agents for treatment and prevention of breast cancer. International journal of clinical practice 61 (12), 2051-2063

7 Waks, A.G. and Winer, E.P. (2019) Breast cancer treatment: a review. Jama 321 (3), 288-300

8 Zhang, X.-F. (2016) Zhi-Guo liu, Wei shen, Sangiliyandi Gurunathan. SilverNanoparticles: Synthesis, Characterization, Properties, Applications, and Therapeutic Approaches. International journal of molecular sciences 17, 1534

9 Zhang, X.-Q. et al. (2012) Interactions of nanomaterials and biological systems: Implications to personalized nanomedicine. Advanced drug delivery reviews 64 (13), 1363-1384

10 Guo, L. et al. (2020) Autophagy Modulated by Inorganic Nanomaterials. Theranostics 10 (7), 3206

11 Bhatia, S. (2016) Nanoparticles types, classification, characterization, fabrication methods and drug delivery applications. In Natural polymer drug delivery systems, pp. 33-93, Springer

12 Khan, I. et al. (2017) Nanoparticles: properties, applications and toxicities. Arabian journal of

chemistry 12: 908.

13 Dhand, C. et al. (2015) Methods and strategies for the synthesis of diverse nanoparticles and their applications: a comprehensive overview. Rsc advances 5 (127), 105003-105037

14 Jamkhande, P.G. et al. (2019) Metal nanoparticles synthesis: An overview on methods of preparation, advantages and disadvantages, and applications. Journal of drug delivery science and technology, 101174

15 Mourdikoudis, S. et al. (2018) Characterization techniques for nanoparticles: comparison and complementarity upon studying nanoparticle properties. Nanoscale 10 (27), 12871-12934

16 Tang, X. et al. (2017) The use of nanoparticulates to treat breast cancer. Nanomedicine 12 (19), 2367-2388

17 Chugh, H. et al. (2018) Role of gold and silver nanoparticles in cancer nano-medicine. Artificial cells, nanomedicine, and biotechnology 46 (sup1), 1210-1220

18 ud Din, F. et al. (2017) Effective use of nanocarriers as drug delivery systems for the treatment of selected tumors. International journal of nanomedicine 12, 7291

19 Xia, L. et al. (2017) Cuprous oxide nanoparticles inhibit the growth of cervical carcinoma by inducing autophagy. Oncotarget 8 (37), 61083

20 Pillai, G. (2014) Nanomedicines for cancer therapy: an update of fda approved and those under various stages of development. SOJ Pharmacy & Pharmaceutical Sciences 1 (2): 13.

21 Wu, M. et al. (2019) Size-dependent cellular uptake and localization profiles of silver nanoparticles. International journal of nanomedicine 14, 4247

22 Foroozandeh, P. and Aziz, A.A. (2018) Insight into cellular uptake and intracellular trafficking of nanoparticles. Nanoscale research letters 13 (1), 339

23 Sun, J. et al. (2015) Tunable rigidity of (polymeric core)–(lipid shell) nanoparticles for regulated cellular uptake. Advanced materials 27 (8), 1402-1407

24 Marano, F. et al. (2011) Nanoparticles: molecular targets and cell signalling. Archives of

toxicology 85 (7), 733-741

25 Schleh, C. et al. (2012) Size and surface charge of gold nanoparticles determine absorption across intestinal barriers and accumulation in secondary target organs after oral administration. Nanotoxicology 6 (1), 36-46

26 Rauch, J. et al. (2013) Big signals from small particles: regulation of cell signaling pathways by nanoparticles. Chemical reviews 113 (5), 3391-3406

27 Behzadi, S. et al. (2017). Cellular uptake of nanoparticles: journey inside the cell. Chemical society reviews 46, 4218-4244

28 Harush-Frenkel, O. et al. (2007) Targeting of nanoparticles to the clathrin-mediated endocytic pathway. Biochemical and biophysical research communications 353 (1), 26-32

29 Pelkmans, L. and Helenius, A. (2002) Endocytosis via caveolae. Traffic 3 (5), 311-320

30 Damm, E.-M. et al. (2005) Clathrin-and caveolin-1–independent endocytosis: entry of simian virus 40 into cells devoid of caveolae. The Journal of cell biology 168 (3), 477-488

31 Lim, J.P. and Gleeson, P.A. (2011) Macropinocytosis: an endocytic pathway for internalising large gulps. Immunology and cell biology 89 (8), 836-843

32 Kuhn, D.A. et al. (2014) Different endocytotic uptake mechanisms for nanoparticles in epithelial cells and macrophages. Beilstein journal of nanotechnology 5 (1), 1625-1636

33 Jovic, M. et al. (2010) The early endosome: a busy sorting station for proteins at the crossroads. Histology and histopathology 25 (1), 99

34 Cordani, M. and Somoza, Á. (2019) Targeting autophagy using metallic nanoparticles: a promising strategy for cancer treatment. Cellular and molecular life sciences 76 (7), 1215-1242

35 Manke, A. et al. (2013) Mechanisms of nanoparticle-induced oxidative stress and toxicity. BioMed research international 2013

36 Ma, W. et al. (2015) Silver nanoparticle exposure induced mitochondrial stress, caspase-3 activation and cell death: amelioration by sodium selenite. International journal of biological

sciences 11 (8), 860

37 Govender, R. et al. (2013) Silver nanoparticles of Albizia adianthifolia: the induction of apoptosis in human lung carcinoma cell line. Journal of nanobiotechnology 11 (1), 5

38 Hulea, L. et al. (2016) Biomedical potential of mTOR modulation by nanoparticles. Trends in biotechnology 34 (5), 349-353

39 Canton, I. and Battaglia, G. (2012) Endocytosis at the nanoscale. Chemical society reviews 41 (7), 2718-2739

40 Miyayama, T. and Matsuoka, M. (2016) Involvement of lysosomal dysfunction in silver nanoparticle-induced cellular damage in A549 human lung alveolar epithelial cells. Journal of occupational medicine and toxicology 11 (1), 1

41 Sheng, R. and Qin, Z.-H. (2019) History and Current Status of Autophagy Research. In Autophagy: Biology and Diseases, pp. 3-37, Springer

42 Yang, J. et al. (2019) Autophagy and Energy Metabolism. In Autophagy: Biology and Diseases, pp. 329-357, Springer

43 Green, D.R. and Levine, B. (2014) To be or not to be? How selective autophagy and cell death govern cell fate. Cell 157 (1), 65-75

44 Li, W. and Zhang, L. (2019) Regulation of ATG and Autophagy Initiation. Advances in experimental medicine and biology, 1206:41-65

45 Kim, J. et al. (2011). AMPK and mTOR regulate autophagy through direct phosphorylation of Ulk1. Nature cell biology 13, 132-141

46 Backer, J.M. (2008) The regulation and function of Class III PI3Ks: novel roles for Vps34. Biochemical journal 410 (1), 1-17

47 Arias, E. et al. (2015) Lysosomal mTORC2/PHLPP1/Akt regulate chaperone-mediated autophagy. Molecular cell 59 (2), 270-284

48 Mijaljica, D. et al. (2011) Microautophagy in mammalian cells: revisiting a 40-year-old

conundrum. Autophagy 7 (7), 673-682

49 Liang, X. et al. (1999) Induction of autophagy and inhibition of tumorigenesis by beclin 1. Nature 402(6762), 672-676

50 Singh, S.S. et al. (2018) Dual role of autophagy in hallmarks of cancer. Oncogene 37 (9), 1142-1158

51 Twig, G. and Shirihai, O.S. (2011) The interplay between mitochondrial dynamics and mitophagy. Antioxidants & redox signaling 14 (10), 1939-1951

52 Chen, H. et al. (2003) Mitofusins Mfn1 and Mfn2 coordinately regulate mitochondrial fusion and are essential for embryonic development. The Journal of cell biology 160 (2), 189-200

53 Trotta, A.P. and Chipuk, J.E. (2017) Mitochondrial dynamics as regulators of cancer biology. Cellular and molecular life sciences 74 (11), 1999-2017

54 Davies, V.J. et al. (2007) Opa1 deficiency in a mouse model of autosomal dominant optic atrophy impairs mitochondrial morphology, optic nerve structure and visual function. Human molecular genetics 16 (11), 1307-1318

55 Van der Bliek, A.M. et al. (2013) Mechanisms of mitochondrial fission and fusion. Cold spring harbor perspectives in biology 5 (6), a011072

56 Sekine, S. and Youle, R.J. (2018) PINK1 import regulation; a fine system to convey mitochondrial stress to the cytosol. BMC biology 16 (1), 2

57 Chan, N.C. et al. (2011) Broad activation of the ubiquitin–proteasome system by Parkin is critical for mitophagy. Human molecular genetics 20 (9), 1726-1737

58 Sarraf, S.A. et al. (2013) Landscape of the PARKIN-dependent ubiquitylome in response to mitochondrial depolarization. Nature 496 (7445), 372-376

59 Geisler, S. et al. (2010) PINK1/Parkin-mediated mitophagy is dependent on VDAC1 and p62/SQSTM1. Nature cell biology 12 (2), 119-131

60 Burman, J.L. et al. (2017) Mitochondrial fission facilitates the selective mitophagy of protein

aggregates. Journal of cell biology 216 (10), 3231-3247

61 McLelland, G.-L. et al. (2018) Mfn2 ubiquitination by PINK1/parkin gates the p97-dependent release of ER from mitochondria to drive mitophagy. Elife 7, e32866

62 Palikaras, K. et al. (2018) Mechanisms of mitophagy in cellular homeostasis, physiology and pathology. Nature cell biology 20 (9), 1013-1022

63 Ding, W.-X. et al. (2010) Nix is critical to two distinct phases of mitophagy, reactive oxygen species-mediated autophagy induction and Parkin-ubiquitin-p62-mediated mitochondrial priming. Journal of biological chemistry 285 (36), 27879-27890

64 Lazarou, M. et al. (2015) The ubiquitin kinase PINK1 recruits autophagy receptors to induce mitophagy. Nature 524 (7565), 309-314

65 He, L. et al. (2017) Prohibitin 2/PHB2 in Parkin-mediated mitophagy: a potential therapeutic target for mitochondrial diseases. Acta biochimica et biophysica sinica 49 (8), 750-751

66 Hernando-Rodríguez, B. and Artal-Sanz, M. (2018) Mitochondrial quality control mechanisms and the PHB (prohibitin) complex. Cells 7 (12), 238

67 Zhan, L. et al. (2016) Drp1-mediated mitochondrial fission promotes cell proliferation through crosstalk of p53 and NF-κB pathways in hepatocellular carcinoma. Oncotarget 7 (40), 65001

68 Wieder, S.Y. et al. (2015) Activation of the mitochondrial fragmentation protein DRP1 correlates with BRAFV600E melanoma. The Journal of investigative dermatology 135 (10), 2544

69 Zhao, J. et al. (2013) Mitochondrial dynamics regulates migration and invasion of breast cancer cells. Oncogene 32 (40), 4814-4824

70 Wan, Y.-Y. et al. (2014) Involvement of Drp1 in hypoxia-induced migration of human glioblastoma U251 cells. Oncology reports 32 (2), 619-626

71 Lee, Y.G. et al. (2020) Androgen-induced expression of DRP1 regulates mitochondrial metabolic reprogramming in prostate cancer. Cancer letters 471, 72-87

72 Qian, W. et al. (2014) Novel combination of mitochondrial division inhibitor 1 (mdivi-1) and

platinum agents produces synergistic pro-apoptotic effect in drug resistant tumor cells. Oncotarget 5 (12), 4180

73 Senft, D. and Ze'ev, A.R. (2015) UPR, autophagy, and mitochondria crosstalk underlies the ER stress response. Trends in biochemical sciences 40 (3), 141-148

74 Qi, Z. and Chen, L. (2019) Endoplasmic Reticulum Stress and Autophagy. In Autophagy: Biology and Diseases, pp. 167-177, Springer

75 Kouroku, Y. et al. (2007) ER stress (PERK/eIF2 α phosphorylation) mediates the polyglutamine-induced LC3 conversion, an essential step for autophagy formation. Cell death & differentiation 14 (2), 230-239

76 Graef, M. and Nunnari, J. (2011) Mitochondria regulate autophagy by conserved signalling pathways. The EMBO journal 30 (11), 2101-2114

77 Lebeau, J. et al. (2018) The PERK arm of the unfolded protein response regulates mitochondrial morphology during acute endoplasmic reticulum stress. Cell reports 22 (11), 2827-2836

78 Oakes, S.A. (2020) Endoplasmic Reticulum Stress Signaling in Cancer Cells. The American journal of pathology

79 Xue, Z. et al. (2011) A conserved structural determinant located at the interdomain region of mammalian inositol-requiring enzyme 1α. Journal of biological chemistry 286 (35), 30859-30866

80 Auf, G. et al. (2010) Inositol-requiring enzyme 1α is a key regulator of angiogenesis and invasion in malignant glioma. Proceedings of the national academy of sciences 107 (35), 15553-15558

81 Chen, X. et al. (2014) XBP1 promotes triple-negative breast cancer by controlling the HIF1α pathway. Nature 508 (7494), 103-107

82 Avril, T. et al. (2017) Endoplasmic reticulum stress signaling and chemotherapy resistance in solid cancers. Oncogenesis 6 (8), e373-e373

83 Feng, Y.-x. et al. (2014) Epithelial-to-mesenchymal transition activates PERK–eIF2α and sensitizes cells to endoplasmic reticulum stress. Cancer discovery 4 (6), 702-715

84 Atkins, C. et al. (2013) Characterization of a novel PERK kinase inhibitor with antitumor and antiangiogenic activity. Cancer research 73 (6), 1993-2002

85 Cullinan, S.B. et al. (2003) Nrf2 is a direct PERK substrate and effector of PERK-dependent cell survival. Molecular and cellular biology 23 (20), 7198-7209

86 Salaroglio, I.C. et al. (2017) PERK induces resistance to cell death elicited by endoplasmic reticulum stress and chemotherapy. Molecular cancer 16 (1), 91

87 Pytel, D. et al. (2016) PERK is a haploinsufficient tumor suppressor: gene dose determines tumor-suppressive versus tumor promoting properties of PERK in melanoma. PLoS genetics 12 (12), e1006518

88 Hanaoka, M. et al. (2018) Expression of ATF6 as a marker of pre-cancerous atypical change in ulcerative colitis-associated colorectal cancer: a potential role in the management of dysplasia. Journal of gastroenterology 53 (5), 631-641

89 Buttacavoli, M. et al. (2018) Anticancer activity of biogenerated silver nanoparticles: an integrated proteomic investigation. Oncotarget 9 (11), 9685

90 Yuan, Y.-G. and Gurunathan, S. (2017) Combination of graphene oxide–silver nanoparticle nanocomposites and cisplatin enhances apoptosis and autophagy in human cervical cancer cells. International journal of nanomedicine 12, 6537

91 Zhang, X.-F. and Gurunathan, S. (2016) Combination of salinomycin and silver nanoparticles enhances apoptosis and autophagy in human ovarian cancer cells: an effective anticancer therapy. International journal of nanomedicine 11, 3655

92 Miyayama, T. et al. (2018) Silver nanoparticles induce lysosomal-autophagic defects and decreased expression of transcription factor EB in A549 human lung adenocarcinoma cells. Toxicology in vitro 46, 148-154

93 Ke, S. et al. (2017) Gold nanoparticles enhance TRAIL sensitivity through Drp1-mediated apoptotic and autophagic mitochondrial fission in NSCLC cells. International journal of nanomedicine 12, 2531

94 Zhang, M. et al. (2017) Near-infrared photothermal therapy using EGFR-targeted gold nanoparticles increases autophagic cell death in breast cancer. Journal of photochemistry and photobiology B: Biology 170, 58-64

95 Wu, Y.-N. et al. (2011) The selective growth inhibition of oral cancer by iron core-gold shell nanoparticles through mitochondria-mediated autophagy. Biomaterials 32 (20), 4565-4573

96 Wu, Y.-N. et al. (2013) The anticancer properties of iron core–gold shell nanoparticles in colorectal cancer cells. International journal of nanomedicine 8, 3321

97 Fageria, L. et al. (2019) Functional Autophagic Flux Regulates AgNP Uptake And The Internalized Nanoparticles Determine Tumor Cell Fate By Temporally Regulating Flux. International journal of nanomedicine 14, 9063

98 De Araújo Jr, R.F. et al. (2018) Apoptosis in human liver carcinoma caused by gold nanoparticles in combination with carvedilol is mediated via modulation of MAPK/Akt/mTOR pathway and EGFR/FAAD proteins. International journal of oncology 52 (1), 189-200

99 Popp, L. et al. (2018) Autophagic response to cellular exposure to titanium dioxide nanoparticles. Acta biomaterialia 79, 354-363

100 Moosavi, M.A. et al. (2016) Photodynamic N-TiO 2 nanoparticle treatment induces controlled ROS-mediated autophagy and terminal differentiation of leukemia cells. Scientific reports 6 (1), 1-16

101 Wang, J. et al. (2018) Zinc oxide nanoparticles induce toxicity in CAL 27 oral cancer cell lines by activating PINK1/Parkin-mediated mitophagy. International journal of nanomedicine 13, 3441

102 Li, X. et al. (2016) Quaternized chitosan/alginate-Fe3O4 magnetic nanoparticles enhance the

chemosensitization of multidrug-resistant gastric carcinoma by regulating cell autophagy activity in mice. Journal of biomedical nanotechnology 12 (5), 948-961

103 Zhang, X. et al. (2016) Iron oxide nanoparticles induce autophagosome accumulation through multiple mechanisms: lysosome impairment, mitochondrial damage, and ER stress. Molecular pharmaceutics 13 (7), 2578-2587

104 Krętowski, R. et al. (2017) The effects of silica nanoparticles on apoptosis and autophagy of glioblastoma cell lines. Nanomaterials 7 (8), 230

105 Laha, D. et al. (2014) Interplay between autophagy and apoptosis mediated by copper oxide nanoparticles in human breast cancer cells MCF7. Biochimica et biophysica acta (BBA)-General subjects 1840 (1), 1-9

106 Huo, L. et al. (2015) Silver nanoparticles activate endoplasmic reticulum stress signaling pathway in cell and mouse models: The role in toxicity evaluation. Biomaterials 61, 307-315

107 Noël, C. et al. (2016) Gold nanoparticles induce apoptosis, endoplasmic reticulum stress events and cleavage of cytoskeletal proteins in human neutrophils. Toxicology in vitro 31, 12-22

108 Peynshaert, K. et al. (2014) Exploiting intrinsic nanoparticle toxicity: the pros and cons of nanoparticle-induced autophagy in biomedical research. Chemical reviews 114 (15), 7581-7609

109 Cao, Y. et al. (2017) A review of endoplasmic reticulum (ER) stress and nanoparticle (NP) exposure. Life sciences 186, 33-42

110 Hou, C.-C. et al. (2013) Pronounced induction of endoplasmic reticulum stress and tumor suppression by surfactant-free poly (lactic-co-glycolic acid) nanoparticles via modulation of the PI3K signaling pathway. International journal of nanomedicine 8, 2689

111 Oakes, S.A. and Papa, F.R. (2015) The role of endoplasmic reticulum stress in human pathology. Annual review of pathology: mechanisms of disease 10, 173-194

112 Ozcan, L. and Tabas, I. (2012) Role of endoplasmic reticulum stress in metabolic disease and other disorders. Annual review of medicine 63, 317-328

113 Shvedova, A.A. et al. (2012) Mechanisms of carbon nanotube-induced toxicity: focus on oxidative stress. Toxicology and applied pharmacology 261 (2), 121-133

114 Sano, R. and Reed, J.C. (2013) ER stress-induced cell death mechanisms. Biochimica et biophysica acta (BBA)-Molecular cell research 1833 (12), 3460-3470

115 Rashid, H.-O. et al. (2015) ER stress: Autophagy induction, inhibition and selection. Autophagy 11 (11), 1956-1977

116 Mohamud, R. et al. (2014) The effects of engineered nanoparticles on pulmonary immune homeostasis. Drug metabolism reviews 46 (2), 176-190

117 Vance, M.E. et al. (2015) Nanotechnology in the real world: Redeveloping the nanomaterial consumer products inventory. Beilstein journal of nanotechnology 6 (1), 1769-1780

118 Luo, Y.-H. et al. (2015) Metal-based nanoparticles and the immune system: activation, inflammation, and potential applications. BioMed research international 2015

119 Park, E.-J. et al. (2014) Magnetic iron oxide nanoparticles induce autophagy preceding apoptosis through mitochondrial damage and ER stress in RAW264. 7 cells. Toxicology in vitro 28 (8), 1402-1412

120 Christen, V. and Fent, K. (2012) Silica nanoparticles and silver-doped silica nanoparticles induce endoplasmatic reticulum stress response and alter cytochrome P4501A activity. Chemosphere 87 (4), 423-434

121 Karthikeyan, B. et al. (2016) Role of ZnS nanoparticles on endoplasmic reticulum stress-mediated apoptosis in retinal pigment epithelial cells. Biological trace element research 170 (2), 390-400

122 Niu, J. et al. (2007) Cardioprotective effects of cerium oxide nanoparticles in a transgenic murine model of cardiomyopathy. Cardiovascular research 73 (3), 549-559

Chapter-2

Gaps in research and objectives

Chapter-2

Gaps in research and objectives

2.1. Gaps in research:

Nanoparticles (NPs) have received global attention due to their extensive applications in the field of biomedical research. However, very few NPs, despite their obvious health benefits, have reached the clinical settings. This gap is partially due to lack of extensive studies understanding the intracellular molecular effects of the NPs, and its variation with the change of physicochemical parameters of the studied NPs. Existing studies provide clear indications towards varied intracellular effects with alterations in the physical property of the NPs; however, there exists an evident dearth of relevant literature that exhaustively defines the same. We hypothesized that a minute variation in the physical property of an NP, for example, its size, or alteration of its chemical property may not only affect the uptake, or the mechanism involved in its internalization but can also have an impact on the overall function of the NPs. These physical variations can thus have a profound effect on the subsequent therapeutic potential of the NPs and can hence be tinkered for additional positive benefits. However, to date, very little research has been channelized in this direction. Furthermore, a holistic study delineating the interconnected string of molecular events, post-exposure of NPs, starting from its mechanism of entry to subsequent intracellular effects, and finally, its impact on the overall cellular health is poorly elucidated. In this regard, earlier studies establish that the cellular homeostatic machinery- autophagy is often de-regulated upon entry of NPs into the tumor cells. However, studies connecting the internalization of NPs, it's trafficking, and the temporal effect on autophagy followed up by its associated impact on subsequent cell fate are poorly explained. Additionally, as per existing literature, autophagy is not only involved in cellular protein homeostasis but can also regulate intracellular organelle dynamicity. The crosstalk between autophagy and organelle dynamicity,

especially mitochondria and endoplasmic reticulum (ER) after exposure to NPs, is poorly defined. Hence, in this study, we make a conscious effort to initially investigate the intracellular impact of alteration of physicochemical properties of metal NPs on tumor cells. We primarily selected silver NPs (AgNPs) for this study, as AgNPs have already shown promise as a therapeutic agent. Briefly, the aspect of internalization and cytotoxic efficacy is investigated with alteration of the size of NPs, herein primarily AgNPs. Variation in AgNPs is executed by combining silver either in core or shell with gold NPs (AuNPs), resulting in the formation of dual or bi-metallic NPs. Thereafter, specifically with AgNPs, we dissect the inter-connected series of molecular events extending from the temporal effect of AgNPs on autophagy, associated intracellular signaling, connected organelle health, and finally cell cytotoxicity. This study not only provides critical information on the size-dependent mechanism of uptake of NPs but also sheds light on how the internalized NPs temporally modulate key intracellular events like autophagy and organelle dynamics. Our research outcome can have potential benefits on the development of NP-based therapy, especially AgNPs and their prospective use in cancer treatment.

2.2 Objectives:

Following objectives were framed to address the above issues:

1. Chemical synthesis and characterization of metal NPs.

2. Analyzing the effect of alteration of size and chemical properties of the NPs on internalization and mechanism of uptake in tumor cells.

3. Mechanistic analysis into temporal modulation of intracellular signaling and organelle dynamics upon internalization of the NPs in tumor cells.

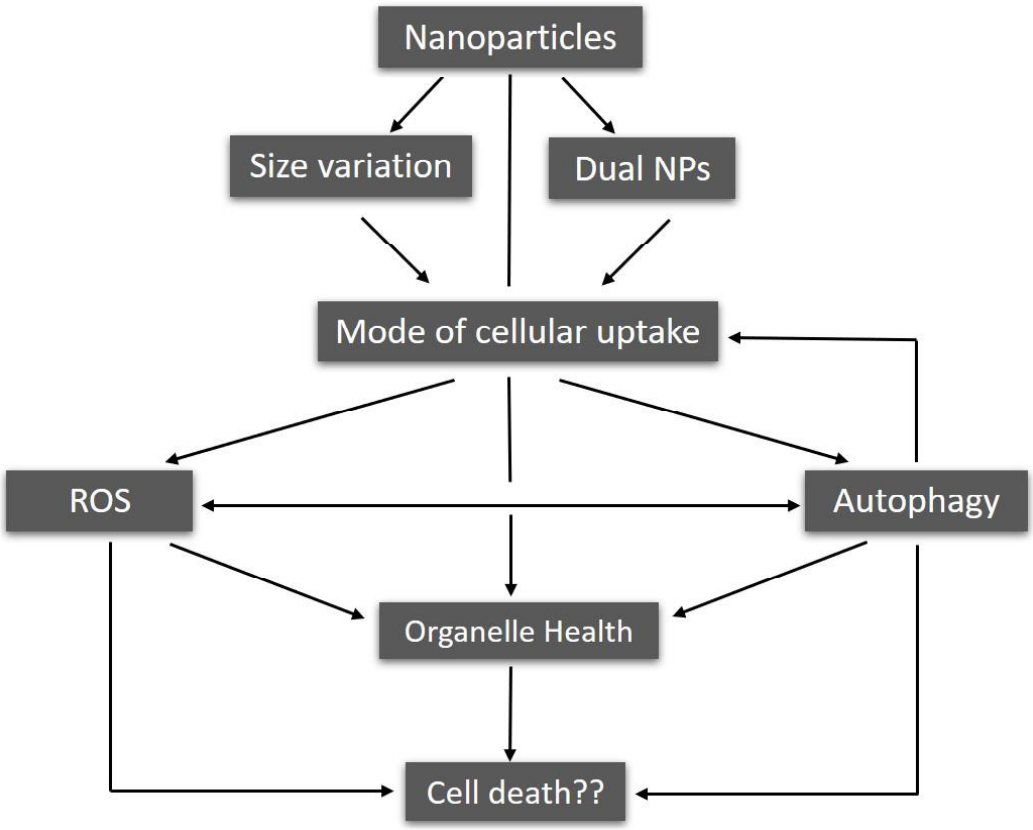

Figure 2.1. Schematic representation of the aspects to be explored after exposure to metal NPs.

Chapter-3

Materials & methods

Chapter-3

Materials & methods

3.1 Materials

Chemicals: Rapamycin (Rapa, #sc-3504A), Nocodazole (Noc, #sc-3518), Chlorpromazine (CPZ, #sc-357313), Tunicamycin (Tun, #sc- 3506A), Dynasore (Dyn, #sc-202592), JC-1 (#sc-364116A) and JNK inhibitor, SP600125 (#sc-200635) were purchased from Santa Cruz Biotechnology. Silver Nitrate ($AgNO_3$, #209139), Gold Chloride ($HAuCl_4$, #484385), 2',7'-dichlorofluorescein diacetate (DCFDA, # D6883), Chloroquine (CQ, #C6628), RIPA Buffer (#R0278), Acridine Orange (AO, #A9231) and Propidium iodide (PI, #P4864) were purchased from Sigma; N-Acetyl-L-cysteine (NAC, #47866), Sodium Hydroxide Pellets (NaOH, #13913) and 3-(4, 5-dimethylthiazol-2-yl)-2,5-di-phenyltetrazolium bromide (MTT, #33611) were obtained from SRL; beta-cyclodextrin (β-CD, #C0900), Genistein (Gen, #G0272) and 3-(2-Benzothiazolyl)-7-(diethylamino)coumarin (C6, #B2088) were purchased from TCI Chemicals. FITC conjugated AnnexinV (#A13199), AnnexinV binding buffer (#V13246), LysoTracker Red DND-99 (LT, # L7528), Lysotracker Green DND-26 (LT, # L7526), Mitotracker Red CMXRos (MT, #M7512), Enhanced Chemiluminescence (ECL, #32106), Antifade mountant (4'-6-diamidino-2-phenylindole, #P36962) and PVDF membrane (#88518) were procured from Thermo Fisher Scientific. Lipofectamine 3000 was from Invitrogen (#L3000-001). mRFP-LC3 was a gift from Dr. Sovan Sarkar, University of Birmingham, UK, GFP-Ub was a gift from Nico Dantuma (Addgene plasmid #11928), mcherry-Parkin was a gift from Richard Youle (Addgene plasmid #23956). The siRNA for ATG5 was a gift from Prof. Santosh Chauhan, ILS Bhubaneswar (Dharmacon#M-004374-04).

Instruments: The major instruments used for the experiments performed are enlisted below

Table 3.1 List of Instruments

Name of the Instrument	Company
Multiskan GO microplate spectrophotometer	Thermo Fisher Scientific
Zetasizer Nano ZS	Malvern Panalytical
Transmission Electron Microscopy Tecnai G^2 20 S-Twin (TEM)	FEI Tecnai, (MNIT JAIPUR, Rajasthan)
ICP-OES	Perkin Elmer, Avio ^{TM} 200
Laminar Air Flow	MAC
Inverted Microscope	Olympus
Fluorescent Microscope/Apotome	ZEISS
Flow Cytometer	Beckman Coulter
Vertical Gel Electrophoresis Unit & Semi-Dry Transfer apparatus	Bio-Rad Laboratories

3.2 Methods

Synthesis of Metal NPs

The nucleation method was used for synthesizing β-CD capped NPs [1]. The general scheme for the synthesis of metal nanoparticles using polymer support via a chemical route is shown below (Fig 3.1).

Scheme:

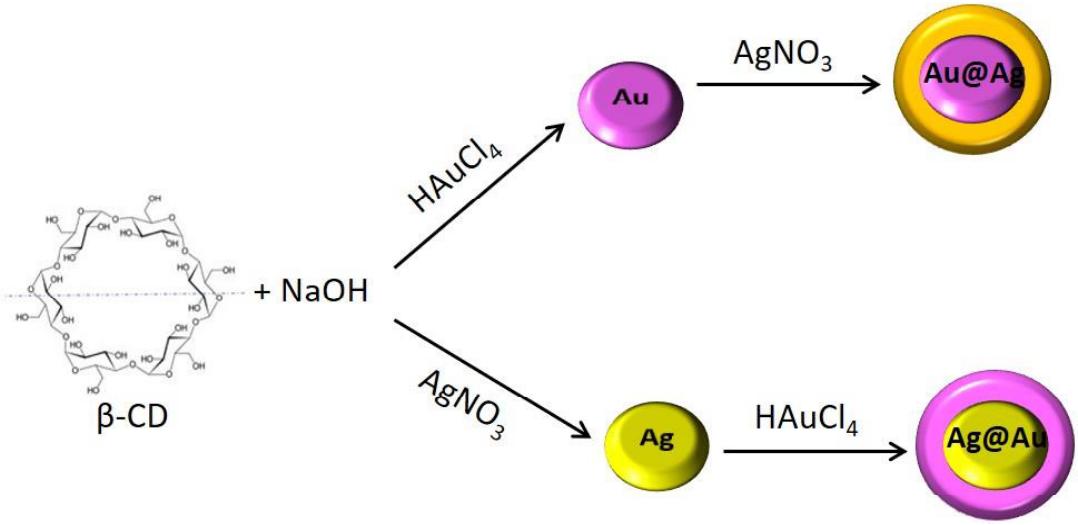

Figure 3.1. ***Representation of scheme for NP synthesis.***

In this process, β-CD was used as a reducing agent and stabilizer. β-CD (0.16 g) was dissolved in autoclaved Milli-Q water (10 mL). After dissolving, 300 µL of 1.0 M NaOH solution was added to increase the pH of the solution to ~10. Different volumes of the corresponding metal salt solution, 0.1 M $AgNO_3$, and 0.01M $HAuCl_4$ was added and mixed properly to get different concentrations of NPs. Then, the reaction mixtures were shaken well and heated on a water bath at 85˚C for 8 minutes while it turned into yellow and pink, indicating the formation of Ag and AuNPs, respectively.

Bi-metallic or dual core@shell were synthesized using a sequential reduction approach [1], which is shown in (Fig 3.1.). For dual NP synthesis, 0.1 M $AgNO_3$ salt was added in the desired volume over the already formed AuNP solution to give rise to Ag shell over Au core (Au@Ag). Similarly, during the synthesis of Au shell over Ag core (Ag@Au), $HAuCl_4$ salt was added in the AgNP solution. The

concentration of synthesized metal NPs was assumed to be same as of the initial concentration of the reactant (metal salt) used. The procedure for the synthesis of metal NPs is shown in (Fig 3.2.):

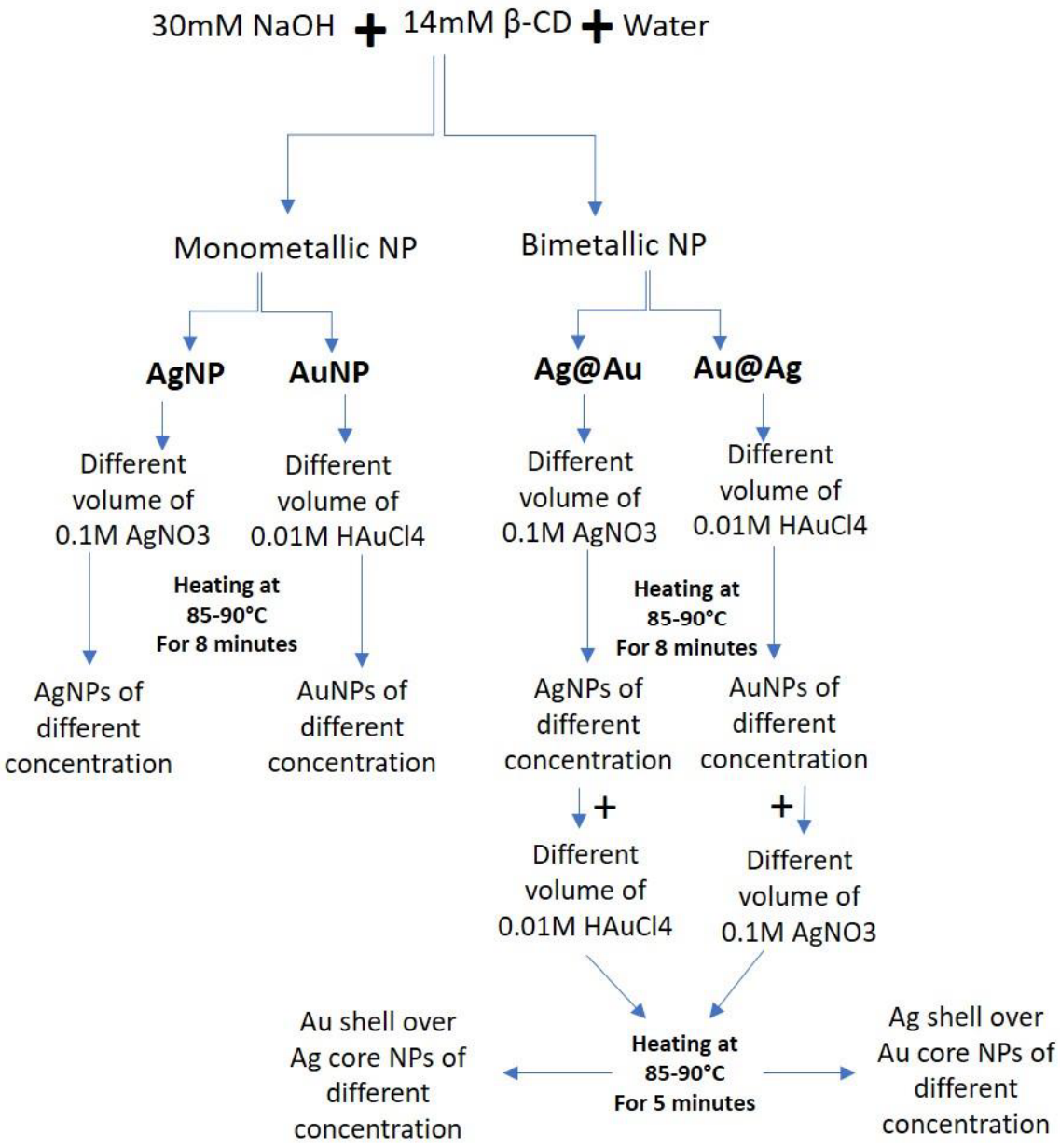

Figure 3.2. Schematic representation of the procedure for the synthesis of metal NPs.

Characterization of NPs

UV-Vis property of synthesized AgNPs was characterized using a Multiskan GO microplate spectrophotometer operated within the range of 300-700 nm at a resolution of 2 nm. Zeta-potential of

AgNPs was measured using Malvern Zetasizer model Nano ZS (ZEN 3600,102 Malvern Instruments, UK). For size and shape determination, the synthesized solution was drop cast onto carbon-coated copper grids, and the grids were kept in a vacuum desiccator overnight for drying. Transmission electron microscopy (TEM) images were taken on a Tecnai G^2 20 S-Twin TEM instrument (FEI Company) at an acceleration voltage of 200 kV, MNIT, Jaipur. For size distribution calculation, ~100 particles were considered.

ICP-OES analysis

Inductively Coupled Plasma - Optical Emission Spectrometry (ICP-OES) was used for the detection of Ag ion concentration in the synthesized metal NPs. The NP solution was diluted (1:10) with MilliQ water and filtered using 0.22 µ syringe filters. The samples were stored at 4°C until analysis. The standard Curve of Ag was plotted by running Ag standards. Syngistix software was used for ICP analysis (Version 3.0).

Cell culture

Human breast cancer cells, MCF-7, MDA-MB-468 (procured from NCCS, Pune, India) and the immortalized keratinocytes, HaCaT cells (a kind gift from Dr. Archana Singh, IGIB, Delhi, India) were cultured at 37 ℃, 5% CO_2, in Dulbecco's modified eagle medium (Invitrogen) supplemented with 10% fetal bovine serum (Invitrogen), 1% Penicillin (100 UmL^{-1}) and streptomycin (100 μgmL^{-1}; Invitrogen) solution. The cells were grown to 70-80% confluency, rinsed in phosphate buffer saline, and placed into the fresh medium before treatments.

Cell viability analysis

The assessment of cell viability was performed by MTT assay [2]. Briefly, 8000 cells per well were seeded in 96-well plate and treated with various concentrations of the desired inhibitor (24 h before

NP treatment) or NPs for desired time points. After that, 20 µl of 5 $mgmL^{-1}$ stock solution of MTT was added and incubated for 3-4 h; post which formazan crystals formed were solubilized in DMSO and absorbance were obtained at 570 nm with a differential filter at 630 nm using a Multiskan GO microplate spectrophotometer. Percentage viable cells were calculated using the formula: viability (%) = (mean absorbance value of treated cells) / (mean absorbance value of un-treated) *100.

Detection of Ag concentration in a cell

Inductively Coupled Plasma - Optical Emission Spectrometry (ICP-OES) was used for the detection of Ag released from the NP inside a cell. Upon treatment of different NPs for desired time points, the cells were collected by trypsinization. The cell pellet obtained was kept overnight for drying, followed by the addition of 65% nitric acid (HNO_3) in a fume hood and then kept in a dry bath at 100°C for 24 h to evaporate acid. After acid digestion, the solution was diluted with MilliQ water (10 mL) and filtered using 0.22 µ syringe filters. The samples were stored at 4°C until analysis.The standard Curve of Ag was plotted by running Ag standards. Syngistix software was used for ICP analysis (Version 3.0).

Microscopic imaging and Analysis of NP internalization

For bright field imaging, cells were cultured in 6 cm dishes and treated with different doses of NPs. Images were captured using Olympus (CKX41). For the internalization study, the NPs were tagged with Coumarin-6 (C6), a green fluorescent dye (2.5 µg/mL) for 1 mL of NPs, and kept overnight in the dark. Subsequently, C6 tagged NPs with or without endocytosis inhibitors (added 30 min before NP treatment) were added to cells in 6 well plates and incubated for 1 h. The samples were then acquired through a flow cytometer (CytoFlex, Beckmann Coulter), and analysis was performed using CytExpert. For fluorescence imaging, cells were seeded on coverslips. After incubation with C6 tagged NPs, the coverslips were washed with PBS and fixed with 4% paraformaldehyde at -room

temperature for 10 min. The coverslips were mounted with antifade containing DAPI. NP internalization was confirmed by visualization through the ZEISS Axio Scope A1 microscope.

Immunoblotting

MCF-7 cells after treatment for desired treatment time were lysed using RIPA buffer (Sigma-Aldrich). Protein concentration was measured using Bradford reagent (Thermo Scientific). 8, 10, and 12% denaturing polyacrylamide gels were used for running the collected protein lysates and, thereafter, transferred to the PVDF membrane for blocking with 5% skimmed milk. The blots were probed with specific primary antibodies (dilution 1:1000). Primary antibodies used were listed in the **Table 3.2**. The blots were stripped and re-probed following conventionally used methods [4]. β-actin or GAPDH (dilution 1:2000) was used as a loading control. The blots were cut to probe with multiple antibodies against proteins of different molecular weights. The secondary antibodies used were horseradish peroxide-conjugated goat anti-rabbit and goat anti-mouse IgG. The protein intensity was measured using Enhanced Chemiluminescence by Chemi-Doc XRS (Bio-Rad) detection system. The expression was densitometrically quantified using ImageJ software.

Table 3.2 List of primary antibodies used in the study.

Antibody	**Catalogue No.**
ATG3	CST, #3415
ATG5	CST, #8540
Beclin-1	CST, #3495
LC3	CST, #3868
P62	BioBharti, #BB-AB0130
LAMP1	CST, #9091
TFEB	CST, #37785

p-JNK	CST, #4370
Total JNK	CST, #4695
Total Ubiquitin	BioBharti, #BB-AB0030
EEA1	CST, #3288
Rab7	CST, #9367
Clathrin	CST, #4796
PARP	CST, #9542
Bax	BioBharti, #BB-AB0250
OPA1	CST, #80471
Mfn2	CST, #11925
P-MFF	CST, #49281
MFF	CST, #84580
TOM20	CST, #42406
Bip	CST, #3177
Calnexin	CST, #2679
IRE1α	CST, #3294
β-actin	Santa Cruz, #Sc-69879
GAPDH	Santa Cruz, #Sc-365062
Anti-rabbit IgG, HRP linked	CST, #7074
Anti-mouse IgG, HRP linked	CST, #7076
Primary antibodies except GAPDH and β-actin were used in 1:1000 dilution, and GAPDH and Actin were used in 1:2000 dilution. Secondary antibodies were used in 1:10,000 dilution.	

Immunofluorescence

The MCF-7 cells were seeded overnight on coverslips. Thereafter, the cells were treated IC_{50} dose of AgNPs in the presence or absence of Dynamin inhibitor for 2 h. Cells were then fixed with 4% paraformaldehyde at room temperature for 10 min. Blocking was done for 2 h with 5% BSA followed by overnight incubation with anti-Clathrin primary antibodies at 4 °C. Similarly, the cells were incubated with anti-TOM20 primary antibody post exposure of NPs for different time points at 4 °C. The secondary antibody used was tagged with Texas-Red. The coverslips were mounted with antifade containing DAPI and visualized through the ZEISS Axio Scope A1 microscope.

Transfection

For visualization of accumulated ubiquitinated proteins, LC3 puncta, and Parkin accumulation, MCF-7 cells were seeded on coverslips. They were transfected with 2 µg of GFP-Ub purified plasmids, RFP-LC3, and mCherry-Parkin plasmid. Lipofectamine 3000 was used for transfection. Approximately, 6 h after transfection, the cells were treated with AgNPs in the medium. Post-treatment, the coverslips were washed and mounted with anti-fade containing DAPI. Green and red fluorescence were analyzed under a fluorescence microscope.

siRNA mediated silencing of ATG5

MCF-7 cells were transfected with siATG5 (a kind gift from Santosh Chauhan, ILS, Bhubaneswar, India) using lipofectamine 3000. Cells were pre-incubated with 20 nM siATG5 for 6 h before the addition of AgNP in the medium [5].

Measurement of LysoTracker (LT) fluorescence

The LysoTracker Red DND-99 and LysoTracker Green DND-26 were used for labeling lysosomes [6]. Cells were cultured till 70-80% confluency. After that, the medium was replaced with pre-

warmed (37 °C), probe (50nM)-containing medium. Cells were then incubated for 20 min. The cells were then observed under a fluorescence microscope (Zeiss), and the intensity of LT fluorescence was measured using Zen 2.3 lite software.

Measurement of Mitotracker (MT) fluorescence

The Mito Tracker Red CMXRos was used for labeling mitochondria [7], MCF-7 cells were incubated with 100nM MT and incubated for around 30 min. The cells were washed with PBS and fixed with DAPI. Cells were observed under a microscope, and the intensity of red fluorescence was measured using Zen 2.3 lite software.

Acridine Orange (AO) staining

MCF-7 cells were trypsinized, collected and stained with AO (final concentration: 0.5 µg/mL) for 10 min. After centrifugation, cells were resuspended in PBS and analyzed through a flow cytometer. Analysis of acquired data was performed using CytExpert software. The percentage of cells showing red fluorescence of AO is represented through a bar diagram [6].

Measurement of intracellular ROS

DCFHDA passively enters the cell, where it reacts with ROS to form the highly fluorescent compound, dichlorofluorescein (DCF). Briefly, cells were seeded in 96 well plates and treated with NPs, ROS scavenger N-acetyl cysteine (NAC) was added 1 h before NP treatment wherever mentioned. Following exposure, cells were washed with PBS, and 10µM of DCFDA was added in each well and incubated for 30 min. The fluorescence of DCF was measured at 485 nm excitation and 530 nm emission using a microplate reader (Fluoroskan Ascent).

Detection of apoptosis by flow cytometry

MCF-7 cells were seeded in 6-well plates for the detection of apoptosis. After attaining 70% confluency, the cells were incubated with different concentrations of NPs for 24 h or 48 h. The cells were collected and washed with PBS and re-suspended in 1X binding buffer. For the detection of both early and late apoptotic cells, 4µL of AnnexinV and 10µl of PI was added to the cells and incubated for 30 min. Cells were acquired and analyzed using a flow cytometer. Percentage of apoptotic cells represent both Annexin+ and Annexin+PI+ cells, and percent of dead cells represent Annexin+, Annexin+PI+, and only PI+ cells in the bar diagram.

Estimation of Mitochondrial Membrane Potential (MMP)

Mitochondrial membrane potential was analyzed using JC-1, a lipophilic cationic fluorescent dye. A shift in red to green fluorescence indicates the depolarization of mitochondrial potential. JC-1 was added to cells in a concentration of 0.5 µgmL $^{-1}$ after treating cells with AgNPs in a 6-well plate and incubated for an additional 30 min at 37 $^{\circ}$C. After washing with PBS, the stained cells were collected and assayed using a flow cytometer [8].

Statistical analysis

The obtained data was analyzed using OriginPro 9.0 and GraphPad Prism (Version 5.01) Software. One-way ANOVA, two-way ANOVA or Student's t-test were used to determine the statistical significance of particular treatment in comparison to control. Bonferroni or Tukey post-tests were used to compare multiple comparisons. All data points represent the mean of independent measurements. If p-value > 0.05 difference is denoted as not significant (ns); if $p \leq 0.05$ or $p \leq 0.01$ the difference is considered significant and is denoted by symbols */#/$ or @, or **/##/$$ or @@ and ***/###/$$$ and @@@ these symbol represents values of p in range from $p \leq 0.0005$ to 0.05 or 0.0001 to 0.01.

3.3 References

1. Pande, S., et al., *Synthesis of normal and inverted gold− silver core− shell architectures in β-cyclodextrin and their applications in SERS.* The journal of physical chemistry C, 2007. **111**(29): p. 10806-10813.
2. Fageria, L., et al., *Biosynthesized protein-capped silver nanoparticles induce ros-dependent proapoptotic signals and prosurvival autophagy in cancer cells.* ACS omega, 2017. **2**(4): p. 1489-1504.
3. Mo, L., et al., *Preparation and characterization of teniposide PLGA nanoparticles and their uptake in human glioblastoma U87MG cells.* International journal of pharmaceutics, 2012. **436**(1-2): p. 815-824.
4. Saini, H., et al., *Autophagy regulated by gain of function mutant p53 enhances proteasomal inhibitor-mediated cell death through induction of ROS and ERK in lung cancer cells.* Journal of oncology, 2019. **2019**.
5. Dash, S., et al., *TGF-β2-induced EMT is dampened by inhibition of autophagy and TNF-α treatment.* Oncotarget, 2018. **9**(5): p. 6433.
6. Fageria, L., et al., *Functional Autophagic Flux Regulates AgNP Uptake And The Internalized Nanoparticles Determine Tumor Cell Fate By Temporally Regulating Flux.* International journal of nanomedicine, 2019. **14**: p. 9063.
7. Cottet-Rousselle, C., et al., *Cytometric assessment of mitochondria using fluorescent probes.* Cytometry part A, 2011. **79**(6): p. 405-425.
8. Liu, J., et al., *Anti-tumor effect of Pinus massoniana bark proanthocyanidins on ovarian cancer through induction of cell apoptosis and inhibition of cell migration.* PloS one, 2015. **10**(11).

Chapter- 4

Synthesis and characterization of metal NPs

Chapter-4

Synthesis and characterization of metal NPs

4.1. Overview

In recent years, nanoparticles (NPs) have emerged as a novel class of materials with the potential for a wide range of applications. In this context, metal NPs, because of their unique physical and chemical properties like plasmonic resonance, catalytic enhancement, their larger surface area to volume ratio, photoluminescence, or superparamagnetic properties, have recently been used in different areas like physics, chemistry, material science, and biomedicine [1]. Also, the intrinsic nature of these NPs, such as their ability to carry other compounds, their ease of cell penetration has made them useful, especially in the field of biomedicine. Especially, NPs have this unique ability to home specifically into tumor tissues by utilizing their leaky vasculature by enhanced permeability and retention (EPR) effect, and that makes them an attractive therapeutic arsenal. In spite of tremendous advances in the use of NPs in healthcare, the key challenge, however, has been how to get these advances into clinics [2]. In this regard, a major lacuna in existing knowledge has been the lack of understanding of the intracellular effects of the NPs with respect to variation in their physicochemical properties. A modification in physical or chemical parameters of the NPs like surface properties or shape can deeply impact its cellular internalization and its function as well [3]. Therefore, to effectively enable NPs with therapeutic potentials to make a significant leap forward, it is essential to have a deeper and comprehensive understanding of the fundamental cellular effects of these NPs with variations in their physicochemical properties. Among various nanomaterials, of late silver nanoparticles (AgNPs) have received considerable attention due to their unique properties like conductivity, chemical stability, relative lower toxicity, and outstanding therapeutic potential, such as anti-inflammatory, antimicrobial and anti-cancerous activities [4]. Today AgNPs have widespread

biological application and one of the highest levels of commercialization amongst nanomaterials. However, how the therapeutic potency of the mono-metallic NPs, like silver, can be improved is of considerable research interest.

Based on the chemical composition of these metallic NPs, they can be classified as simple or composite. Simple NPs are made of a single metal, whereas composite or core/shell particles are made of two or more metals. Because of the modification of optoelectronic and catalytic properties, bi-metallic NPs compared to mono-metallic ones are often explored as a multifaceted tool in disease management with functionality extending from photothermal therapy, targeted drug delivery, nano theranostics, cell labeling and even gene delivery in a more effective way [5, 6]. In this regard, high stability, inertness, and biocompatibility of gold (Au) and silver (Ag) NPs together make them a prospective candidate for use in various medicinal systems [7, 8]. We assume that the core/shell, bi-metallic silver/gold nanosystems can significantly improve therapeutic efficacy compared to their mono-metallic counterparts by maintaining the general biocompatibility of the nanoparticles, especially AuNPs, while, at the same time, decreasing the relatively high toxicity of AgNPs toward healthy human cells.

Therefore, in this chapter, we describe the synthesis of both mono-metallic and bi-metallic NPs composed of silver and gold. Synthesis methods of NPs are broadly divided into 3 categories, namely, physical, chemical, and biological methods. Physical synthesis may include pulse laser ablation, pulse wired discharge, and mechanical synthesis like high energy ball milling [9]. Chemical synthesis of NPs can include chemical reduction method, which is one of the most used methods, chemical oxidation method, sol-gel method, solvothermal decomposition, electrochemical, and sonochemical process [10]. Most of these chemical and physical methods used are energy and capital intensive, employ toxic chemicals, and often yield particles in non-polar organic solutions, thus hindering their biomedical applications. On the other hand, biological or green synthesis of NPs using bacteria, fungi, algae, yeast, or plant extracts is considered eco-friendlier and more sustainable

[11]. However, this method has disadvantages, like the formation of non-homogenous NPs, occasional pathogenicity, etc. To overcome these drawbacks, an alternative bio-compatible and eco-friendly procedure would be an advantage. In this regard, cyclodextrins (CDs), a class of oligosaccharides made of glucopyranose subunits having a unique cone shape structure, with a hydrophobic center and hydrophilic outer surface is coming out to be a widely used in pharmaceuticals [12]. CDs are known as stabilizing agents as they strongly get located on the surface of NPs [13]. Among all other CDs, β-CD is mostly used because of its internal cavity diameter, which is about 6 to 6.5 Å, suitable for host and guest interaction. β-CD has high biosorbent ability, drug solubility, increased encapsulation efficiency [14]. In this chapter, we describe the synthesis of mono-metallic Ag, Au, and bi-metallic NPs composing of Ag and Au of different molar ratios using β-CD and characterized.

4.2. Results

4.2.1 Synthesis of NPs

The metal NPs were synthesized following the procedure discussed in chapter 3. In brief, 14 mM β-CD and 30 mM NaOH were dissolved in water, followed by the addition of different volumes of 0.1M stock solution of $AgNO_3$ and 0.01 M stock solution of $HAuCl_4$ and boiling at a higher temperature (85 °C) for 8-10 mins. Similarly, bi-metallic NPs were prepared by sequential reduction of metal salt over the NP solution of other metal to form core@shell nanomaterials.

Following NPs (**Table 4.2.1**) were prepared using the above procedure. NPs suspended in a clear aqueous solution of varying colors were synthesized, as observed in the below **Fig 4.2.1.**

Table 4.2.1 List of the synthesized mono and bi-metallic NPs.

0.16 g β-CD and 300 µl of 1 M NaOH was added in each test tube the final volume (10mL) was made by water		
NPs (10 mL)	**0.1 M $AgNO_3$ (µl)**	**0.01 M $HAuCl_4$ (µl)**
100 µM AgNP	**10**	**-**
500 µM AgNP	**50**	**-**
100 µM AuNP	**-**	**100**
100:100 Au@Ag	**10**	**100**
100:100 Ag@Au	**10**	**100**

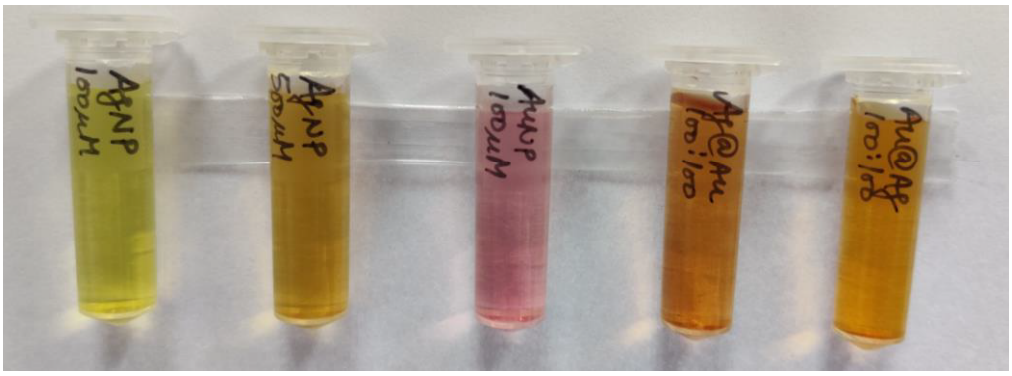

Figure 4.2.1. Image representing different NP solutions.

4.2.2 Characterization of NPs

The synthesized NPs were characterized by performing UV-Vis spectroscopy, Zeta potential analysis, transmission electron microscopy (TEM), and inductively coupled plasma optical emission spectrum (ICP-OES) techniques.

UV-Vis Spectroscopy:

Every metallic compound can absorb light and emit a particular wavelength in the visible region, which explains the color of the above shown NPs. Metal NPs has a characteristic surface plasmon resonance (SPR) property. SPR is a resonance effect induced by the interaction of incident photons with the conducting electrons of metal surface. AuNPs shows a plasmon band in the range of 500-600 nm whereas AgNPs shows at 400-500 nm [11, 15]. The resonance, determined from absorption spectroscopy can help in detection of properties of NPs. Hence, UV-vis spectroscopy was performed to analyze the maximum absorbance of the synthesized NPs. The absorption spectrum obtained was ranging from 300-700 nm, and the absorbance was taken at a resolution of 2 nm. Absorption maxima for AgNPs were obtained at 400-420 nm while for AuNPs was at around 520-540 nm (Fig 4.2.2.1). Furthermore, in case of bi-metallic NPs the core is not completely covered because of presence of Au and Ag in 1:1 ratio hence; a broader absorption spectrum is observed (Fig 4.2.2.1). The UV-Vis absorption peaks of bi-metallic NPs depends on the metal present on the outer shell.

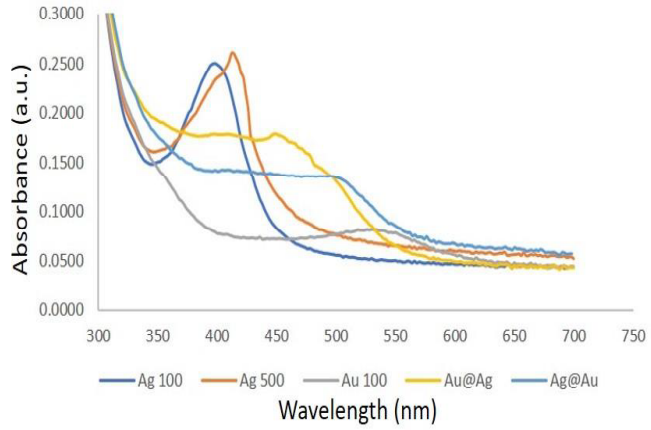

Nanoparticles	λmax (nm)
100 µM AgNP	406
500 µM AgNP	412
100 µM AuNP	536
Au@Ag (100:100)	450
Ag@Au (100:100)	496

Figure 4.2.2.1. UV-Vis absorption spectra of synthesized NPs.

Zeta potential measurement:

Zeta potential analysis is the technique for determination of the surface charge of NPs. The surface of nanoparticle attracts layer of counter ions. The electric potential at boundary of double layer formed, is known as zeta potential of particles [15, 16]. From the below-described **Table 4.2.2,** it can be observed that the prepared NPs have around 30 mV with the voltage being negative. Negative voltage indicates that the NPs are negatively charged, which is due to the presence of β-CD.

Table 4.2.2 Zeta potential of synthesized NPs

NPs	Zeta Potential (mV)
100 µM AgNP	**-31.0**
500 µM AgNP	**-29.8**
100 µM AuNP	**-30.0**
100:100 Au@Ag	**-34.2**
100:100 Ag@Au	**-31.2**

Transmission electron microscopy (TEM):

The above characterized NPs were analyzed for determination of their size and shape by TEM. The synthesized NP solutions were drop casted onto carbon-coated copper grids, and the grids were kept in a vacuum desiccator overnight for drying. TEM images were taken at an acceleration voltage of 200 kV. High-resolution transmission electron microscopy (HRTEM) was also performed, and the size distribution of these nanoparticles was evaluated. The size and shape of 100 and 500 µM Ag clusters were uniform, monodisperse, and spherical particles with diameters 9±2.2 nm and 19±2 nm. Hence AgNPs 100 µM and AgNPs 500 µM were termed as "small-sized" (ss) and "large-sized" (ls) NPs, respectively (**Fig 4.2.2.2 a**). The 100 µM AuNPs also showed the same pattern of size and shape, these spherical NPs were also found to lie in the range of 9 to 12 nm (**Fig 4.2.2.2 b**). Bi-

metallic NPs, Ag@Au were spherical, having a size of around 10±2 nm, whereas Au@Ag NPs were of around 11±3 nm with spherical shape (**Fig 4.2.2.2 c**). The size and shape of bi-metallic NPs were almost similar to their mono-metallic counterparts; thus, we can say that conjugation of these two metals to form bi-metallic nanosystems does not affect size and shape.

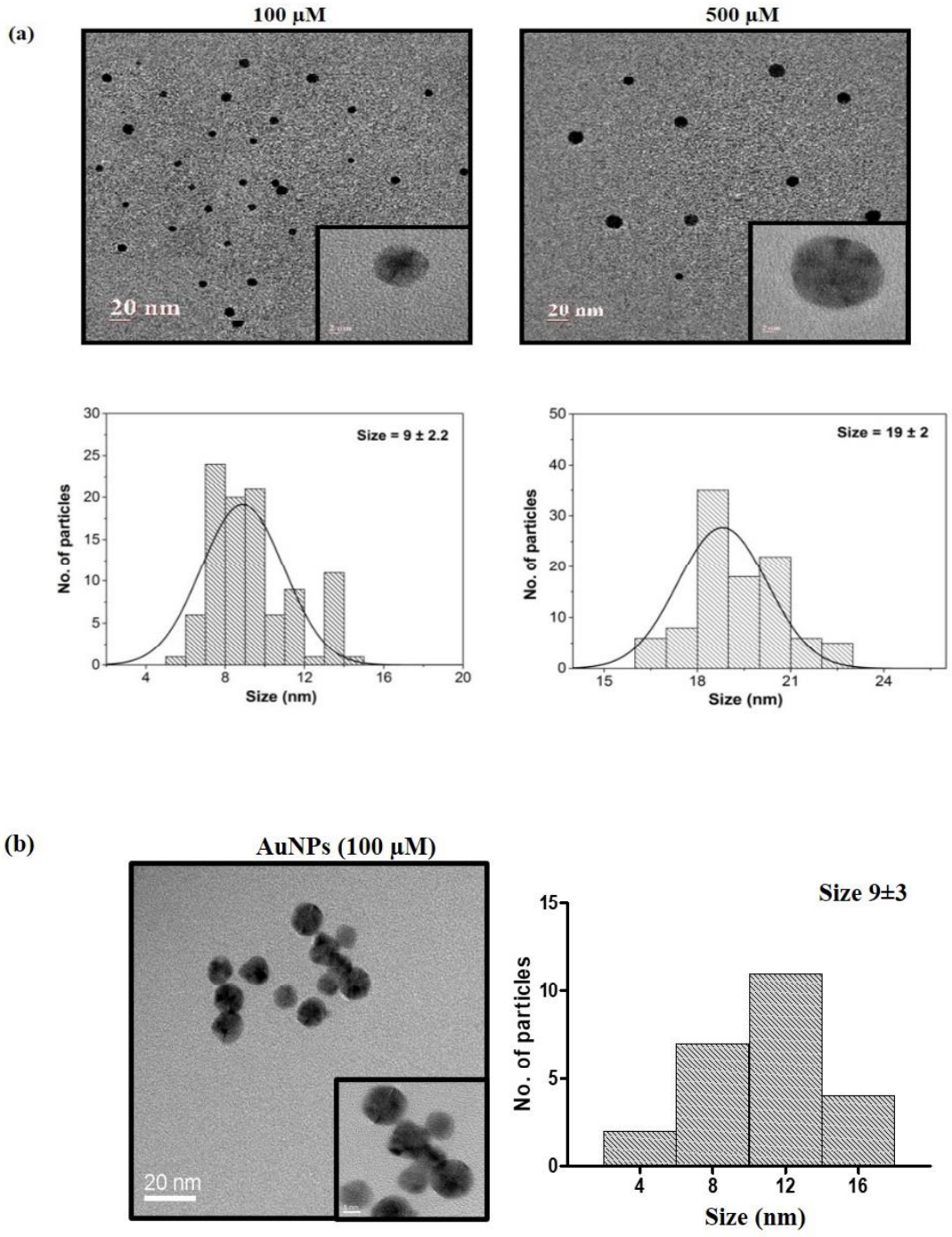

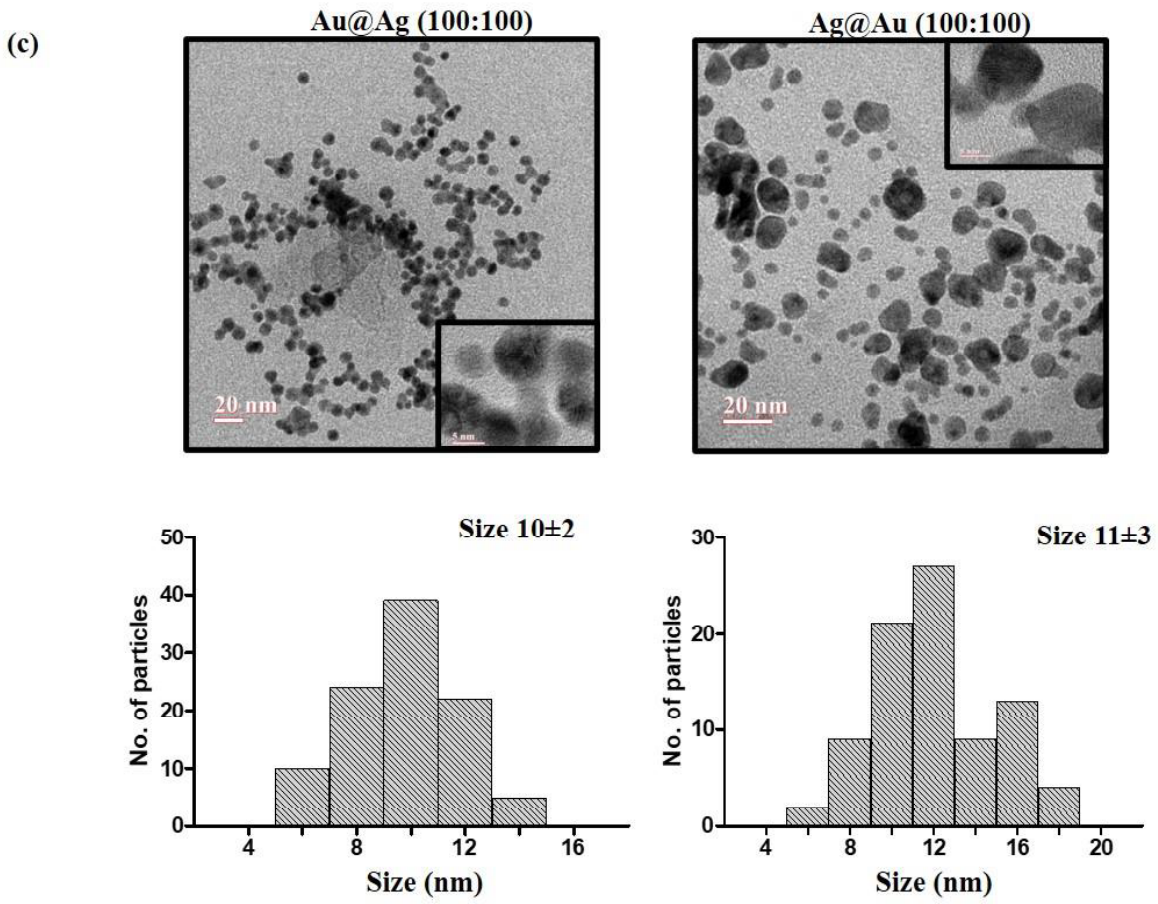

Figure 4.2.2.2. TEM analysis of NPs. TEM images with particle size distribution histogram of 100 and 500 µM AgNPs **(a)** 100 µM AuNPs **(b)** and 100:100 Au@Ag and Ag@Au NPs **(c).** Inset shows the HRTEM images of NPs.

Inductively Coupled Plasma-Optical Emission Spectroscopy (ICP-OES)

ICP-OES analysis is done for determining the concentration of elements present even in a meager amount in the sample. It is a technique that produces excited atoms by using plasma; these excited atoms emit electromagnetic radiations at a wavelength of the characteristic element [17]. The NPs were filtered and analyzed as discussed in chapter 3; the results obtained are represented below in **Table 4.2.3**. The results indicate that the concentration of Ag in mono and bi-metallic NPs is same.

Table 4.2.3 ICP-OES analysis of NPs

NPs (100 µM)	Concentration (mg/L or ppm)
Ag	15.98
Ag@Au	15.54
Au@Ag	15.06

4.3 Discussion

In this chapter, we have discussed the successful synthesis of mono-metallic (Ag or Au NPs) and core@shell type dual/ bi-metallic nanoparticles (Ag@Au, Au@Ag) of varying molar ratios using β-CD as a reducing as well as the stabilizing agent. These NPs would be utilized for further biological studies, and hence a proper characterization of the synthesized NPs was important. Initially, the synthesis of the mono-metallic and dual NPs was confirmed by UV-visible spectroscopy. Further, the zeta potential analysis showed that the NP surface possesses a negative charge attributed to the β-CD capping. Negative values of zeta potential served to indicate successful capping and hence the putative stability of the NPs as well. Thereafter the shape and size of the NPs were confirmed through TEM analysis. The mono-metallic AgNPs were synthesized in different sizes to understand functional variation correlated with size. TEM analysis confirmed the size of the smaller NPs (ss-AgNPs) in the range from 8-12 nm, while the relatively larger ones (ls-AgNPs) had size ranging from 19-21 nm. Further biological studies in subsequent chapters would provide insights into whether such a relatively small variation in size can have a significant effect on the intracellular internalization or cytotoxicity of the NPs. As part of our study, we planned to explore the functional deviation of AgNPs when in the mono-metallic state or core@shell bi-metallic state. We, therefore, synthesized the dual NPs as well with gold in its core or shell. The size of the mono-metallic AuNPs and the dual NPs was purposefully maintained close to the size of the mono-metallic ss-AgNPs so that subsequent comparative biological analysis could be successfully carried out. Also, an ICP-OES

analysis was performed to confirm that the concentration of Ag in dual NPs was close to the mono-metallic AgNPs, thus allowing fruitful comparisons in subsequent studies. **Figure 4.3** illustrates the type of NPs synthesized and their dimensions as well. Further, elucidation of the biological efficacy of these characterized NPs in terms of their cellular uptake route and their anti-cancerous potential shall be discussed in the following chapters.

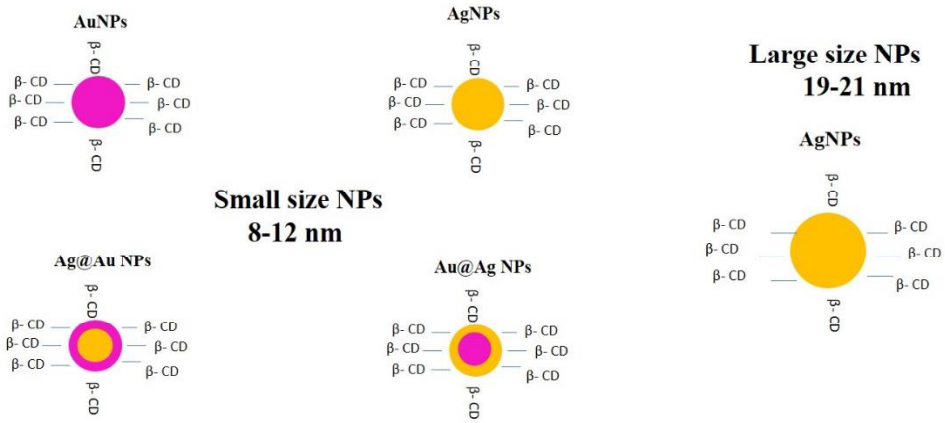

Figure 4.3. Pictorial representation of synthesized metal NPs.

4.4 References

1 Alaqad, K. and Saleh, T. (2016) Gold and silver nanoparticles: synthesis methods, characterization routes and applications towards drugs. *Journal of environmental & analytical toxicology* 6 (4), 525-2161

2 Greish, K. (2010) Enhanced permeability and retention (EPR) effect for anticancer nanomedicine drug targeting. In *Cancer nanotechnology*, pp. 25-37, Springer

3 Ghosh Chaudhuri, R. and Paria, S. (2012) Core/shell nanoparticles: classes, properties, synthesis mechanisms, characterization, and applications. *Chemical reviews* 112 (4), 2373-2433

4 Kulkarni, N. and Muddapur, U. (2014) Biosynthesis of metal nanoparticles: a review. *Journal of nanotechnology* 2014

5 Zaleska-Medynska, A. et al. (2016) Noble metal-based bimetallic nanoparticles: the effect of the structure on the optical, catalytic and photocatalytic properties. *Advances in colloid and interface science* 229, 80-107

6 Zeng, L. et al. (2015) Raman reporter-coupled Agcore@ Aushell nanostars for in vivo improved surface enhanced Raman scattering imaging and near-infrared-triggered photothermal therapy in breast cancers. *ACS applied materials & interfaces* 7 (30), 16781-16791

7 Lomelí-Marroquín, D. et al. (2019) Starch-mediated synthesis of mono-and bimetallic silver/gold nanoparticles as antimicrobial and anticancer agents. *International journal of nanomedicine* 14, 2171

8 Katifelis, H. et al. (2018) Ag/Au bimetallic nanoparticles induce apoptosis in human cancer cell lines via P53, CASPASE-3 and BAX/BCL-2 pathways. *Artificial cells, nanomedicine, and biotechnology* 46 (sup3), S389-S398

9 Satyanarayana, T. and Reddy, S.S. (2018) Methods of Nanomaterials. *International journal for research in applied science & engineering technology. 6 (1), 2885-2889*

10 Reverberi, A. et al. (2016) Systematical analysis of chemical methods in metal nanoparticles synthesis. *Theoretical foundations of chemical engineering* 50 (1), 59-66

11 Mariadoss, A.V.A. et al. (2019) Green synthesis, characterization and antibacterial activity of silver nanoparticles by Malus domestica and its cytotoxic effect on (MCF-7) cell line. *Microbial pathogenesis* 135, 103609

12 Shelley, H. and Babu, R.J. (2018) Role of cyclodextrins in nanoparticle-based drug delivery systems. *Journal of pharmaceutical sciences* 107 (7), 1741-1753

13 Mellet, C.O. et al. (2011) Cyclodextrin-based gene delivery systems. *Chemical society reviews* 40 (3), 1586-1608

14 R Kanwar, J. et al. (2011) The use of cyclodextrins nanoparticles for oral delivery. *Current medicinal chemistry* 18 (14), 2079-2085

15 Laban, B. et al. (2020) Green synthesis and characterization of nontoxic L-methionine capped silver and gold nanoparticles. *Journal of inorganic biochemistry* 204, 110958

16 Gupta, A. et al. (2020) Synthesis of Silver Nanoparticles Using Curcumin-Cyclodextrins Loaded into Bacterial Cellulose-Based Hydrogels for Wound Dressing Applications. *Biomacromolecules*

17 Figueroa, J.A.L. et al. (2016) Metal ion transport quantified by ICP-MS in intact cells. *Scientific reports* 6, 20551

Chapter- 5

Variation in physical and chemical property of NPs, its effect on cellular uptake and associated cytotoxicity

Chapter-5

Variation in physical and chemical property of NPs, its effect on cellular uptake and associated cytotoxicity

5.1 Overview:

In the previous chapter, we have discussed the procedure by which we have synthesized metal nanoparticles using β-CD and their characterization using various conventionally used techniques. Since NPs have this unique ability to home, particularly into tumor tissues exploiting the leaky vasculature of tumors, it makes them an essential component of the therapeutic arsenal against cancer [1, 2]. However, the uptake efficiency and cytotoxic efficacy of the NPs post variation of their physical or chemical parameters have not been deeply investigated, so far. Hence, in this study, we planned to explore the effect of the synthesized NPs following variation in their physicochemical properties on breast cancer cells. Primarily, all biomolecules, for example, bacteria, viruses, have been evolved in particular sizes and shapes to perform their precise functions and interactions. Similarly, we propose that not random, but an optimum dimension or physical parameter of an NP is required for a robust therapeutic effect on the cells. This might have a subsequent impact on the successful entry of the NPs into cells, which might further be a determining factor for its cytotoxic efficacy. Existing reports already hint that factors like size, shape, charge, and stiffness of NPs can affect their uptake by a cell [3, 4]. Even modifying the surface of NPs with two different ligands targeting the same receptor can alter the uptake and cytotoxic potential of NPs. Further, in animals, for example, positively charged NPs were found to be cleared rapidly from the bloodstream as they get adsorbed by serum proteins marking them for degradation by phagocytosis in the liver [5]. In contrast, few reports contradict this statement suggesting a high positive charge increases the uptake efficiency of the NPs [6]. Furthermore, existing studies show that for NPs of a size larger than 100

nm, rod-shaped NPs were found to exhibit higher efficiency of uptake followed by spherical, cylindrical, and cubical NPs. However, for sizes smaller than 100 nm, spherical shaped NPs were preferred over rod [7-9]. Based on existing literature, it is evident that the physical properties of NPs define their role; however, the scale of this variation and its associated effect on the cellular system is poorly defined. Also, the size-dependent uptake of NPs is reported to be related to the membrane wrapping process. Different discrete pathways for cellular internalization of NPs exist, which might be critical for exerting an effect at the cellular level. Currently, a vast majority of research suggests that metal NPs enter the cell primarily *via* endocytosis [10]. Based on the proteins involved, it can be mainly classified as caveolae-mediated, clathrin-mediated, or clathrin- and caveolae-independent endocytosis [11, 12]. However, what property of the NPs regulates the mode of entry of the NPs and how it affects subsequent intracellular trafficking, and critical intracellular processes are under-explored. In this chapter, we shall explore and present the comparative involvement of pathways for the uptake of NPs and how it varies with alteration in the physical parameters of the NPs. Furthermore, the subsequent effect on cell viability shall be evaluated.

5.2 Results:

5.2.1 Variation in the physicochemical properties of NPs affects their sensitivity

As discussed in the previous chapter, we have synthesized mono and bi-metallic NPs of Ag and Au. We have investigated the cell viability upon exposure of these NPs to breast cancer cells.

5.2.1.1 Analysis of cell viability of AgNPs

We initially examined the dose-dependent effect of AgNPs on human breast cancer cells, MCF-7 and MDA-MB-468, MCF-7 having wild type p53 whereas MDA-MB-468 have R273H mutant form of p53 gene. **Figure 5.2.1.1 a** shows phase contrast images of MCF-7 and MDA-MB-468 cells exposed to AgNPs. A distinct difference in cell shape with consistent rounding up of cells was observed after

treatment with ss-AgNPs (small size, ~9nm) and ls-AgNPs (large size, ~19nm). Both the cell types studied were significantly (***) more sensitive to ss-AgNPs with an IC_{50} of ~25 µM compared to ls-AgNPs (IC_{50}~100 µM), as shown by MTT assay **(Fig 5.2.1.1 b)** and AnnexinV/PI staining (**Fig 5.2.1.1 c)**. These results indicate that AgNP induces size and dose-dependent toxicity, and the pattern was same for both cell types, which suggest toxicity was independent of p53 status in these cells. The concentration of β-CD and $AgNO_3$ used for the synthesis of NPs was not toxic (**Fig 5.2.1.1 d**). To check the effect of these AgNPs on non-cancerous, we treated HaCaT cells (immortalized keratinocytes). We observed less cytotoxicity as compared to MCF-7 cells confirming their sensitivity for cancer cells only (**Fig 5.2.1.1 e & f**).

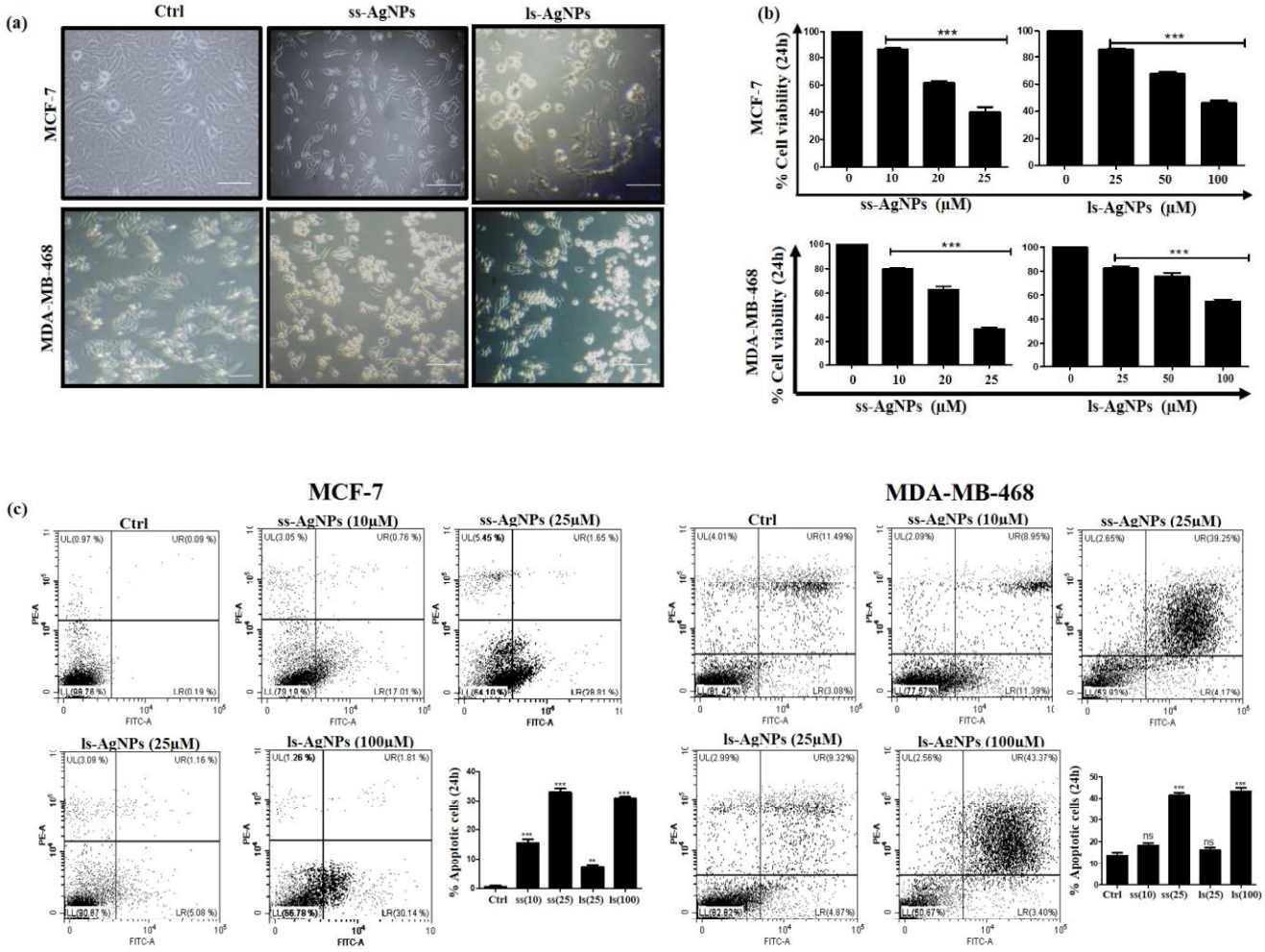

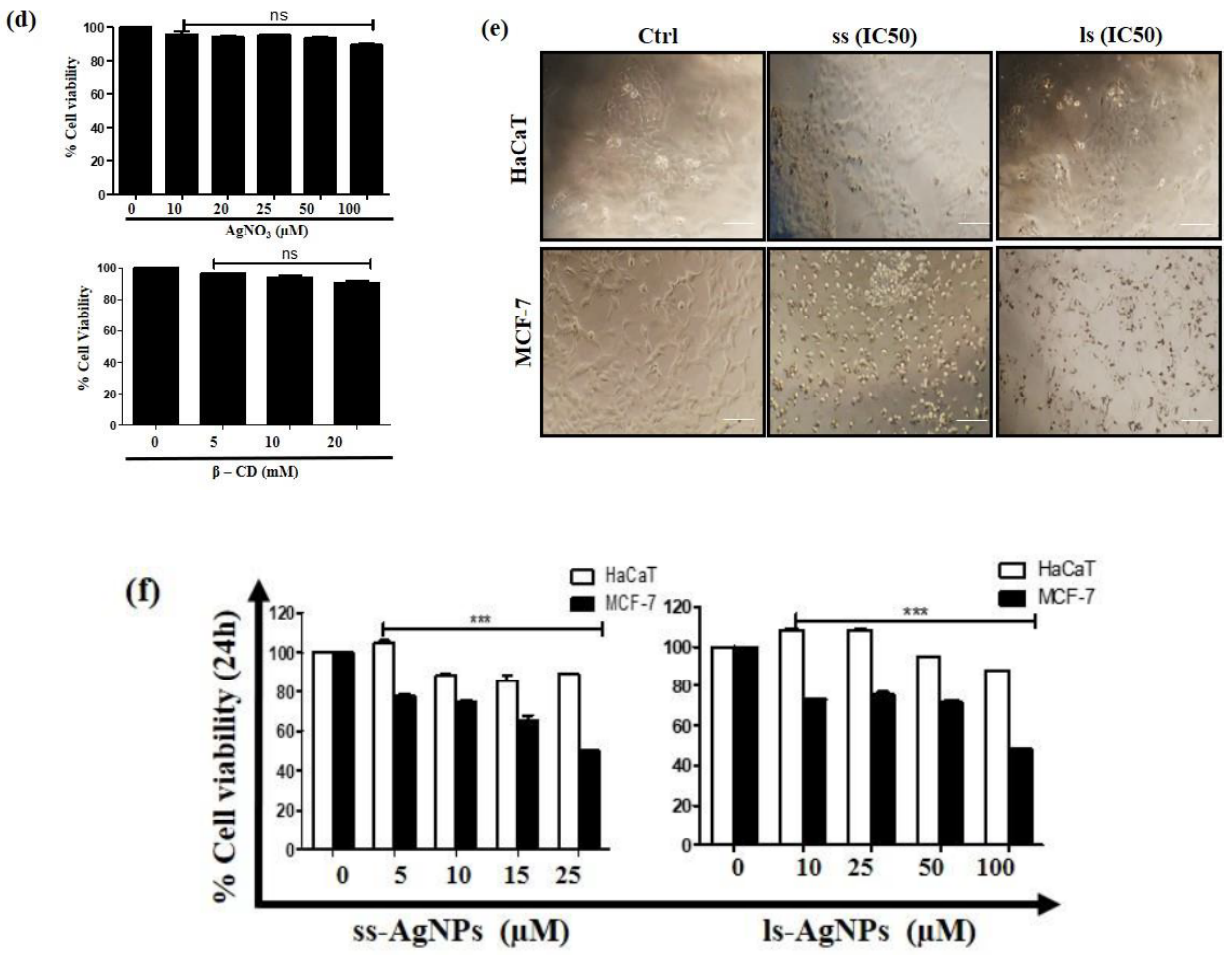

Figure 5.2.1.1. Analysis of cell viability upon AgNP treatment. **(a)** Phase-contrast images of cells after treatment with AgNPs for 24 h. "Ctrl" represents untreated cells. Scale bar- 100 µm (**b)** MTT assay analyzing cell viability after 24 h of treatment with different doses of AgNPs. **(c)** AnnexinV/PI staining representing the percentage of dead cells post-exposure to low and IC_{50} doses of AgNPs for 24 h. **(d)** MTT assay analyzing cell viability after treatment with different doses of β-CD and $AgNO_3$. **(e)** Phase-contrast images of HaCaT and MCF-7 cells after treatment with IC_{50} dose of AgNPs for 24 h. "Ctrl" represents untreated cells. Scale bar- 100 µm. **(f)** Cell viability of HaCaT in comparison to MCF-7 cells after treatment of AgNPs (IC_{50} dose) for 24 h. [Symbol (*) represents a statistically significant difference with respect to untreated cells].

5.2.1.2 Analysis of cell viability of AuNPs

Similar to the AgNPs, we treated the MCF7 cells with different doses of AuNPs. As discussed in the earlier chapter, the metal Au was utilized to prepare the dual NPs, and the objective behind that was to understand how the functional behavior of AgNPs varies when in combination with Au forming dual NPs of approximately the same size. So, before we proceeded with analyzing cytotoxicity of Ag-Au-NPs, we evaluated the cytotoxicity of the AuNPs at similar concentrations to the ss-AgNPs. As mentioned earlier, the size range of the AuNPs was also kept close to the ss-AgNPs. Different doses of AuNPs were used to treat the MCF-7 cells. Importantly, the AuNPs were comparatively significantly (ns) less toxic to the cells even after 48 h of treatment, as observed by MTT assay and Annexin/PI staining (**Fig 5.2.1.2 a & b**).

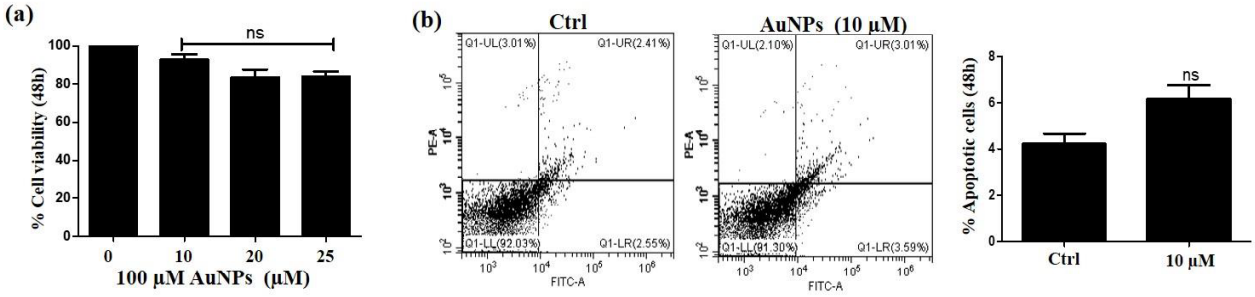

Figure 5.2.1.2. Analysis of cell viability upon AuNP treatment. **(a)** MTT assay analyzing cell viability after 48 h of treatment with different doses of AuNPs. **(b)** AnnexinV/PI staining representing the percentage of dead cells post-exposure to AuNPs for 48 h. [Symbol (ns) stands for non-significant difference].

5.2.1.3 Cell viability of bi-metallic NPs

Bi-metallic nano-composites often exhibit properties that are different from their respective independent mono-metallic NPs. Therefore, there has been a recent surge in synthesis, characterization, and functional evaluation of bi-metallic NPs and its comparison with mono-metallic

ones. As per existing literature, bi-metallic NPs have been used as substrates for SERS (Surface Enhanced Raman Spectroscopy), which can be used to detect biomolecules present in blood and body fluids and for detection of biomarkers for cancer [13]. Here, we have synthesized the bi-metallic NPs, Au@Ag (Au_{core}; Ag_{shell}) and Ag@Au (Ag_{core}; Au_{shell}) in 1:1 ratio using β-CD, as discussed in Chapter 4. The synthesized bi-metallic NPs were then analyzed for their internalization and cytotoxicity in MCF-7 cells. Interestingly, these NPs showed comparatively reduced cytotoxicity as compared to the mono-metallic AgNPs, but were more toxic than AuNPs after 48 h of treatment as analyzed by MTT assay and Annexin/PI staining experiment using flow cytometry (**Fig 5.2.1.3 a & b).** We speculate that the reduced cytotoxicity observed can be attributed either to their less cellular uptake or the slow release of Ag ions from the bi-metallic NPs when compared to the mono-metallic ones. To confirm the same, we analyzed the release of Ag ions by ICP-OES analysis. Interestingly, it showed an increased intracellular accumulation of Ag ions, after 24 h, in cells treated with AgNPs than the cells treated with dual NPs. A further increase in ion concentration was observed after dual NP treatment for 48h (**Table 5.2.1**), at this time point mono-metallic AgNPs were very toxic to the cells studied; hence, we were not able to harvest cells at the same dose.

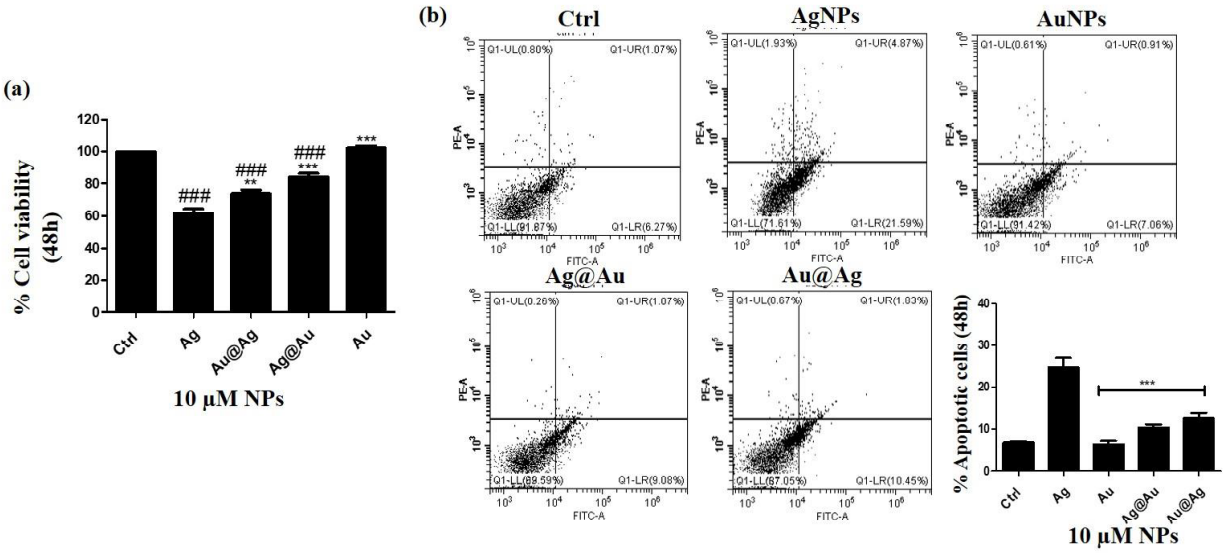

Figure 5.2.1.3. Analysis of cell viability upon bi-metallic NP treatment. **(a)** MTT assay analyzing cell viability after 48 h of treatment with different doses of NPs. Symbol (* and #) denote statistically

significant difference with respect to AgNP and untreated cells, respectively **(b)** AnnexinV/PI staining representing the percentage of dead cells post-exposure to NPs for 48 h. Symbol (*) denote statistically significant difference with respect to AgNP treated cells.

Table 5.2.1 ICP-OES analysis of NP treated cells

NPs (25 µM)	Concentration of Ag (mg/L or ppm)	Cells treated with NPs (25 µM)	Concentration (mg/L or ppm)
Ag NP	2.545	Ag, 24 h	1.118
Ag@Au 100:100	2.472	Ag@Au 100:100, 24 h	0.632
Au@Ag 100:100	2.341	Au@Ag 100:100, 24 h	0.536
		Ag@Au 100:100, 48 h	1.012
		Au@Ag 100:100, 48 h	0.992

5.2.2 Cellular uptake of NPs

For assessment of internalization, the NPs were tagged with Coumarin-6 (C6), a green fluorescent dye following the procedure, as discussed in the material & methods section for their visualization [14]. These C6 tagged NPs were used to treat MCF-7 cells for the desired time at specific concentrations.

5.2.2.1 Size and time-dependent internalization of AgNPs (mono-metallic)

We monitored the cellular uptake of mono-metallic AgNPs, presuming that a variation in size might result in differential uptake**. Figure 5.2.2.1 a** indicates that there was more intense green fluorescence for ss-AgNPs compared to ls-AgNps reflecting their better internalization. Uptake of free C6 was also monitored (**Fig 5.2.2.1 b**). The microscopic observation was further confirmed through flow cytometry with ss-AgNPs showing significantly (***) increased internalization at

similar concentrations than ls-AgNPs (**Fig 5.2.2.1 c**). The uptake also increased with time (**Fig 5.2.2.1 d**). It can be inferred from above that the uptake of AgNPs is size and time-dependent with enhanced permeability potential for small-sized NPs.

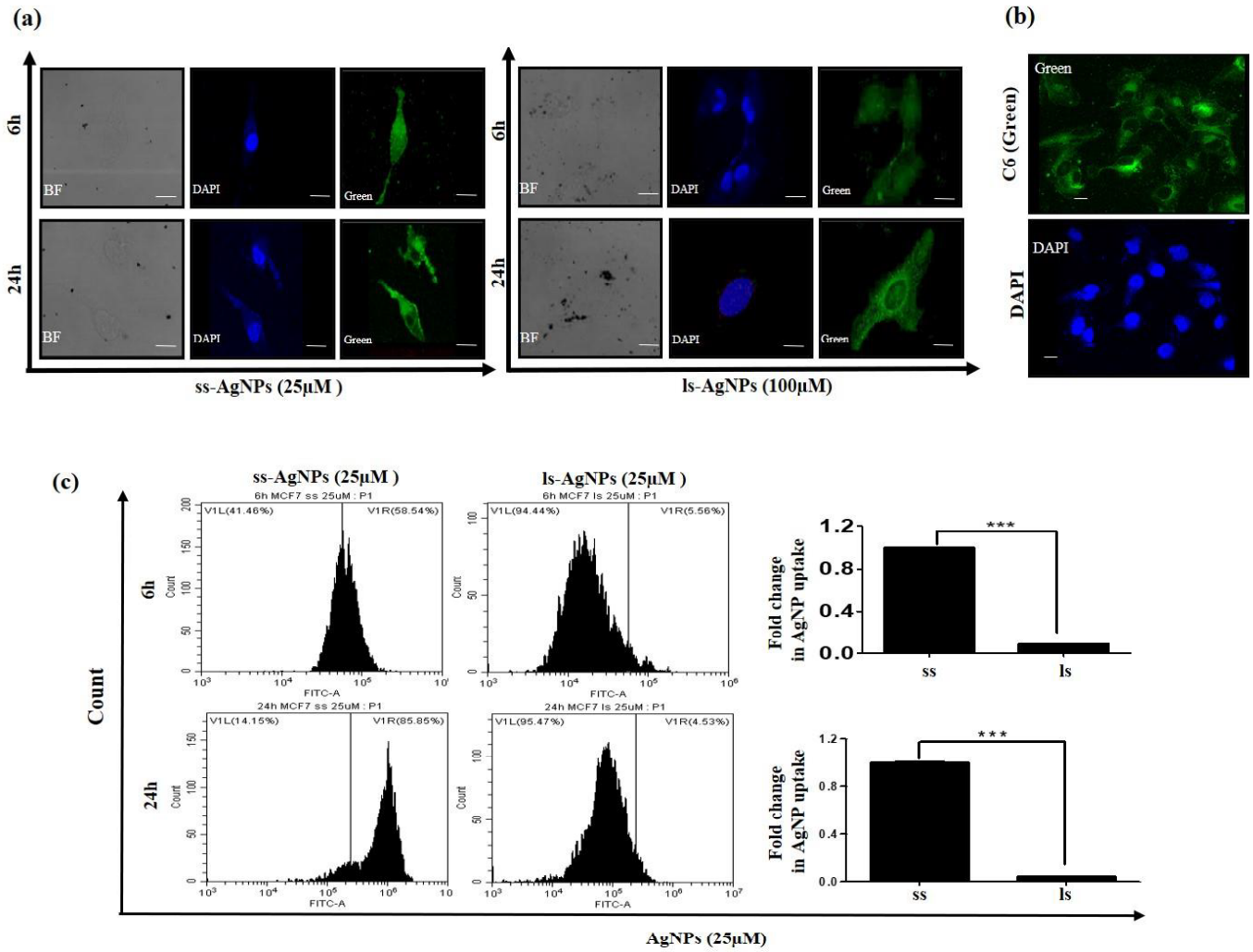

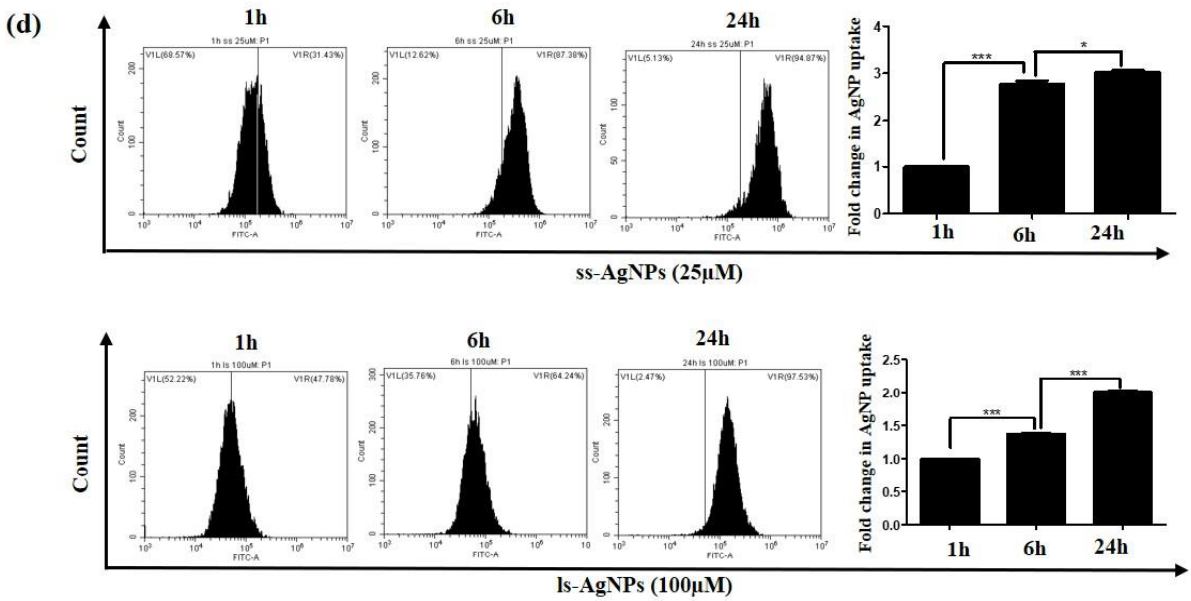

Figure 5.2.2.1. Analysis of internalization of AgNPs. **(a)** Fluorescent microscopic images of MCF-7 cells after treatment with IC_{50} dose of C6 tagged AgNPs for 6 h and 24 h. **(b)** Fluorescent microscopic images of MCF-7 cells after treatment with free Coumarin-6 (C6). Scale bar- 200 µm. **(c)** A comparative fold change between C6 tagged ss-AgNP and ls-AgNp uptake (25 µM) measured through flow cytometry at different time points. **(d)** A comparative difference in uptake of C6 tagged AgNPs (IC_{50}) at different time points (1, 6 & 24 h) as measured through flow cytometry. The symbol (*) represents a significant difference between different treatments.

5.2.2.2 Cellular uptake of NPs is an energy-dependent process

Endocytosis is a form of active transport that occurs by using ATP as energy [15]. To confirm a primarily energy-dependent internalization, we treated cells with AgNPs and incubated them at 4°C and 37°C. We observed that the uptake of NPs was significantly (***) decreased in cells incubated at lower temperature irrespective of the differential size-dependent uptake observed earlier **(Fig 5.2.2.2)**. However, we assume that at low temperature, the metabolic activity of the cell reduces, and hence an ATP dependent process is not feasible. Had the internalization been mostly due to diffusion, the cells could have shown accumulation of the NPs synthesized.

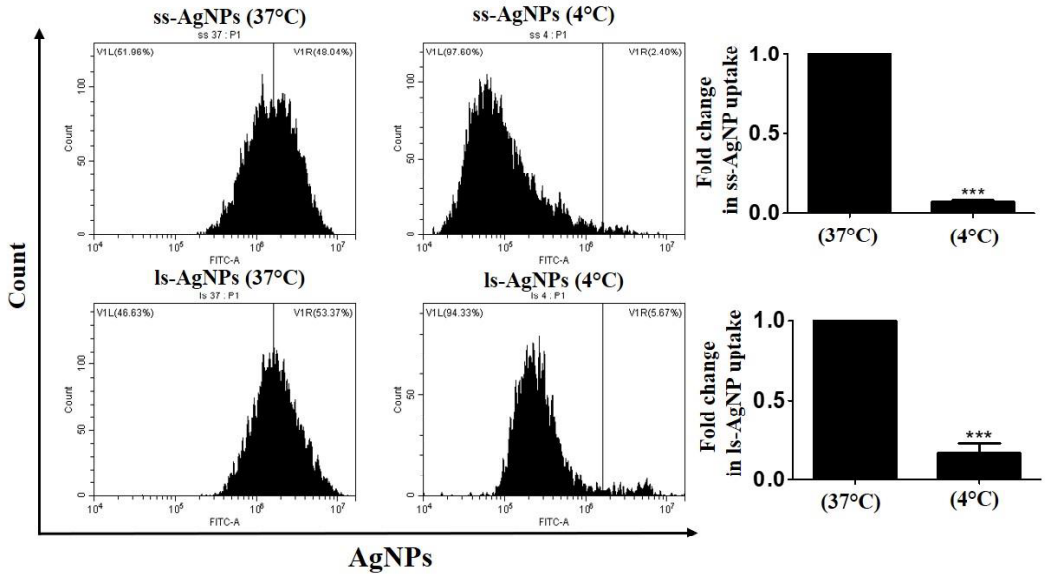

Figure 5.2.2.2. Analysis of internalization of AgNPs at different temperatures. A comparative fold change between C6 tagged ss-AgNP and ls-AgNP uptake (IC_{50} dose) measured through flow cytometry at different temperatures. The symbol (*) represents a significant difference between different treatments.

5.2.2.3 Effect of variation in physicochemical properties of NPs on cellular uptake

Different small molecules inhibit respective intracellular route of entry

Internalization of NPs can occur through various mechanisms like clathrin-mediated endocytosis (CME), caveolae-mediated endocytosis (CVE), and clathrin-caveolae independent endocytic mechanisms (CCIE), as well as by phagocytosis or macropinocytosis [11]. We took the commonly used inhibitors of endocytosis, for example, chlorpromazine (CPZ), which inhibits CME [16]; genistein (Gen), an inhibitor of CVE; nocodazole (Noc), that inhibit actin driven macropinocytosis; and finally, dynasore (Dyn), that inhibit dynamin from blocking dynamin-dependent endocytosis. The internalization parameters were analyzed after 1 h of exposure to the NPs, as preventing a particular route of entry into the cells may activate another compensatory pathway of endocytosis at later time points, thus complicating analysis [17]. The time and dose of each inhibitor were selected

based on prior published reports; a non-cytotoxic dose was selected based on viability assay performed (**Fig 5.2.2.3**).

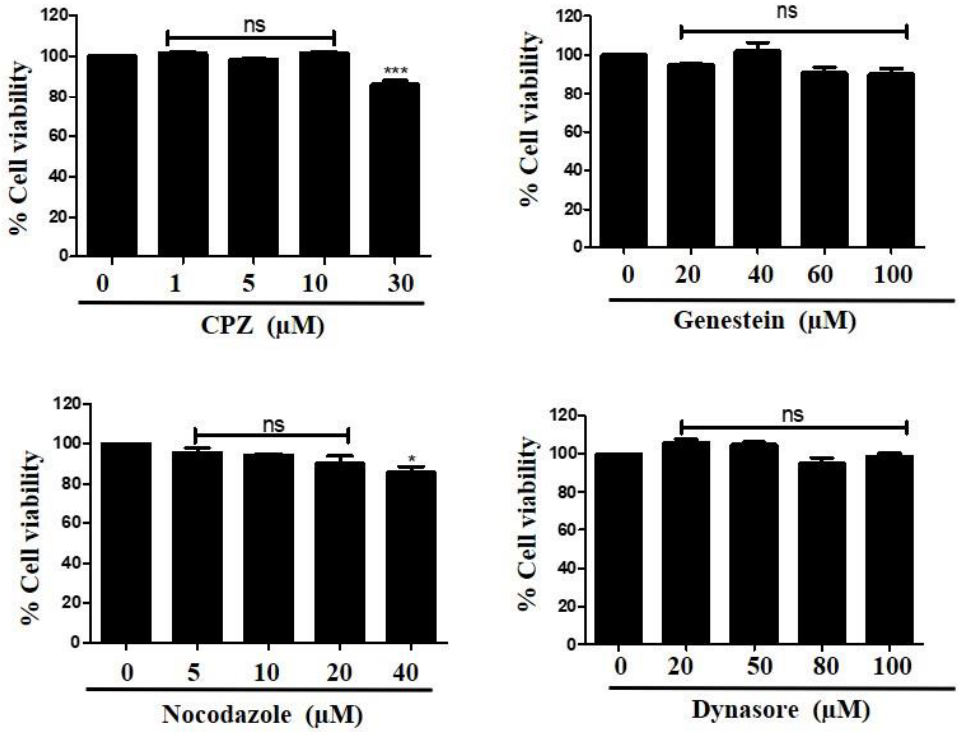

Figure 5.2.2.3. Analysis of cell viability after treatment with different endocytic pathway inhibitors. MTT assay analyzing cell viability after 6 h of treatment with varying doses of inhibitors of various endocytosis pathway. The symbol (*) represents the level of significance with respect to untreated cells. Symbol (ns) represents, the difference is not significant.

5.2.2.3.1 Internalization mechanism of NPs is affected by size of the NPs

Upon treatment with mono-metallic NPs, we observed that internalization alters with their size. To further understand the effect of size on the internalization pathway of NPs, we treated cells with ss and ls-AgNPs. Interestingly, unlike ss-AgNPs, Dyn did not have a profound impact on the uptake of ls-AgNPs (**Fig 5.2.2.3.1 a & b**). Rather, a significant impediment (***) in the uptake of ls-AgNPs

was observed when specific inhibitors of CME and CVE were used (**Fig 5.2.2.3.1 b**). Though, the difference in level of internalization between AgNPs and AuNPs was non-significant, ss-AgNPs were significantly (***) affected by the use of Dyn when compared to Gen. The effect of CPZ treatment had a diverse effect on the uptake of NPs; it moderately affected the uptake of AgNPs but not the AuNPs (**Fig 5.2.2.3.1 c**). This observation confirmed that change in type or size of the NPs, the mode of entry of NPs, also varies. **Figure 5.2.2.3.1 d** represents co-localization of clathrin protein, with AgNPs. Importantly, the addition of Dyn before AgNP treatment reduced the co-localization of clathrin (red) with ss-AgNPs but not ls-AgNPs (green). Existing reports are suggesting that dynamin and clathrin co-localize, and dynamin is required for clathrin-dependent vesicle formation. Hence, pre-treatment with Dyn, which acts as an inhibitor of endocytic pathways that are known to depend on dynamin by inhibiting vesicle formation, showed reduced co-localization of AgNPs and clathrin [18, 19]. Dyn, though an inhibitor of dynamin-1 and 2 dependent segregation of endocytic vesicles from the cell membrane, is also involved in dynamin-independent effects as well [20]. We assume that ss-AgNPs, by virtue of their small size, might involve both dynamin-dependent and independent mechanisms for their internalization.

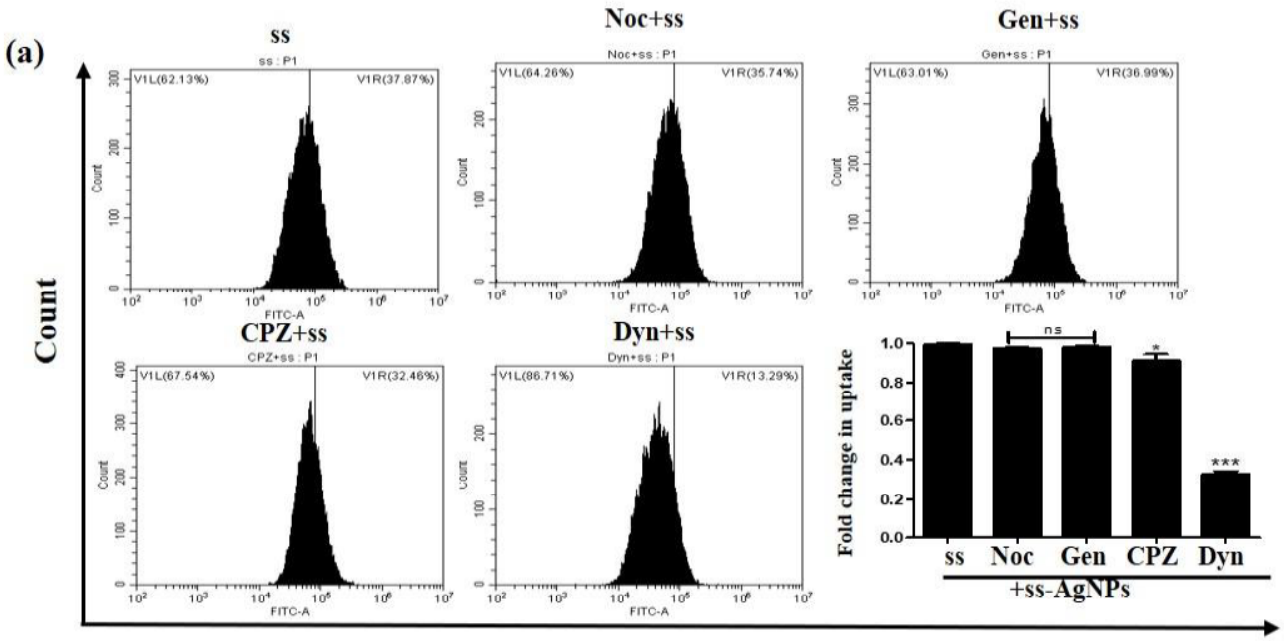

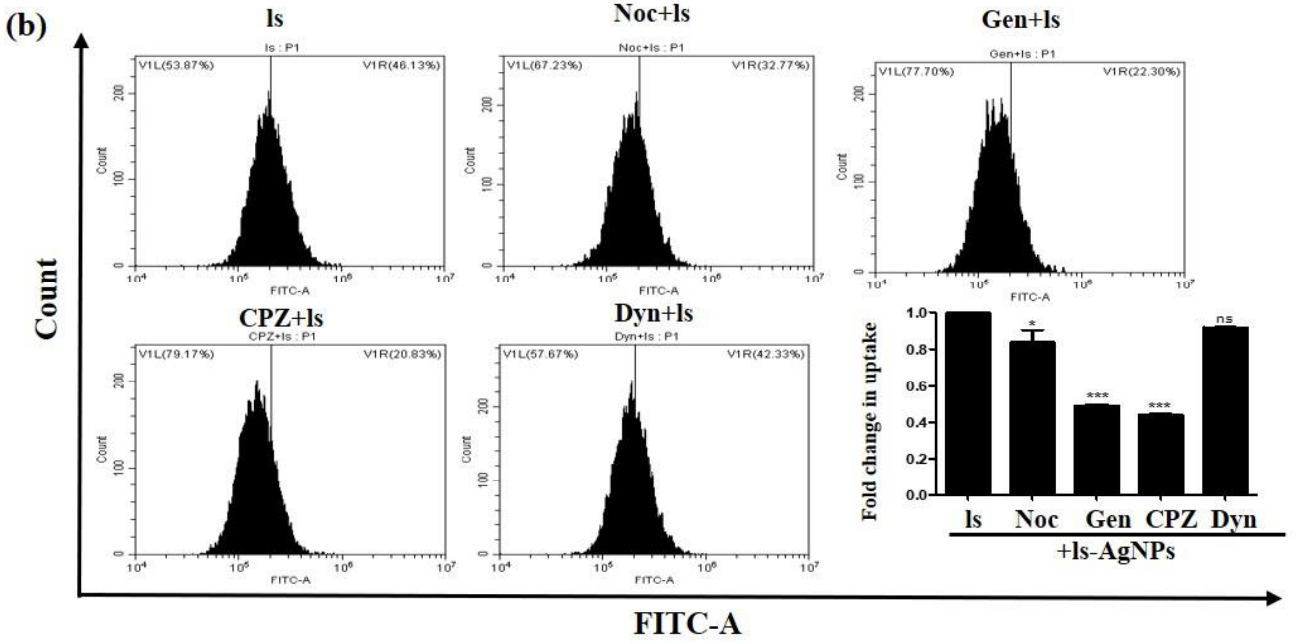
(b)
Is
Noc+Is
Gen+Is
CPZ+Is
Dyn+Is
V1L(53.87%)
V1R(46.13%)
V1L(67.23%)
V1R(32.77%)
V1L(77.70%)
V1R(22.30%)
V1L(79.17%)
V1R(20.83%)
V1L(57.67%)
V1R(42.33%)
Count
FITC-A
Fold change in uptake
Is
Noc
Gen
CPZ
Dyn
+Is-AgNPs

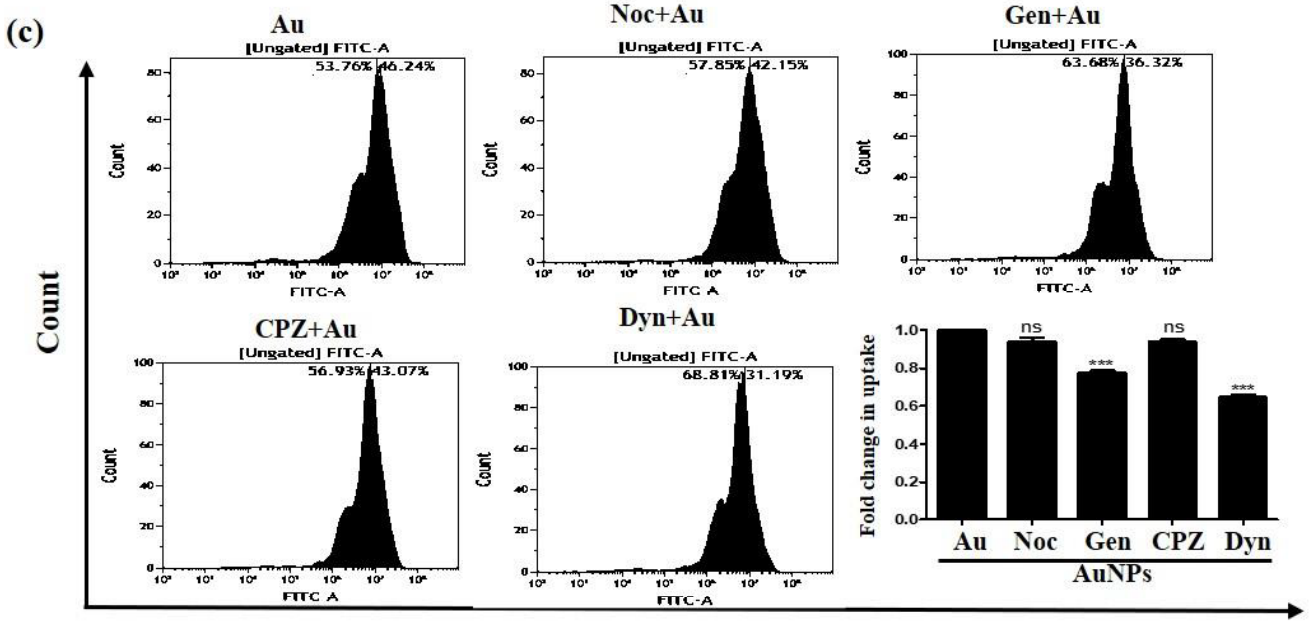
(c)
Au
Noc+Au
Gen+Au
CPZ+Au
Dyn+Au
[Ungated] FITC-A
53.76%
46.24%
57.85%
42.15%
63.68%
36.32%
56.93%
43.07%
68.81%
31.19%
Count
FITC-A
Fold change in uptake
Au
Noc
Gen
CPZ
Dyn
AuNPs

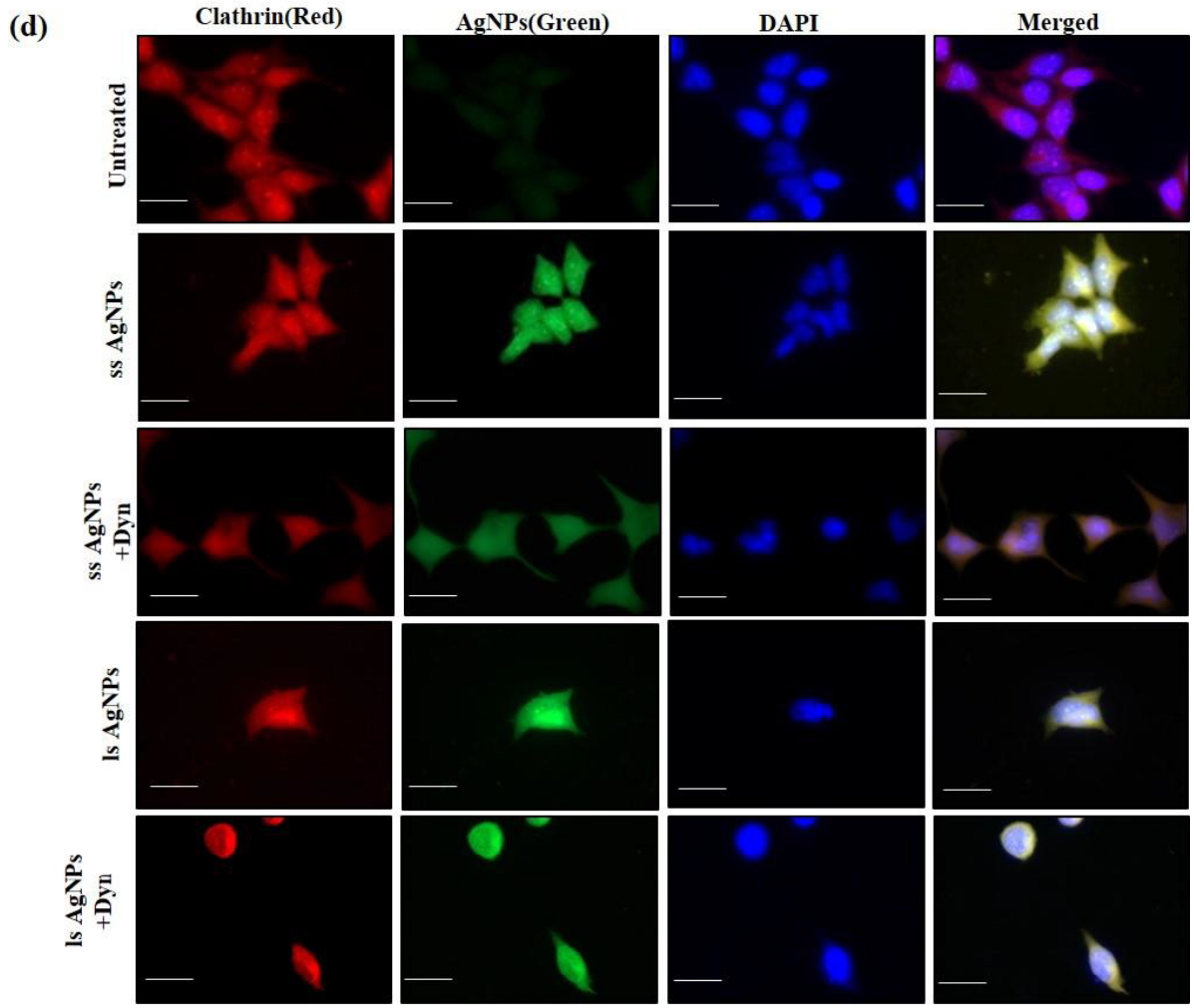

Figure 5.2.2.3.1. Analysis of the intracellular uptake mechanism of AuNPs and AgNPs. Flow cytometric analysis of the uptake of AuNPs **(a)**, ss-AgNPs **(b),** and ls-AgNPs **(c)** (at IC_{50} dose) 1 h after treatment with NPs. The inhibitors used were- Nocodazole (Noc; 0.5 µM), Genistein (Gen; 10 µM), Chlorpromazine (CPZ; 5 µM) and Dynasore (Dyn; 50 µM). **(d)** Immunofluorescence images of cells treated with IC_{50} dose of ss and ls-AgNPs (green) with and without Dyn. Cells were stained with anti-rabbit TR conjugated secondary antibody against clathrin (red). Scale bar- 200 µm. The symbol (*) represents a significant difference with respect to AgNP-treated cells.

5.2.2.3.2 Intracellular route of entry of bi-metallic NPs

Following the observation of the internalization mechanism of the mono-metallic NPs, we investigated for the bi-metallic ones. The Ag@Au and Au@Ag NPs had size comparatively similar to their mono-metallic forms. Also, from cell viability assays, we have found that the bi-metallic NPs were less toxic to the MCF-7 cells. To confirm whether these NPs show reduced intracellular entry, we treated the cells with a similar dose of bi-metallic NPs, as per the dose used for mono-metallic AgNPs. Interestingly, flow cytometry analysis revealed that rather than a decreased internalization, the uptake of bi-metallic NPs, however, was more as compared to the mono-metallic AgNPs (**Fig 5.2.2.3.2 a**). To follow the uptake route of these bi-metallic NPs, we treated the cells with inhibitors of endocytic pathways in a similar manner as discussed above. Interestingly, we observed that Noc and Dyn both significantly (***) affected the entry of both Ag@Au and Au@Ag bi-metallic NPs (**Fig 5.2.2.3.2 b & c**). However, CPZ was also found to affect the uptake of Ag_{core} significantly (***), but not the Au_{core} bi-metallic NPs (**Fig 5.2.2.3.2 b & c**). One significant observation analyzing the entry route of the bi-metallic ones was that their internalization was affected by the use of multiple inhibitors suggesting utilization of multiple cellular internalization mechanisms. However, it remains to be analyzed why bi-metallic NPs showed more uptake.

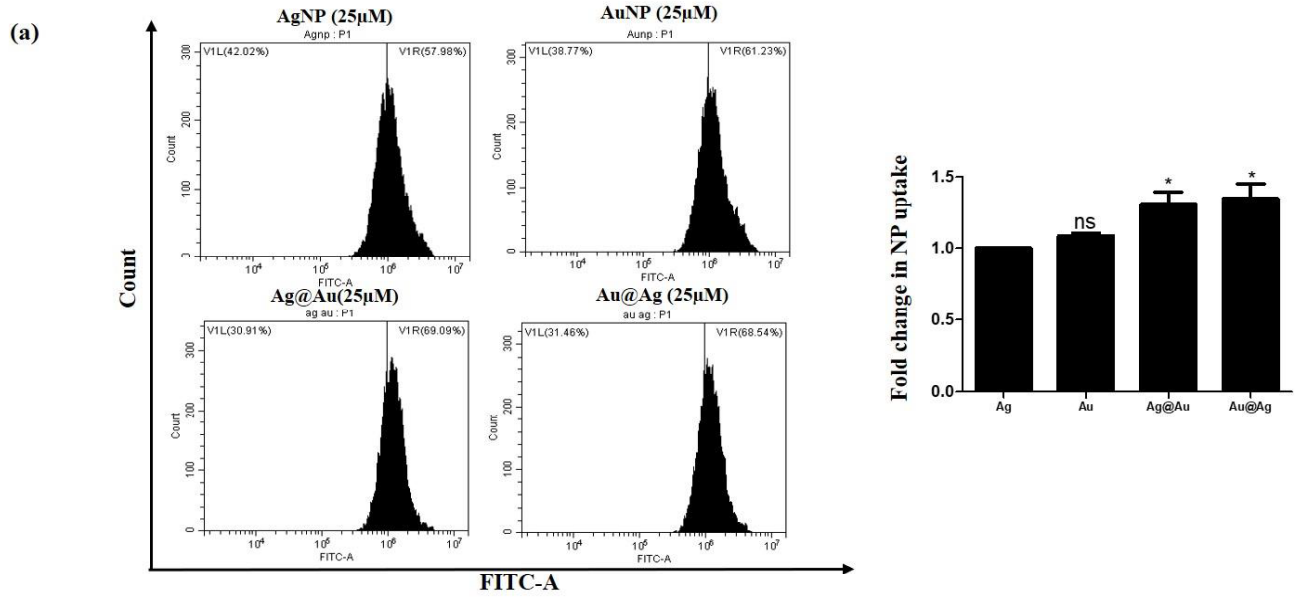

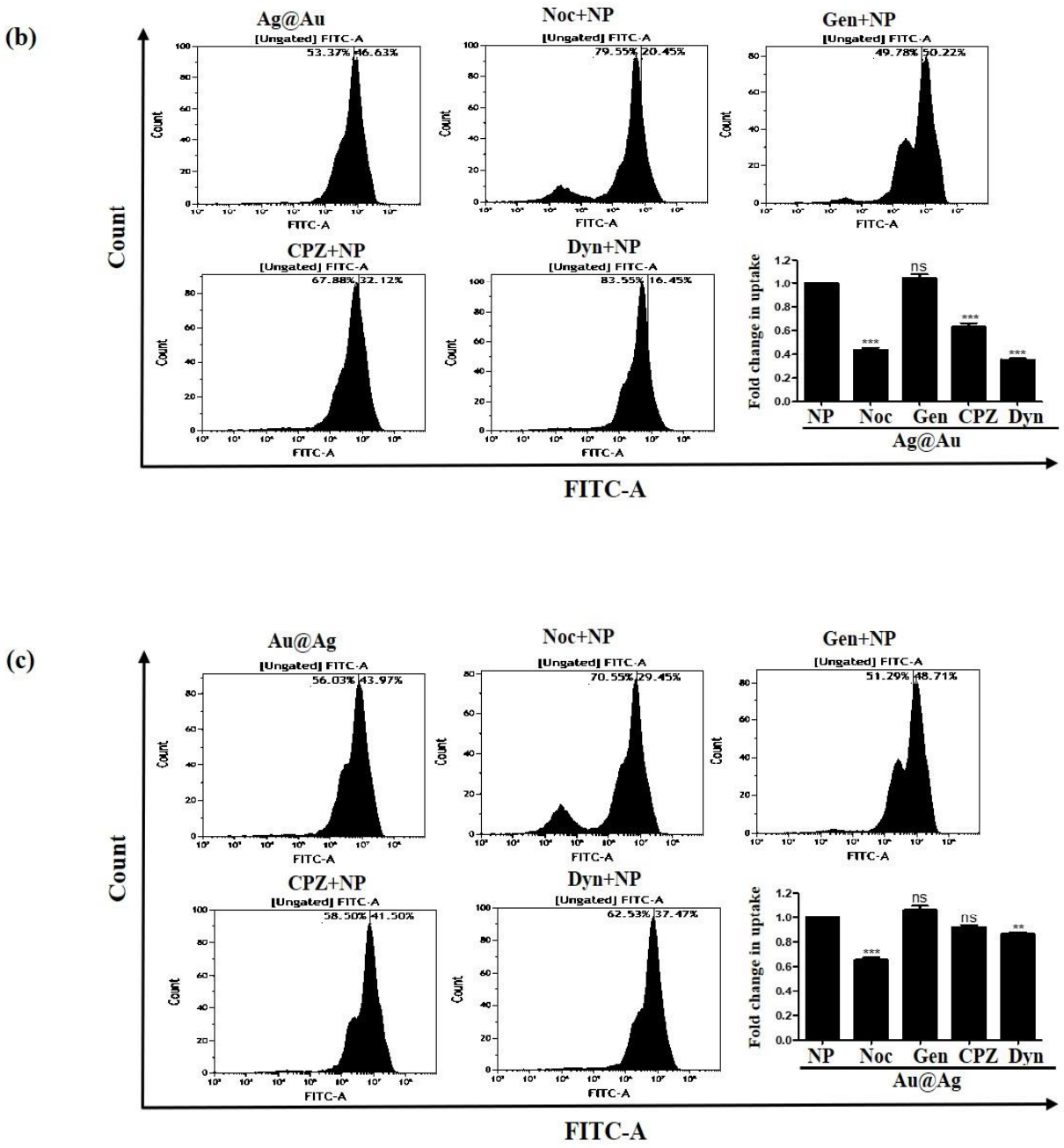

Figure 5.2.2.3.2. Analysis of internalization of bi-metallic NPs. **(a)** A comparative fold change between C6 tagged Ag@Au, Au@Ag, AuNP, and AgNP uptake (25 µM) measured through flow cytometry after 6 h of NP treatment. **(b) & (c)** Fold change in the uptake of Ag@au and Au@Ag, respectively, after treatment with different endocytic pathway inhibitors. The symbol (*) represents a significant difference between different treatments, (ns) denotes difference is not significant.

5.3 Discussion

In this chapter, we show that the β-CD coated metal NPs, both mono-metallic and bi-metallic NPs, are internalized by the cultured tumor cells by an energy-driven process. The mechanism of internalization is strictly dependent on the type and size of the NPs. A significant observation was that the ss-AgNPs were comparatively more internalized than the ls-AgNPs after a similar period in the cells studied. We thus prove that a small variation in the size of NPs (~10 nm) has an impact on the internalization potential of the NPs. Furthermore, we observed that the mechanism of internalization also varied with a change in the size of the NPs. Upon pharmacological inhibition of the different endocytic pathways, we found that the endocytic route involving Dynamin was especially associated with the uptake of ss-AgNPs. At the same time, it had a comparatively less effect on the ls-AgNPs, as analyzed through flow cytometry and fluorescence microscopy. On the other hand, AuNPs followed caveolin and dynamin-dependent endocytosis. This further establishes that the composition of the NPs also has an impact on the mechanism of internalization involved. However, interestingly, though the mechanism of entry varied, there was a minimal or in-significant difference in the internalization potential of the AgNPs compared to the AuNPs when cells were harvested after a similar time interval. Finally, the bi-metallic NPs showed a skewed preference towards internalization through macropinocytosis, as Nocodazole significantly decreased uptake of both types of dual NPs. We speculate that in the bi-metallic NPs, there is an alteration in the physico-chemical property, leading to differential uptake mechanism. Further studies are required in this direction to understand this differential uptake. The ss-AgNPs showed high cytotoxic potential. Interestingly, the bi-metallic NPs showed lower cytotoxicity after a similar time interval compared to the mono-metallic AgNPs. ICP-OES analysis confirmed that the presence of intracellular Ag ions upon bi-metallic NP treatment in MCF7 cells was low, providing a probable cause towards reduced cytotoxicity observed. Further future studies are required in this direction to precisely understand the role of size or physical parameters in the internalization of the NPs, say, how it varies with cell type

or change in the microenvironment. In the subsequent chapters, we analyze the intracellular effect of the internalized NPs, especially the AgNPs.

5.4 References

1 Heiligtag, F.J. and Niederberger, M. (2013) The fascinating world of nanoparticle research. *Materials today* 16 (7-8), 262-271

2 Liu, P. et al. (2013) Silver nanoparticles: a novel radiation sensitizer for glioma? *Nanoscale* 5 (23), 11829-11836

3 Zhang, S. et al. (2015) Physical principles of nanoparticle cellular endocytosis. *ACS nano* 9 (9), 8655-8671

4 Truong, N.P. et al. (2015) The importance of nanoparticle shape in cancer drug delivery. *Expert opinion on drug delivery* 12 (1), 129-142

5 Albanese, A. et al. (2012) The effect of nanoparticle size, shape, and surface chemistry on biological systems. *Annual review of biomedical engineering* 14, 1-16

6 Foroozandeh, P. and Aziz, A.A. (2018) Insight into cellular uptake and intracellular trafficking of nanoparticles. *Nanoscale research letters* 13 (1), 339

7 Wang, W. et al. (2019) The impact of nanoparticle shape on cellular internalisation and transport: what do the different analysis methods tell us? *Materials horizons* 6 (8), 1538-1547

8 Zhao, J. and Stenzel, M.H. (2018) Entry of nanoparticles into cells: The importance of nanoparticle properties. *Polymer chemistry* 9 (3), 259-272

9 Chithrani, B.D. et al. (2006) Determining the size and shape dependence of gold nanoparticle uptake into mammalian cells. *Nano letters* 6 (4), 662-668

10 Hsiao, I.L. et al. (2017) Effects of silver nanoparticles on the interactions of neuron-and glia-like cells: Toxicity, uptake mechanisms, and lysosomal tracking. *Environmental toxicology* 32 (6), 1742-1753

11 Sahay, G. et al. (2010) Endocytosis of nanomedicines. *Journal of controlled release* 145 (3), 182-195

12 Kou, L. et al. (2013) The endocytosis and intracellular fate of nanomedicines: Implication for rational design. *Asian journal of pharmaceutical sciences* 8 (1), 1-10

13 Horikoshi, S. and Serpone, N. (2013) *Microwaves in nanoparticle synthesis: fundamentals and applications*, John Wiley & Sons

14 Zucker, R. et al. (2013) Detection of silver nanoparticles in cells by flow cytometry using light scatter and far-red fluorescence. *Cytometry part A* 83 (10), 962-972

15 Feher, J. (2012) 2.5-Passive Transport and Facilitated Diffusion. Quantitative Human Physiology. Academic Press, Boston

16 Vercauteren, D. et al. (2010) The use of inhibitors to study endocytic pathways of gene carriers: optimization and pitfalls. *Molecular therapy* 18 (3), 561-569

17 Harush-Frenkel, O. et al. (2007) Targeting of nanoparticles to the clathrin-mediated endocytic pathway. *Biochemical and biophysical research communications* 353 (1), 26-32

18 Preta, G. et al. (2015) Dynasore-not just a dynamin inhibitor. *Cell commun signal* 13 (1), 24-31

19 Basagiannis, D. et al. (2017) Dynasore impairs VEGFR2 signalling in an endocytosis-independent manner. *Scientific reports* 7, 45035

20 Preta, G. et al. (2015) Dynasore-not just a dynamin inhibitor. *Cell communication and signaling* 13 (1), 24

Chapter- 6

Crosstalk between AgNPs and autophagy

Chapter-6

Crosstalk between AgNPs and autophagy

6.1 Overview

In the previous chapter, we have analyzed the route of entry of the synthesized NPs into the tumor cells. We have shown how the mechanism of entry varies with change in physicochemical parameters of the NPs. Thereafter, the associated cytotoxic potential of the NPs was also evaluated. The cytotoxic effect of the NPs was positively correlated with the proportion of entry of the mono-metallic NPs, and with the change in physical dimensions, the cytotoxic effect varied. Thereafter to have a holistic understanding of the intracellular phenomenon triggered by the NPs contributing to their cytotoxicity post internalization, we performed a further set of experiments. In this context, currently, it is unanimously accepted that AgNPs impart cytotoxicity in a dose-dependent manner in tumor cells, primarily through the generation of reactive oxygen species (ROS), and consequent activation of apoptosis or necrosis [1,2]. The other reported intracellular death-inducing mechanism, autophagy, is known to be induced by AgNPs as well; however, the role of autophagy in this context is controversially discussed in the literature. This cellular homeostatic process has been highly implicated in cancer and is often found to be imperative to tumor cell adaptation to stress; on the contrary, autophagy has also been reported to accentuate cell death [3]. We, along with few other studies have previously reported activation of protective autophagy upon exposure of tumor cells to AgNPs [4]; in a different context, we have also shown that conversely, autophagy can act as a pro-death mechanism [5]. Based on our understanding and existing evidence, we assume that the critical cellular process- autophagy cannot be strictly demarcated as pro-survival or pro-death; instead, it is dynamic, and its role can change temporally and, in a context, dependent manner. We also postulated that it might have a strong connection with other cellular processes like cellular internalization or

endocytic mechanisms. Regarding endocytosis, it is often considered that for an efficient autophagy a functional endocytic pathway is essential [6]; therefore, we assumed that the molecular forces driving autophagy in tumor cells might be cross-linked with activities at the plasma membrane level itself and hence might have a role in NP internalization, discussed in the earlier chapter. Therefore, analyzing the process of AgNP internalization, subsequent effect on intracellular trafficking might be tightly linked and associated with autophagy. Understanding these connections might be necessary for developing ways to allow AgNPs into the tumor cells and impart a higher curative effect.

In this chapter, we have used AgNPs of two different sizes ss-AgNP (small-sized AgNP, ~9 nm) and ls-AgNP (large-sized AgNP, ~19 nm) to explore how AgNPs modulate associated cellular events like autophagy and have made efforts to establish the connection between AgNP internalization, consequent trafficking and associated mechanism of toxicity with autophagy.

6.2 Results

6.2.1. AgNPs cause initial induction of autophagy-mediated by JNK activation

We investigated the effect of AgNPs on autophagy. As expected, both ss-AgNPs and ls-AgNPs at their IC50 dose led to an increase in LC3B-II, Beclin1, and Atg3 protein levels (**Fig 6.2.1 a, b & c**), predominant markers of autophagy. However, an increase in LC3B-II doesn't always correlate with autophagic flux, as it may indicate a blockage of autophagic flux as well [7]. We, hence, analyzed the expression level of p62, which, when degraded, means induction of flux and, when accumulates, signifies inhibition. At 1 and 6 h, an increase in LC3B-II was coupled with decreased p62 protein levels indicating induction of autophagy and probable trafficking of NPs towards lysosomes (**Fig 6.2.1 b & c**). The MAPK-JNK pathway has been implicated in the regulation of autophagy [4]. We observed that both ss-AgNPs and ls-AgNPs, at IC_{50} dose resulted in phosphorylation of JNK (**Fig 6.2.1 b**). Interestingly, pharmacological inhibition of JNK by SP600125 led to a drastic decrease in

LC3B-II levels (**Fig 6.2.1 d**). After 6 h of AgNP exposure, we also observed co-localization of transfected RFP-LC3 puncta with lysosomes (LysoTracker), which further confirmed autophagic flux induction (**Fig 6.2.1 e**).

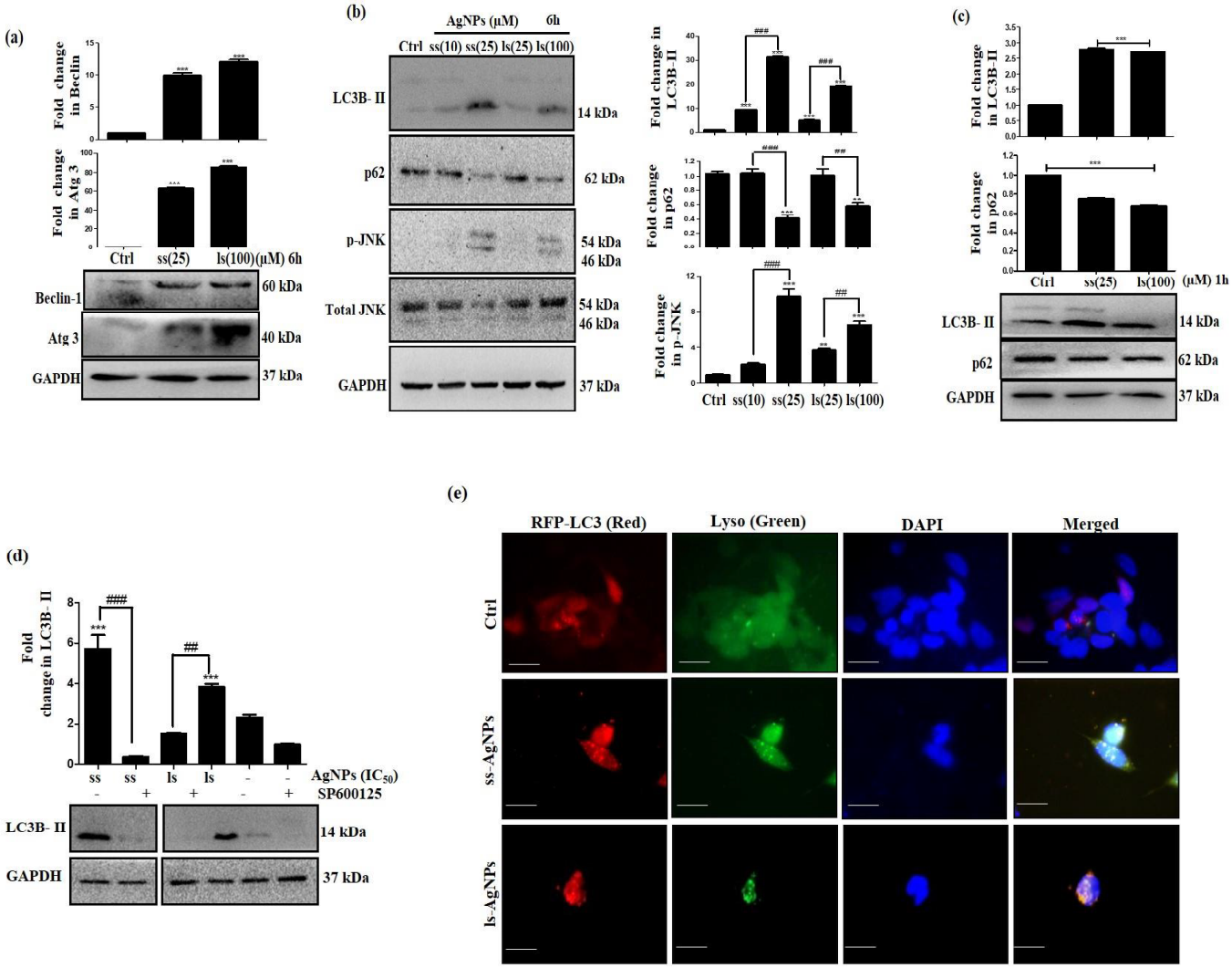

Figure 6.2.1. Analysis of early induction of autophagy and JNK signaling after AgNP exposure. **(a)** Immunoblot showing expression of Beclin1 and Atg3 after 6 h of treatment with AgNPs. (**b)** Immunoblot showing expression of LC3B-II, p62, and JNK after treatment with AgNPs for 6 h. **(c)**. Immunoblot showing expression of LC3B-II and p62 after 1 h of treatment with AgNPs **(d)**. Immunoblot showing expression of LC3B-II upon AgNPs treatment for 6 h after inhibiting JNK by

SP600125. Wherever mentioned, SP600125 (25 µM) was added 24 h before AgNP treatment. GAPDH served as a loading control. **(e)** Fluorescent microscopic images showing co-localization of LC3 (red) with lysosomes (LysoTracker green) after 6 h of AgNP treatment. Scale bar- 200 µm. [Symbol (*), (#), and ($) represent statistically significant differences with respect to untreated cells, AgNP-treated cells, and AgNP with inhibitor/inducer, respectively].

6.2.2. JNK activation and autophagy facilitate uptake of AgNPs

Several reports confirm a strong correlation between endocytosis and autophagy [8], we were, therefore, interested to know whether modulation of autophagy or JNK signaling has any effect on endocytosis of AgNPs as well. To prove the connection between autophagic flux and endocytic trafficking, we inhibited autophagic flux with CQ and monitored the endosomal marker, Rab7. Rab7 is implicated in the maturation of endosomes and autophagosomes, directing their fusion with lysosomes [9]. We observed an accumulation of Rab7 protein when cells were treated with both CQ and AgNPs when compared to only CQ **(Fig 6.2.2 a**), indicating that a flux blockage can affect trafficking. Interestingly, inhibition of autophagy or JNK signaling with CQ or SP600125, respectively, resulted in reduced uptake of AgNPs with a more pronounced effect on autophagy inhibition (**Fig 6.2.2 b**). In contrast, enhancing autophagy by Rapa, increased uptake of AgNPs (**Fig 6.2.2 c)**.

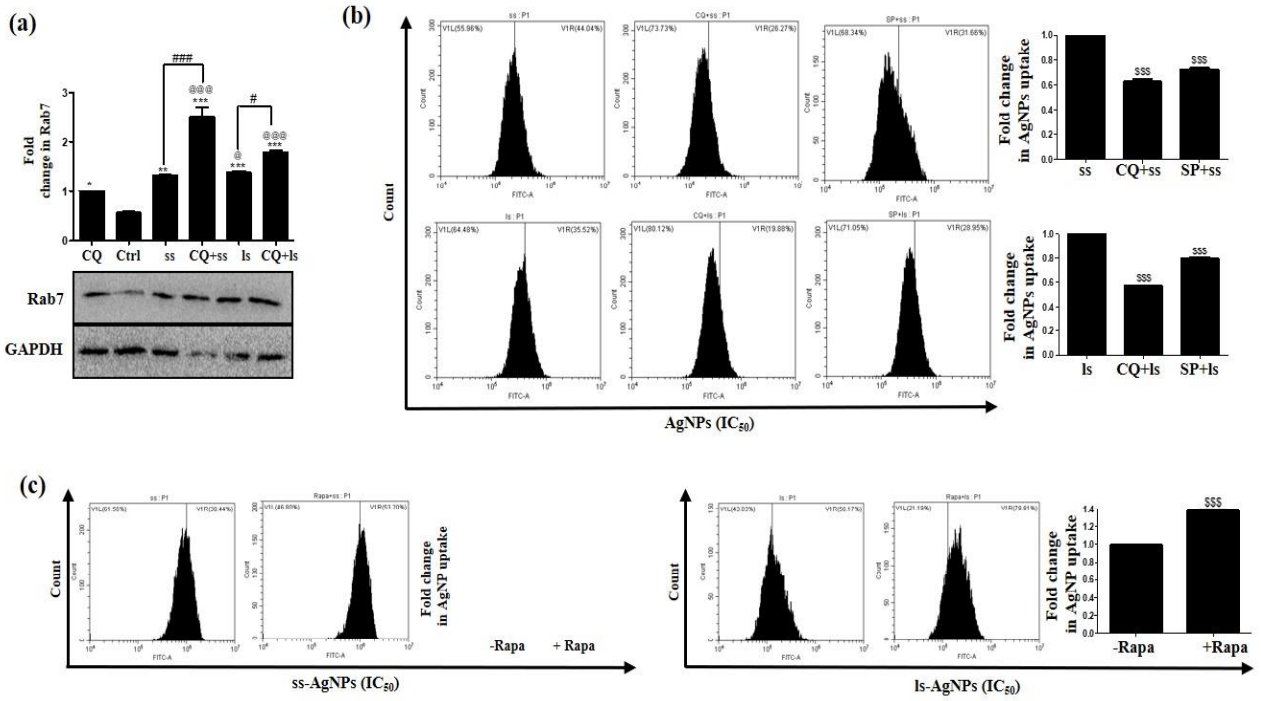

Figure 6.2.2. Correlation of JNK activation and autophagy signaling with NP uptake. **(a)** Immunoblot showing expression of Rab7 after treatment with IC_{50} dose of AgNPs for 6 h in the presence or absence of CQ (20 µM). [Symbol *, @ and # represent significant difference with respect to untreated cells, CQ-treated cells, and CQ plus NP treatment, respectively]. **(b)** Flow cytometric analysis of the uptake of AgNPs post inhibition of autophagy and JNK signaling. SP600125 (25 µM) was used to inhibit JNK signaling. **(c)** Flow cytometric analysis of the uptake of AgNPs post-treatment with Rapa (500 nM). [$ represents a significant difference with respect to AgNP treatment].

6.2.3. AgNP accumulation over time, in turn, disrupts trafficking and autophagic flux

Though there are previous reports that show activation of autophagic flux upon AgNP exposure [10], reports are scarce, demonstrating delayed effects of the NPs on the endo-lysosome trafficking. Interestingly we observed that prolonged exposure to ss-AgNPs/ls-AgNPs led to an increased accumulation of both LC3B-II and p62 protein, indicating a blockage of autophagic flux (**Fig 6.2.3 a**). We further observed an accumulation of Rab7 in a time-dependent manner upon AgNP exposure,

with maximal accumulation at 24 h. We also found a gradual increase in early endosomal marker EEA1 (early endosome antigen 1) after 24 h of AgNP treatment, suggesting that AgNPs perturb the endocytic trafficking process (**Fig 6.2.3 b**). The efficient management of protein aggregates is essential for cell viability, and autophagy primarily ensures this homeostasis [3]. AgNP exposed cells showed increased green ubiquitin (GFP-Ub) punctate dots with considerably more at 24 h than 6 h (**Fig 6.2.3 c**). Also, the total ubiquitinated protein content was higher at 24 h compared to 6 h of AgNP treatment (**Fig 6.2.3 d**). Induction of flux with Rapa promoted clearance of aggregates, and hence less ubiquitinated protein accumulation was observed with AgNP plus Rapa compared to only NPs (**Fig 6.2.3 d**).

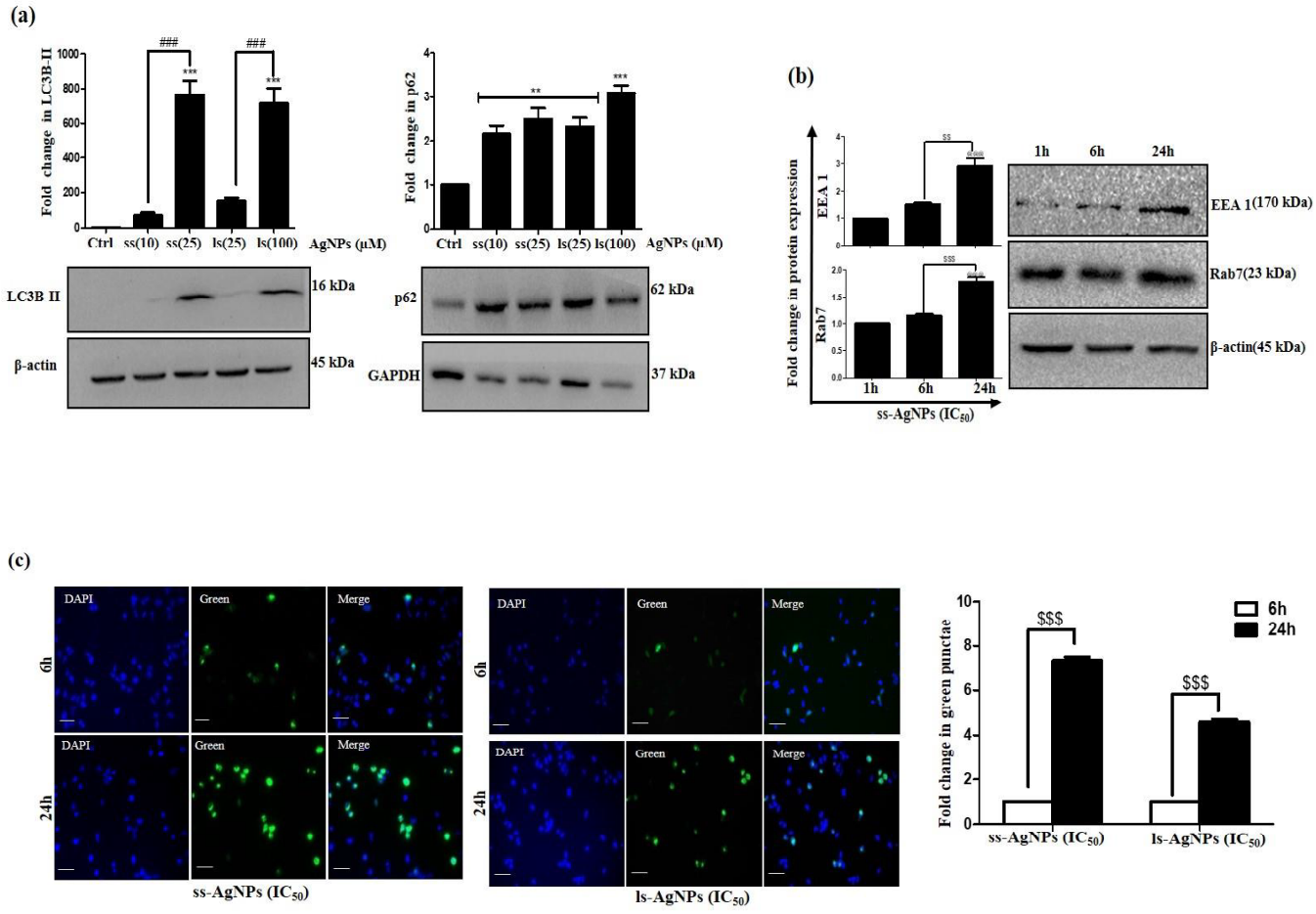

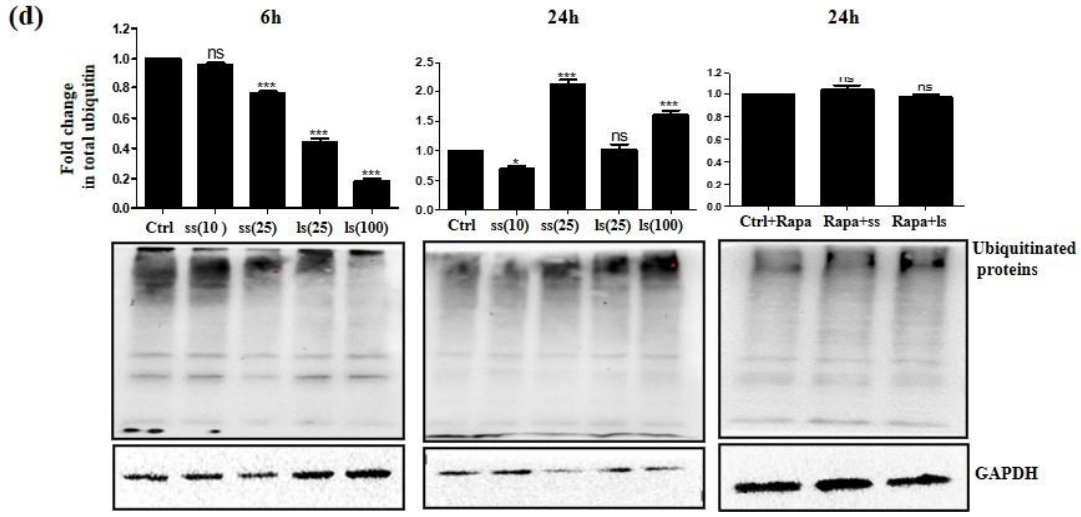

Figure 6.2.3. Analysis of temporal effect of AgNPs on vesicular markers and autophagic flux. **(a)** Immunoblots showing expression of LC3B-II and p62 after AgNP exposure for 24 h. **(b)** Immunoblots showing expression of EEA1 and Rab7 at different time points post-exposure to IC_{50} dose of AgNPs. **(c)** A comparative analysis of GFP-ub punctae green fluorescence after 6 h and 24 h of AgNP exposure. Scale bar- 200 µm. **(d)** Immunoblots showing total ubiquitinated protein after exposure to AgNPs. [Symbol *, #, @ and $ represent statistically significant difference with respect to untreated cells, AgNP-treated, 1 h AgNP treatment & 6/24 h of AgNP treatment respectively].

6.2.4. Prolonged AgNP exposure affects lysosomal stability

From the above experiment, we observed the blockage of trafficking and inhibition of autophagic flux to find the reason for the same. We checked the expression of LAMP1, a lysosomal-associated membrane protein, which was significantly ($$$) reduced at 24 h when compared to cells treated with AgNPs for 1 h or 6 h (**Fig 6.2.4 a**). We further observed a significant ($$$) decrease in LysoTracker (LT) fluorescence after 24 h of AgNP exposure (**Fig 6.2.4 b**). To further determine the stability of lysosomes in cells exposed to the NPs, we used acridine orange (AO). A loss of lysosomal integrity is generally quantified as a loss of AO red dots [11]. We observed a time-

dependent variation in AO red fluorescence, with a high red fluorescence at 6 h followed by a decrease by 24 h. This suggested there is probable lysosomal membrane permeabilization (LMP) or disruption of lysosomal integrity upon prolonged AgNP exposure (**Fig 6.2.4 c**). Interestingly, cells, when treated with Rapa along with AgNPs, did not show the decrease in LT fluorescence, as observed with only NP (**Fig 6.2.4 d**). Moreover, there was also increased retention of AO-red fluorescence with Rapa plus NP, indicating the existence of more functional lysosomes when Rapa is added (**Fig 6.2.4 e**).

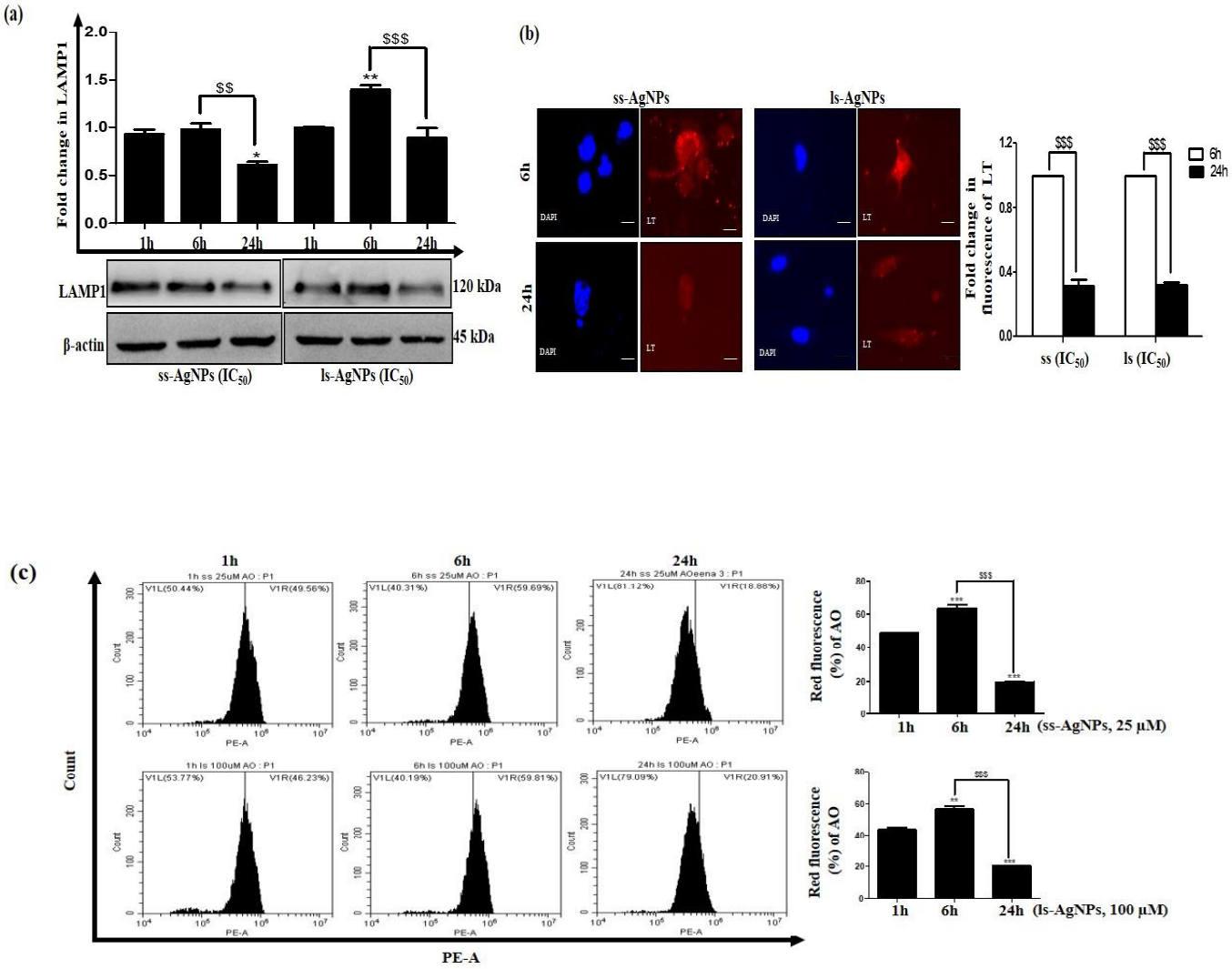

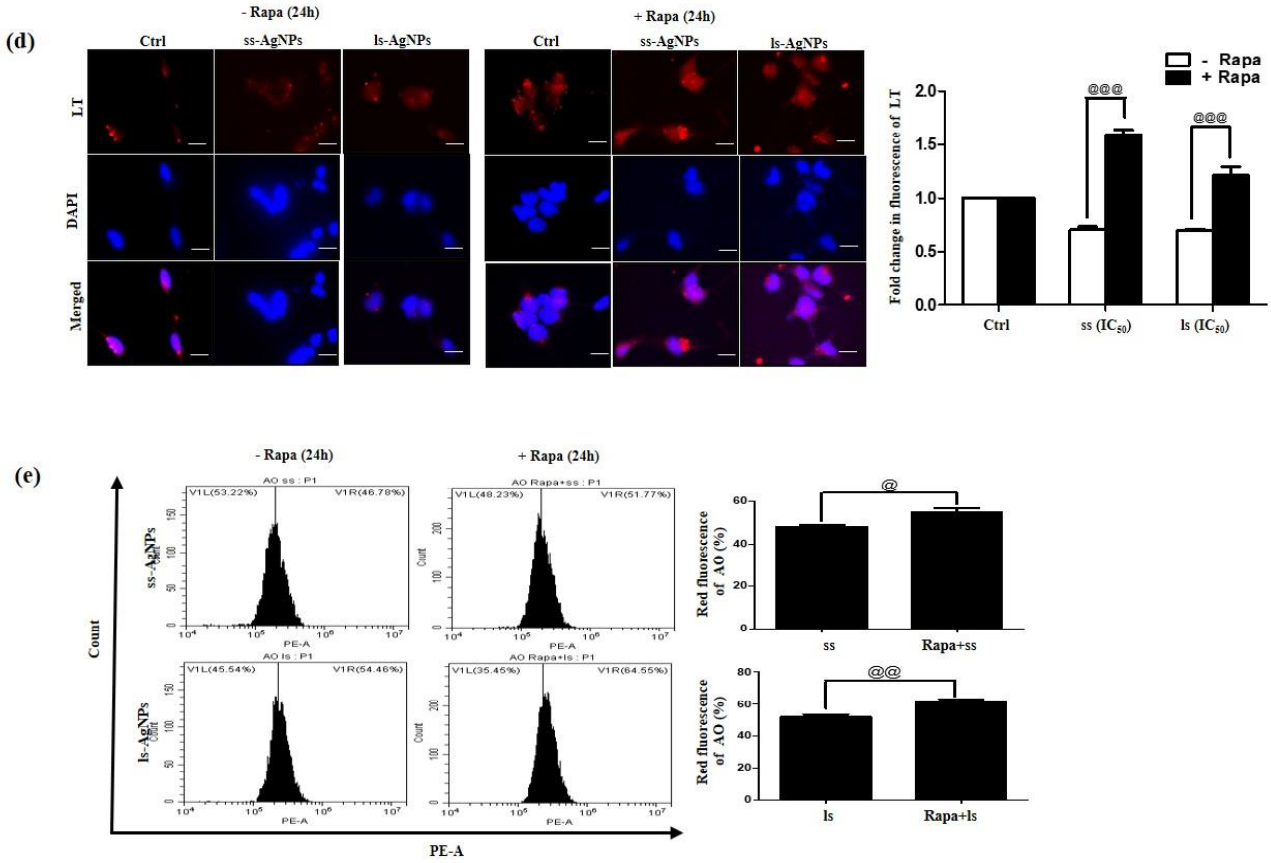

Figure 6.2.4. Effect of prolonged AgNP exposure on lysosomes. **(a)** Immunoblot showing relative LAMP1 expression at different time points post-AgNP exposure. **(b)** A comparative analysis of LysoTracker Red fluorescence between 6 h and 24 h post-exposure to AgNPs. **(c)** A comparative analysis of AO red fluorescence at different time points as analyzed through flow cytometer post-exposure to AgNPs. [Significant difference between 6 h and 24 h of AgNP treatment with respect to 1 h is represented as (*), whereas as ($) represents a significant difference between 6 h and 24 h]. **(d)** A comparative analysis of LysoTracker Red fluorescence with or without Rapa, post-exposure to AgNPs at IC_{50} dose for 24 h. **(e)** A comparative analysis of AO red fluorescence, in the presence or absence of Rapa, post-exposure to AgNPs at IC_{50} dose for 24 h. [Symbol @ represents statistically significant difference with respect to AgNP-treated cells]. Scale bar- 200 µm.

6.2.5. Autophagy regulates intracellular ROS and associated cytotoxicity as well

Autophagy is known to play a role in the regulation of intracellular ROS [12]. At an early time point (6 h), when enhanced autophagic flux was observed, ROS levels were low; however, at 24 h when flux was inhibited, we found a significantly (***) increased ROS [**Fig 6.2.5 a(i)**]. An increased ROS is a cause towards cytotoxicity, was proved when a ROS quencher, N-acetyl cysteine (NAC) resulted in significantly (###) increased cell viability after AgNP treatment, more prominently at 24 h [**Fig 6.2.5 a(ii)**]. We thereafter inhibited autophagy by CQ and measured ROS. An enhanced ROS accumulation was observed along with increased cytotoxicity [**Fig 6.2.5 b(i) & (ii)**]. Interestingly, a significant (***) decrease in expression of LC3B-II protein levels was also observed after AgNP treatment in cells pre-exposed to NAC; this confirms the role autophagy in reducing ROS levels [**Fig 6.2.5 b(iii)**]. Further, upon genetic ablation of ATG5 with si-ATG5, increased cytotoxicity to ss-AgNPs (~1.5 fold) and ls-AgNPs (~1.4 fold) was observed [**Fig 6.2.5 b(iv) & (v**)]. AgNP-induced accumulation of ROS and associated cytotoxicity was reduced when the cells were treated with Rapa before NP exposure (**Fig 6.2.5 c**). We thereafter checked for mitochondrial membrane potential (MMP; $\Delta\Psi M$) after AgNP exposure using JC-1. Flow cytometric analysis showed a collapse in MMP in cells treated with AgNPs for 24 h (**Fig 6.2.5 d**). As expected, a decrease in MMP was associated with apoptosis as confirmed by AnnexinV and PI staining; however, further extending AgNP exposure to 48 h increased cell population positive for PI only [**Fig 6.2.5 e(i**)]. AgNP induced apoptosis was further confirmed by observing a reduction in expression of total PARP protein upon exposure to IC_{50} dose of AgNPs for 24 h [**Fig 6.2.5 e(ii**)].

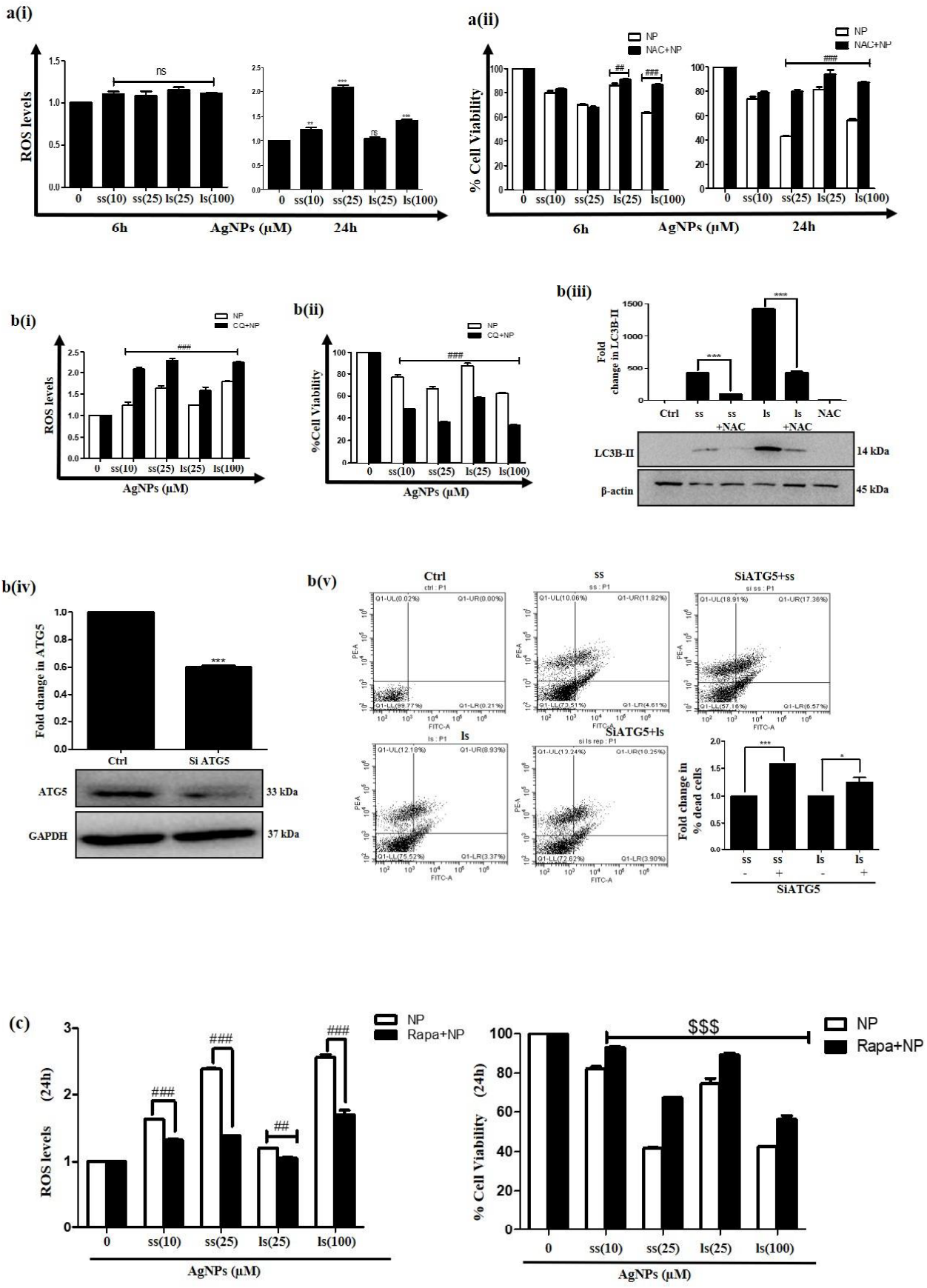
a(i)
ROS levels
ns
0 ss(10) ss(25) ls(25) ls(100)
6h
AgNPs (µM)
24h
a(ii)
NP
NAC+NP
% Cell Viability
##
###
6h
AgNPs (µM)
24h
b(i)
NP
CQ+NP
ROS levels
###
AgNPs (µM)
b(ii)
NP
CQ+NP
%Cell Viability
###
AgNPs (µM)
b(iii)
Fold change in LC3B-II
Ctrl ss ss ls ls NAC
+NAC +NAC
LC3B-II
14 kDa
β-actin
45 kDa
b(iv)
Fold change in ATG5
Ctrl
Si ATG5
ATG5
33 kDa
GAPDH
37 kDa
b(v)
Ctrl
ss
SiATG5+ss
ls
SiATG5+ls
Fold change in % dead cells
SiATG5
c
NP
Rapa+NP
ROS levels (24h)
AgNPs (µM)
$$$
% Cell Viability (24h)
AgNPs (µM)

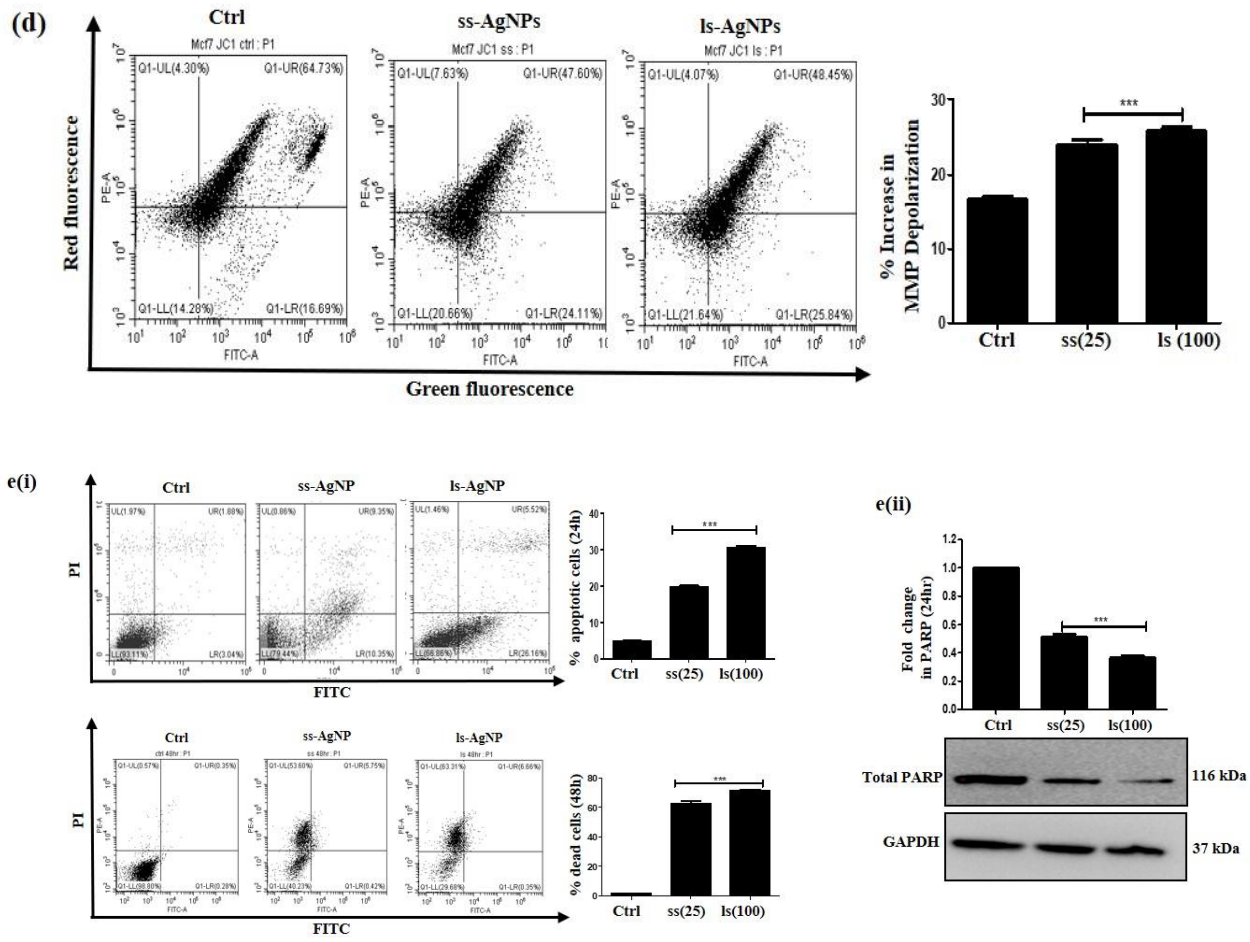

Figure 6.2.5. Analysis of intracellular ROS generation and cytotoxicity in context to autophagy status. **[a(i)]** Fold change in intracellular ROS levels post-exposure to AgNPs for 6 h & 24 h, **(ii)** MTT assay analyzing cell viability after 6 h & 24 h of AgNP treatment, in presence or absence of NAC (20 mM). **[b(i)]** Fold change in intracellular ROS levels post-exposure to AgNPs for 6 h in the presence or absence of CQ (20 µM). **(ii)** MTT assay measuring cell viability post-exposure to AgNPs for 6 h in the presence or absence of CQ. **(iii)** Immunoblots showing expression of LC3B-II protein after 24 h of AgNP treatment with or without NAC. **(iv)** Immunoblots showing expression of ATG5 after treating the cell with siATG5. **(v)** AnnexinV/PI staining representing the percentage of dead cells post-exposure to IC_{50} dose of AgNPs for 24 h, with or without silencing of ATG5, as analyzed through flow cytometry. **(c)** Fold change in intracellular ROS levels and cell viability analysis post-exposure to AgNPs for 24 h in the presence or absence of Rapa. **(d)** Flow cytometric analysis of

MMP with JC-1 dye in cells treated with IC_{50} dose of AgNPs for 24 h. **[e (i)]** Dot plots of AnnexinV/PI staining post-exposure to IC_{50} dose of AgNPs for 24 h and 48 h, respectively, as analyzed through flow cytometry. **(ii)** Immunoblots showing expression of total PARP after exposure of IC_{50} dose of AgNPs for 24 h. [Symbol (*) and (#) represent a significant difference in AgNP-treated cells with respect to untreated control and specific inhibitor, respectively].

6.3 Discussion

In this chapter, we have characterized the dynamic crosstalk that exists between AgNP and autophagy in the tumor cells. We have shown that a perturbation of functional autophagic flux by CQ, an autophagy inhibitor, significantly affects the internalization of AgNPs. The internalized AgNPs, in turn, shows a temporal effect on the process of autophagy as well. Contrarily, the autophagy inducer Rapa enhances the intracellular uptake of the NPs. Post internalization, we analyzed the signaling pathways triggered by the NPs and their correlation with autophagy. The ss-AgNPs and ls-AgNPs, at their respective IC_{50} doses, exhibited induction of autophagy-mediated through upstream activation of JNK signaling. Autophagy induction was marked by increased LC3B-II and decreased p62 protein levels. Since LC3B-II was cleared by autophagy, we observed a co-localization of LC3B-II with the labeled lysosomes post-AgNP exposure. However, this induction of flux was restricted to early time points of exposure only, like 1 h and 6 h. But, at the later time-point like 24 h post-exposure, increased protein levels of p62, LC3B-II, and ubiquitinated proteins was observed, indicating inhibition of flux, associated with pronounced cytotoxicity. We further found that at later time points, and inhibition of flux was also associated with a disruption of vesicular trafficking and lysosomal damage. We assume that post-exposure to NPs, the tumor cells uptake the NPs, and a functional flux is required for this uptake. Thereafter, cells direct and converge the endocytic route towards lysosomes in an attempt to probable sequestration and degradation of the

internalized NPs in the lysosomes. Here, functional autophagy also helps to limit intracellular ROS. However, prolonged exposure, in turn, negatively impacts the lysosomal function and hence a subsequent inhibition of autophagic flux over time. Impaired autophagy thus is also associated with enhanced intracellular accumulation of ROS, after prolonged AgNP exposure. Again, the use of autophagy inducer, rapamycin diminished ROS levels, and mitigated ROS-induced cytotoxicity. **Figure 6.3** is the schematic representation of summarized results. Overall, from this study, we show that autophagy dynamically changes over time, suggesting that it might be misleading to assign one particular function to autophagy. This temporal divergence of autophagy and its association with ROS necessitates further investigations into selective autophagy like, mitophagy, which we have studied in the next chapter.

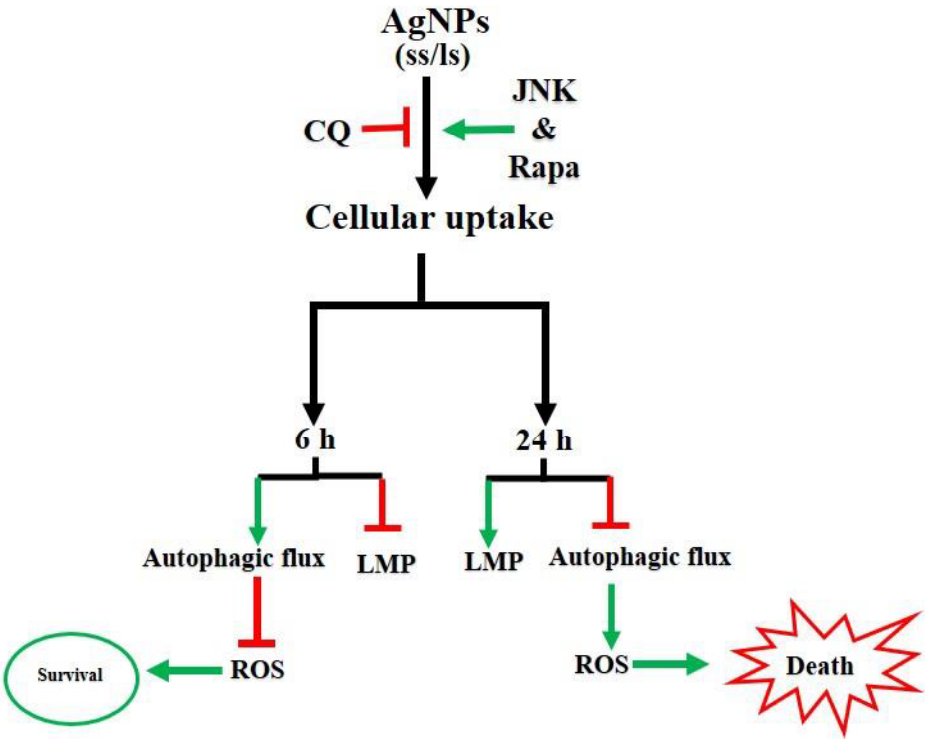

Figure 6.3. Schematic representation of the crosstalk between AgNPs and autophagy.

6.4 References:

1 Carlson, C. et al. (2008) Unique cellular interaction of silver nanoparticles: size-dependent generation of reactive oxygen species. *The journal of physical chemistry B* 112 (43), 13608-13619

2 Hussain, S.M. et al. (2005) In vitro toxicity of nanoparticles in BRL 3A rat liver cells. *Toxicol in vitro* 19 (7), 975-983

3 Galluzzi, L. et al. (2017) Molecular definitions of autophagy and related processes. *EMBO J* 36 (13), 1811-1836

4 Fageria, L. et al. (2017) Biosynthesized protein-capped silver nanoparticles induce ros-dependent proapoptotic signals and prosurvival autophagy in cancer cells. *ACS omega* 2 (4), 1489-1504

5 Xu, Y. et al. (2015) Silver nanoparticles impede phorbol myristate acetate-induced monocyte–macrophage differentiation and autophagy. *Nanoscale* 7 (38), 16100-16109

6 Lamb, C.A. et al. (2013) Endocytosis and autophagy: Shared machinery for degradation. *Bioessays* 35 (1), 34-45

7 Zhang, X.J. et al. (2013) Why should autophagic flux be assessed? *Acta pharmacol sin* 34 (5), 595-599

8 Tooze, S.A. et al. (2014) Endocytosis and autophagy: exploitation or cooperation? *Cold spring harb perspect biol* 6 (5), a018358

9 Jager, S. et al. (2004) Role for Rab7 in maturation of late autophagic vacuoles. *Journal of cell science* 117 (Pt 20), 4837-4848

10 Lee, Y.-H. et al. (2014) Cytotoxicity, oxidative stress, apoptosis and the autophagic effects of silver nanoparticles in mouse embryonic fibroblasts. *Biomaterials* 35 (16), 4706-4715

11 Paglin, S. et al. (2001) A novel response of cancer cells to radiation involves autophagy and formation of acidic vesicles. *Cancer research* 61 (2), 439-444

12 Dash, S. et al. (2018) TGF-β2-induced EMT is dampened by inhibition of autophagy and TNF-α treatment. *Oncotarget* 9 (5), 6433

Chapter- 7

Effect of AgNPs on organelle homeostasis

Chapter-7

Effect of AgNPs on organelle homeostasis

7.1 Overview

In the previous chapter, we have discussed the crosstalk between AgNPs and autophagy. The NPs exerted a temporal effect on the autophagic flux. Autophagy, in turn, was responsible for the regulation of intracellular ROS levels, and inhibition of flux resulted in varied effects extending from oxidative stress, ubiquitinated protein accumulation, and lysosomal dysfunction leading to cell death. The generation of oxidative stress and associated intracellular effects are intricately linked to the health of vital cellular organelles like mitochondria and endoplasmic reticulum (ER). This prompted us to investigate mitochondrial dynamics after NP exposure and associated events like mitophagy, ER stress, which might help in better understanding of AgNP induced effects on organelle function and how it changes with autophagy dynamics observed earlier in the breast cancer cells.

Mitochondria undergo dynamic changes that are crucial for maintaining the proper functioning of mitochondria, and its deregulation can contribute to the onset of cellular or metabolic dysfunction leading to diseases [1]. Importantly, the accumulation of dysfunctional mitochondria is often a source of enhanced ROS, which in turn results in increased oxidative stress. Mitochondria undergo repetitive cycles of fusion or fission, which have evolved as a protective mechanism in response to stress. In other words, the cellular mitochondrial quality control system continuously maintains stringent regulation of mitochondrial dynamicity [2]. For example, mitochondrial damage or depolarization is often succeeded by fission event removing dysfunctional mitochondria through selective autophagy, like, mitophagy.

Interestingly, the endoplasmic reticulum (ER) has emerged as an organelle that is reported to contribute in regulating mitochondrial health, introducing a relatively new model

that links ER with cellular death involving changes in mitochondrial dynamicity [3]. The disturbed proteostasis of a cell can give rise to ER stress, a common phenomenon in different disorders, including cancer. During ER stress, a cascade of events including unfolded protein response (UPR), ER-associated degradation (ERAD) coupled to autophagy, and regulation of mitochondrial dynamics is initiated by the cell to restore the cellular function [4]. Thus, understanding the regulation of ER stress and mitochondrial network regulation may facilitate the understanding of the precise cellular events induced by AgNPs coupled to autophagy.

In this chapter, we shall investigate how ss-AgNPs affect organelles like, mitochondria and ER. The changes in organelle dynamicity shall be monitored and correlated with cellular autophagy status. Further, how this dynamicity regulates the fate of tumor cells shall be explored.

7.2 Results

7.2.1 AgNP treatment induces accumulation of TOM20 protein

Though mitochondria have their own genome, around 90% of mitochondrial proteins are encoded in the nucleus, which is synthesized by ribosomes in the cytoplasm and then transported to the mitochondria. TOM20, a translocase of the outer mitochondrial membrane (OMM), is a multiunit translocase involved in the import of cytoplasmic proteins into mitochondria [5]. To check for the effect of AgNPs on mitochondrial dynamicity, we labelled mitochondria with anti-TOM20 antibody and also analyzed protein levels of TOM20 after AgNP treatment for 1, 6, and 24 h through immunoblotting and compared it with untreated control. The TOM20 protein is anchored to OMM and hence its distribution provides an idea about the mitochondrial network and its interconnectivity. The fluorescence microscopy enabled us to visualize that there was a drastic change in mitochondrial dimensions and

significant loss of mitochondrial interconnectivity overtime after AgNP exposure. While untreated cells showed a highly connected elongated network of mitochondria, a disperse morphology without extended and elongated inter-cellular connection shown with white and yellow arrows, (**Fig 7.2.1 a)** was visible at later time points, more prominent at 6 h. Further, in a number of cells, at later time points, like 24 h, we noted mitochondrial clustering more preferentially close to the nucleus shown with green arrows, (**Fig 7.2.1 a)** after NP exposure; this was also accompanied by an overall decrease in the surface area of the cell. This peri-nuclear clustering was in contrast to untreated cells where mitochondria were found to be evenly distributed in a more homogenous pattern. In addition, immunoblot analysis showed an accumulation of TOM20 protein over time (**Fig 7.2.1 b**). The above experiments are indicative of a disruption of mitochondrial distribution and hence putatively a dysregulation of its function after AgNP exposure, which was further investigated.

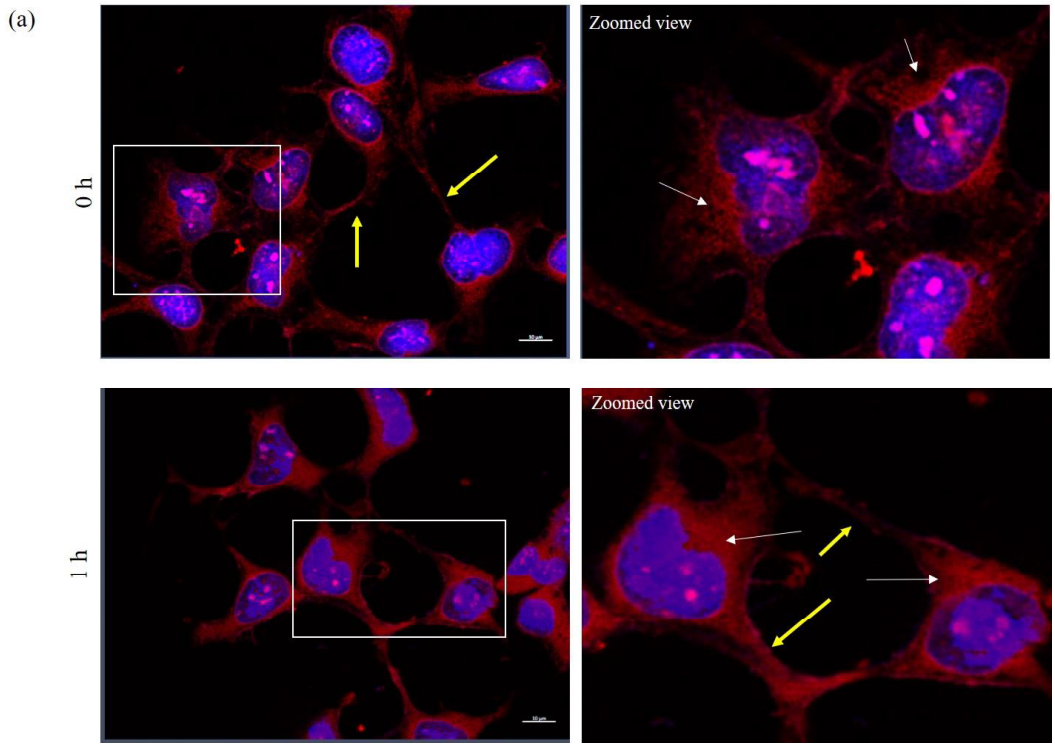

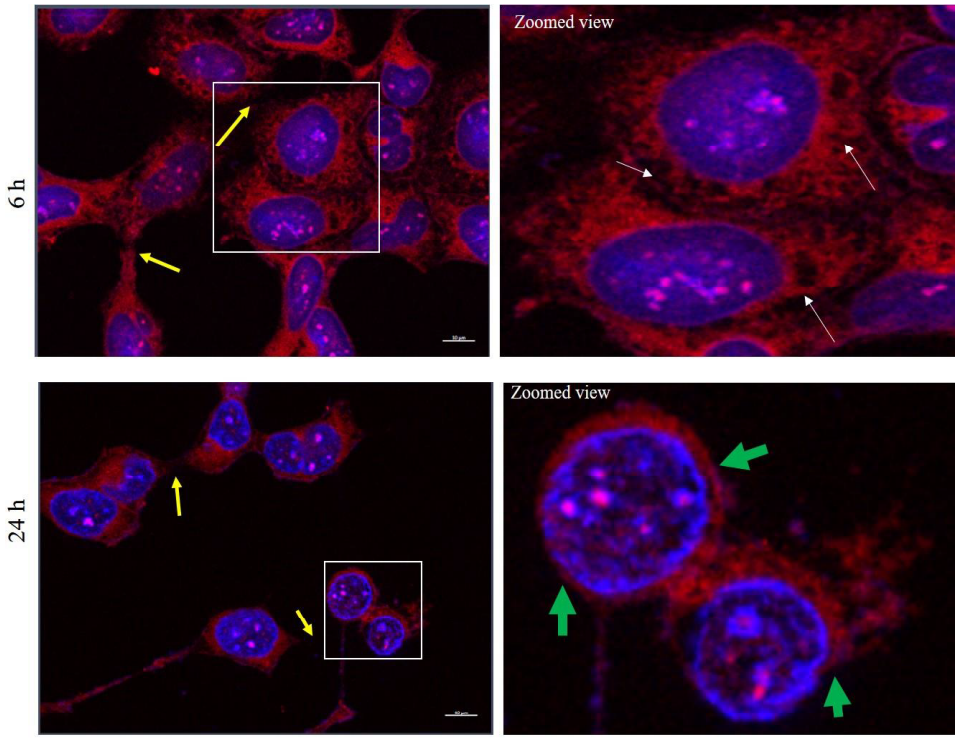

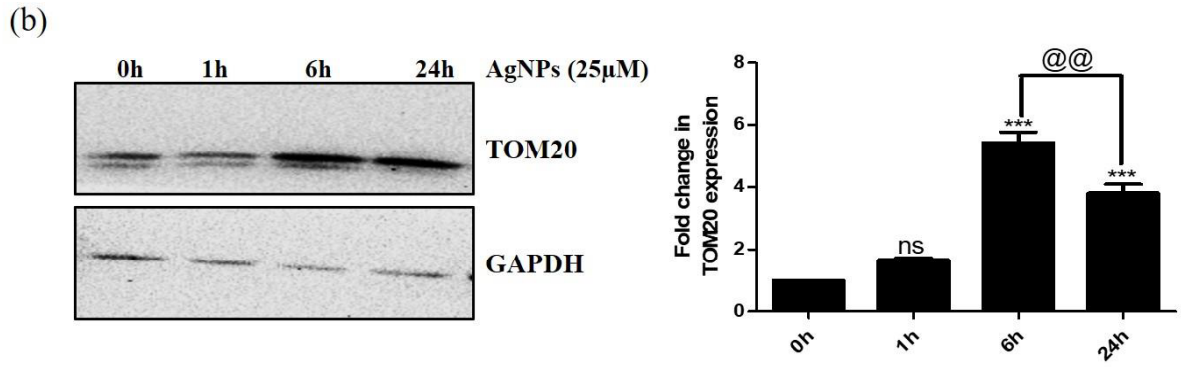

Figure 7.2.1. Analysis of mitochondrial TOM20 protein expression upon AgNP treatment. **(a)** Immunofluorescence images of MCF-7 cells treated with AgNPs (25 µM) for different time points. Cells were stained with anti-rabbit TR conjugated secondary antibody against TOM20 (red). Scale bar- 10 µm. The area in the inset is zoomed and represented with each image. **(b)** Immunoblots showing the expression of TOM20 after AgNP treatment for 1, 6, and 24 h. GAPDH was used as a loading control. The symbol (*) represents the significance

level of with respect to untreated cells, (@) represents a significant difference between 6 and 24 h AgNP treated cells.

7.2.2 AgNPs cause change in Mitotracker (MT) Red fluorescence

Mitochondria are a dynamic organelle that undergoes continuous fission and fusion cycles in response to stimuli, and we are aware that tumor cells modulate their mitochondrial dynamicity and its associated function to adapt to various stressful conditions [6]. To confirm alteration in the TOM20 expression pattern, as observed above, we further analyzed mitochondrial distribution after AgNP exposure by staining the cells with MT. **Figure 7.2.2** represents fluorescence microscopy images of treated cells along with the zoomed view of inset. As evident from the images, the mitochondria were evenly distributed in the cellular cytoplasm with prominent interconnections visible at both 0 h (untreated) and 1 h of exposure; however, the interconnections were lost at 6 h, and 24 h and the localization was more clustered at the later time points. Also, the number of fragmented punctate morphology of mitochondria was more evident at 24 h of exposure suggesting probable fission like process that sets in after prolonged exposure; however, at 6 h elongated mitochondrial structures were still visible. We speculate that the cells at 6 h of exposure might try to combat the stress; however, at 24 h, increased fission predominates, leading to loss of mitochondrial function and cell death, as observed earlier. Interestingly, an analysis of overall red fluorescence intensity showed the highest at 24 h (Fig 7.2.2); and the fluorescence observed might be directly proportional to the mitochondrial content or mass [7]. Generally, the fission of mitochondria is reported to cause its fragmentation, followed by its clearance through mitophagy [8]. The increase in fluorescence intensity thus might indicate the lack of removal of the mitochondrial fragments leading to their accumulation. This might be attributed to an inhibition of autophagic flux observed at 24 h.

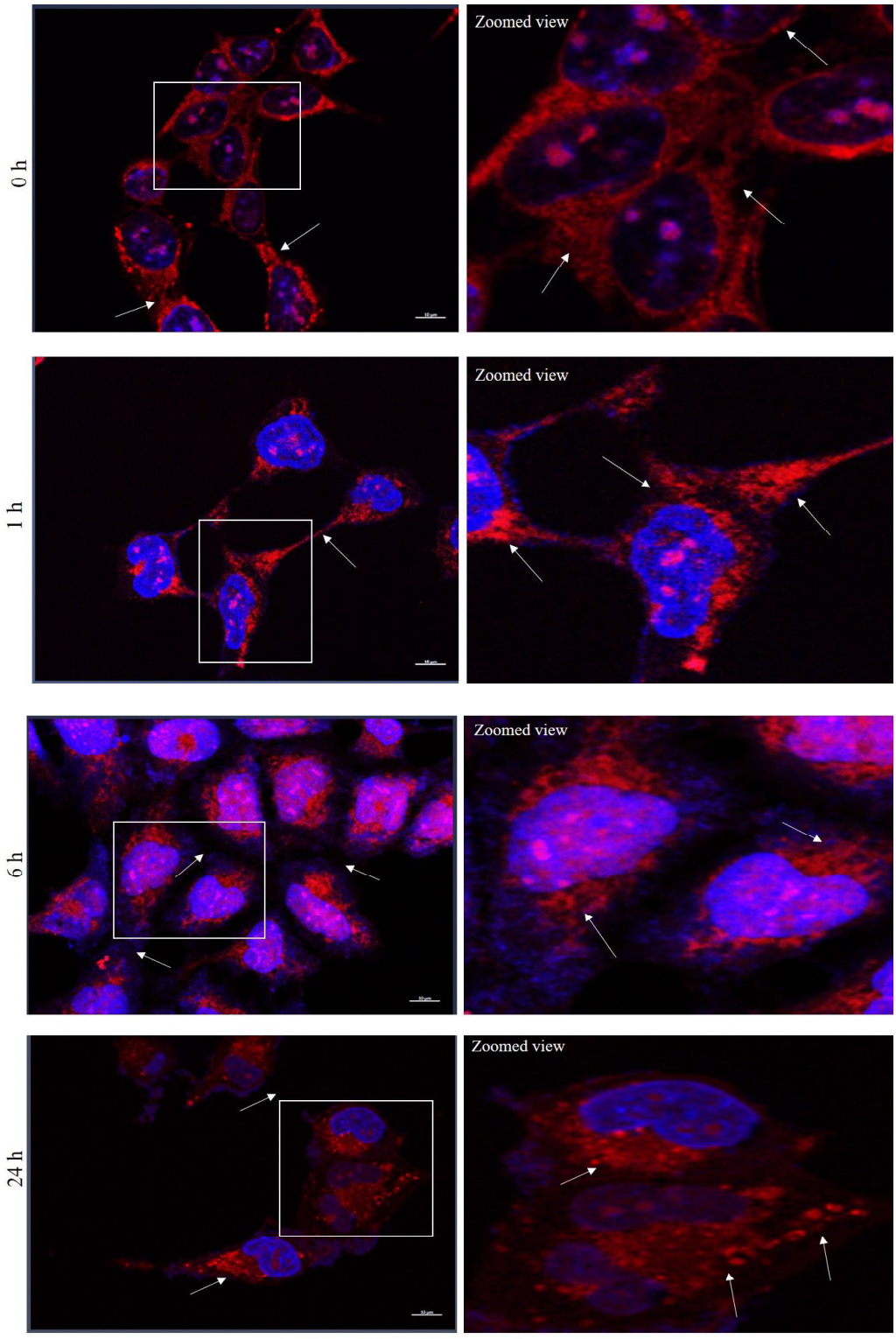

AgNPs (25 µM), Mitotracker (red), DAPI (blue)

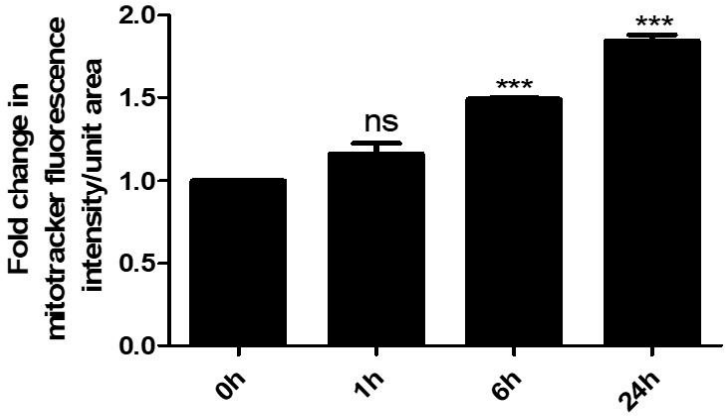

Figure 7.2.2. Visualization of mitochondria after AgNP exposure. Fluorescence microscopic images of MT (red) stained MCF-7 cells after treatment with AgNPs (25 µM) for 1, 6, and 24 h. The area in the inset is zoomed and represented with each image. Scale bar- 10 µm. Fluorescence intensity was calculated and represented as a bar graph. The symbol (*) denotes the significance level with respect to untreated cells, (@) represents a significant difference between 6 and 24 h AgNP treated cells.

7.2.3 Prolonged exposure of AgNPs recruits the ubiquitin ligase- Parkin

As discussed above in the earlier experiments, we observed an increased accumulation of fragmented mitochondria with an amplified intensity of Mitotracker Red fluorescence at 24 h of AgNP exposure. A selective degradation of mitochondria- mitophagy is frequently coupled with mitochondrial fragmentation. The mitophagy pathway is often triggered by inducing the translocation and recruitment of Parkin, a ubiquitin ligase from the cytoplasm to fragmented mitochondria [9], which tags the mitochondria for clearance through lysosomes [10, 11]. We transfected the MCF-7 cells with mcherry-Parkin plasmid and then exposed them to the AgNPs. Interestingly, we observed a distinct accumulation of Parkin-Red fluorescence after 24 h of AgNP exposure compared to either untreated control (0 h) or 6 h (**Fig 7.2.3. a**). This is indicative of an increased Parkin recruitment at 24 h coupled to fragmented mitochondria

observed earlier. We hypothesized that inhibition of autophagic flux, as observed at 24 h, prevents the tagged mitochondria from getting cleared off by mitophagy, though they are marked for degradation by Parkin recruitment. To confirm the same, we stained the cells with AO, that stains acidic compartments in a cell, primarily the lysosomes [12]. **Figure 7.2.3 b** confirms a decrease in AO fluorescence at 24 h of AgNP exposure, indicating that coupled to inhibition of autophagic flux observed earlier, at 24 h, there is also a reduction in the cellular lysosomal number thus hindering clearance and resulting in accumulation of Parkin tagged mitochondria at 24 h.

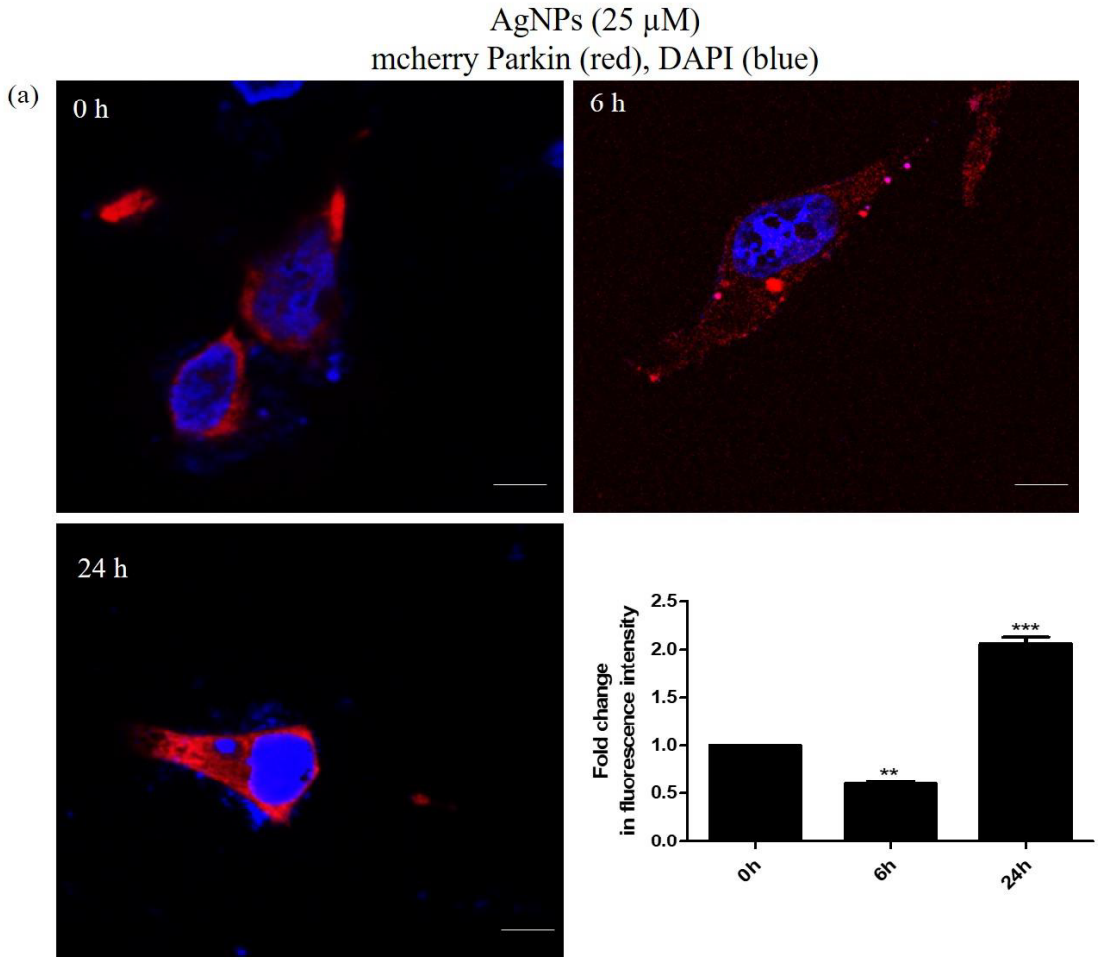

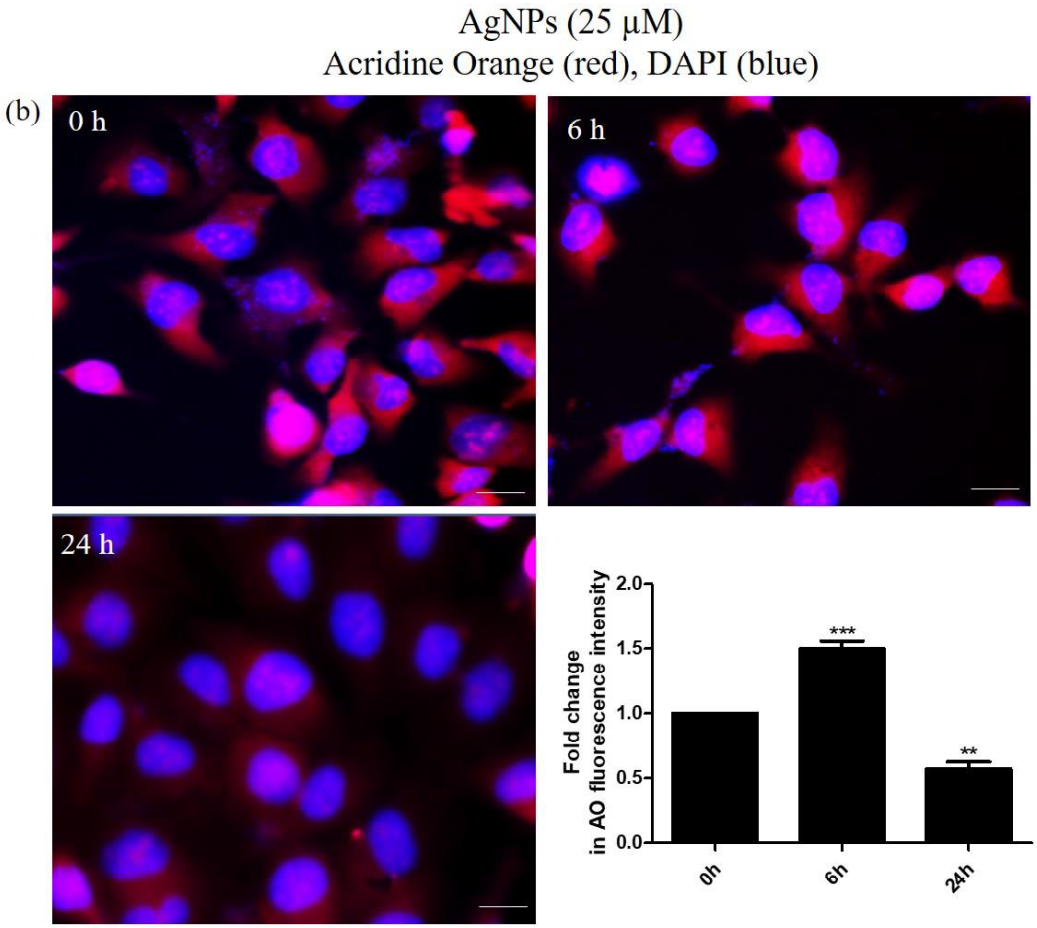

Figure 7.2.3. Analysis of Parkin expression after AgNP treatment. **(a).** Fluorescence images of cells transfected with mCherry Parkin (red) followed by exposure to AgNPs for 6 and 24 h. Fold change in fluorescence intensity is represented as bar graphs. **(b).** Fluorescence images of AgNP treated cells for 6 and 24 h after staining with AO. The bar graph represents the fold change in fluorescence intensity. Scale bar- 10 µm. The symbol (*) denotes the significance difference levels of AgNP treated cells with respect to untreated cells.

7.2.4 Inhibition of autophagic flux causes early mitochondrial fission

From the above results, we conclude that prolonged exposure to AgNPs inhibits autophagic flux, reduces the lysosomal number, and results in increased accumulation of mitochondria with fragmented morphology due to lack of clearance of Parkin tagged mitochondria. Here,

we hypothesized that an inhibition of flux associated with increased ROS generation, as shown earlier, is the cause towards the observation of mitochondria with fragmented morphology after AgNP exposure. To confirm the same, we treated the cells with chloroquine diphosphate (CQ), an inhibitor of autophagic flux, or Rapamycin (Rapa), a known autophagy inducer alongside AgNP exposure for 6 and 24 h. Interestingly, inhibition of flux by CQ resulted in the appearance of fragmented morphology of mitochondria even at 6 h of exposure to the NPs, quite unlike to what observed earlier with only NP treatment. Further, the intercellular connections almost disappeared upon CQ treatment, as early as 6 h (**Fig 7.2.4 a**). These events were strikingly similar to 24 h AgNP treated cells. However, the addition of Rapa had a contrasting effect, as it prevented the appearance of fragmented morphology and mitochondrial interconnections were still visible at 24 h after AgNP and Rapa treatment (**Fig 7.2.4 a**). The fact that fragmentation sets in earlier, if the flux is inhibited pharmacologically authenticates the contribution of AgNP induced inhibition of autophagic flux in the deterioration of mitochondrial health and/or appearance of fragmented morphology of mitochondria. This was further confirmed when we observed a significant ($^{###}$) decrease in the protein expression level of OPA1 (optic atrophy 1), a protein of the inner membrane of mitochondria involved in the fusion of mitochondria, in AgNP plus CQ treated cells compared to only AgNP at 6 h of exposure [13]. In contrast, the protein MFF (mitochondrial fission factor), known to recruit Drp1 (dynamin-related protein 1) [14], showed increased expression with AgNP plus CQ treatment (**Fig 7.2.4 b**). This further proves that inhibition of flux reduces mitochondrial fusion and induces fission factors resulting in mitochondrial fragmentation.

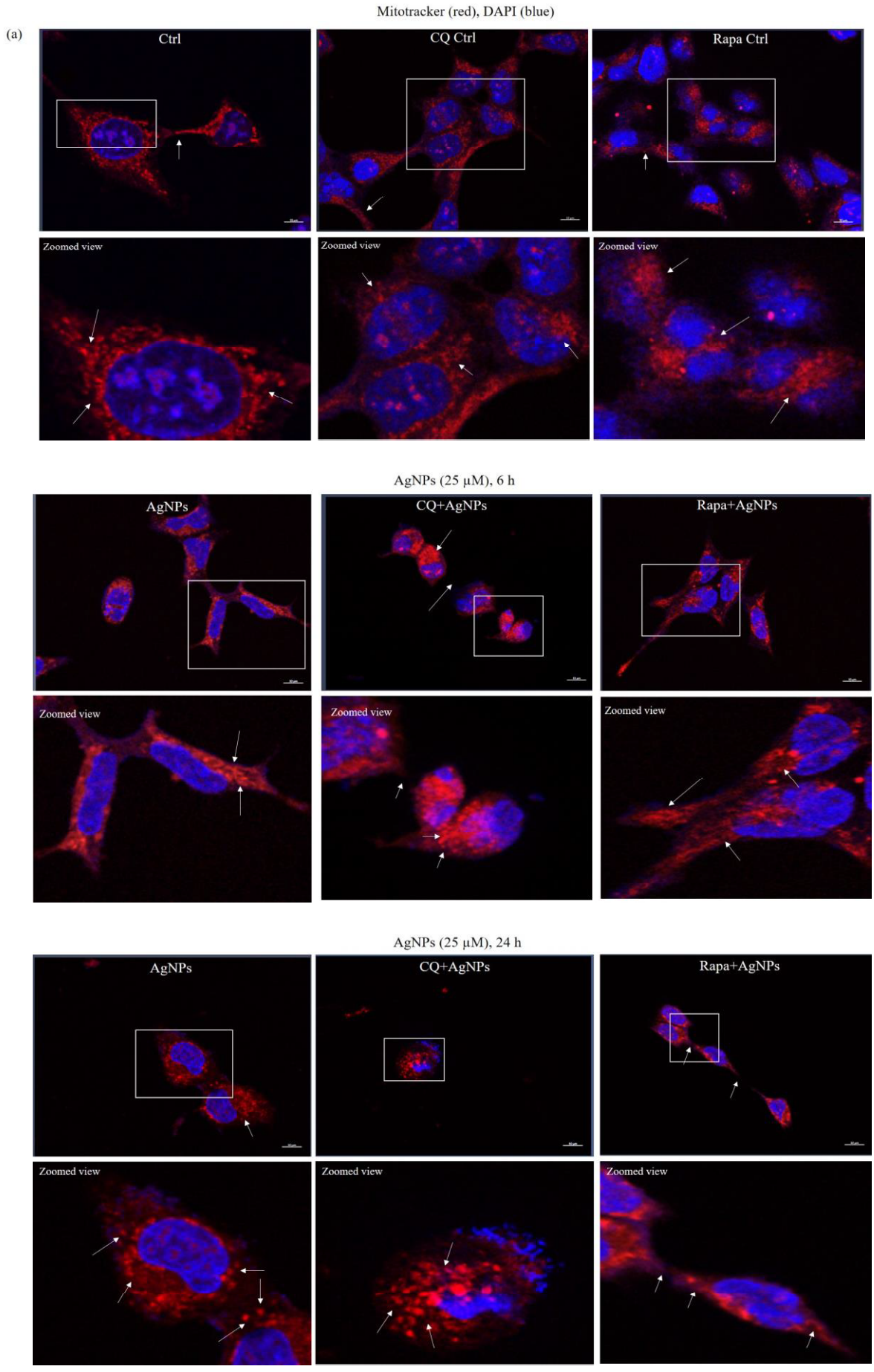
Mitotracker (red), DAPI (blue)
(a)
Ctrl
CQ Ctrl
Rapa Ctrl
Zoomed view
Zoomed view
Zoomed view
AgNPs (25 μM), 6 h
AgNPs
CQ+AgNPs
Rapa+AgNPs
Zoomed view
Zoomed view
Zoomed view
AgNPs (25 μM), 24 h
AgNPs
CQ+AgNPs
Rapa+AgNPs
Zoomed view
Zoomed view
Zoomed view

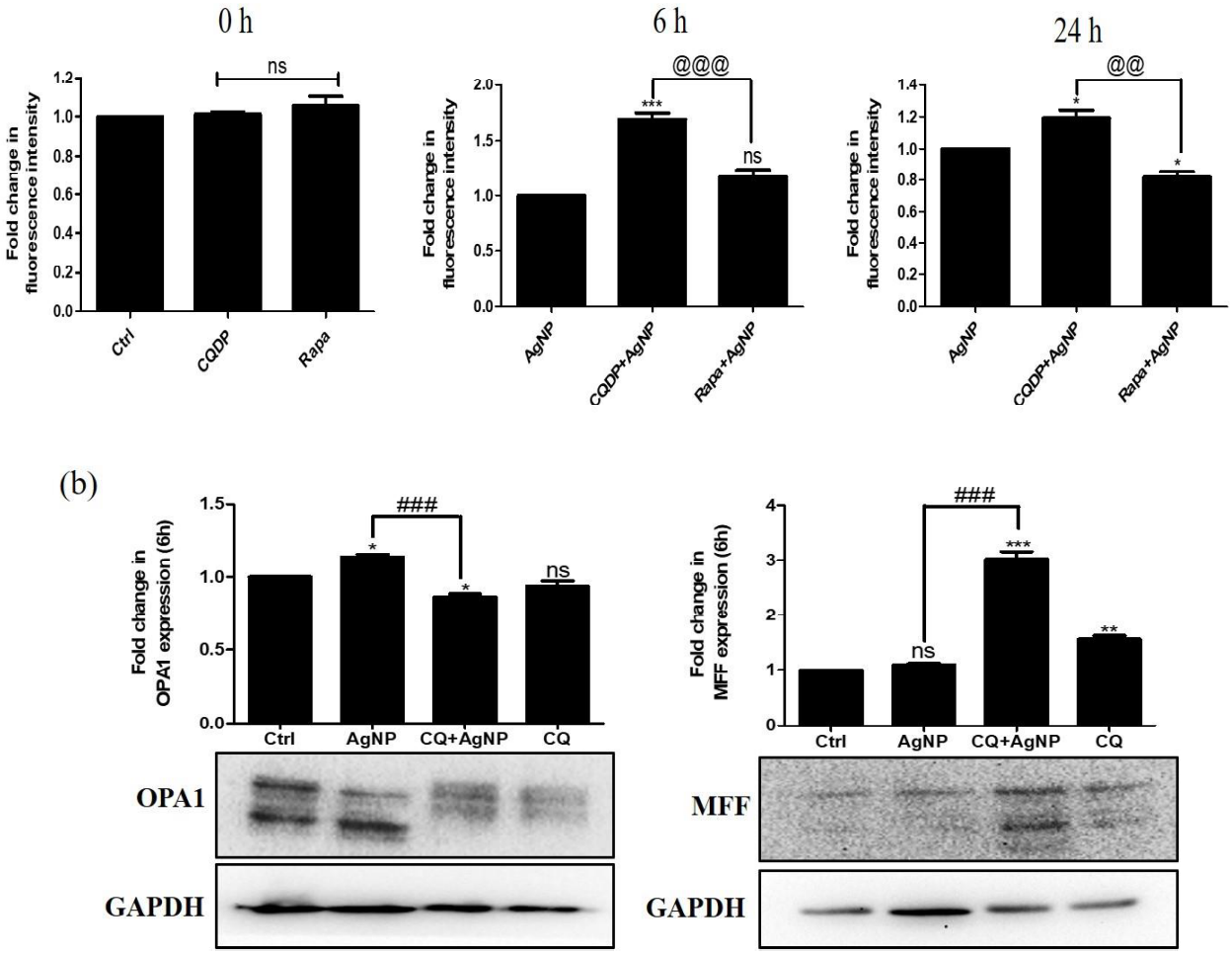

Figure 7.2.4. Analysis of mitochondrial dynamics upon autophagy modulation. **(a).** Fluorescence images of cells stained with MT red after AgNP treatment for 6 and 24 h with or without CQ or Rapa. Fold change in fluorescence intensity is represented as bar graphs. Scale bar- 10 µm. **(b).** Immunoblots showing the change in expression of OPA1 and MFF after 6 h of AgNP treatment with or without CQ. The symbol (*) represents significance difference levels with respect to AgNP treated cells, (#) represents the significance levels between AgNP and CQ+AgNP treated cells, and (@) denotes the significance level between CQ+AgNP and Rapa+AgNP treated cells.

7.2.5 Autophagy inhibition causes mitochondrial depolarization resulting in apoptosis

As described above, prolonged exposure to AgNPs resulted in a significant accumulation of

fragmented mitochondria, which further increased with CQ. A depolarization of mitochondrial membrane potential is often known to be a major driver for the initiation of mitochondrial fission. Therefore, we hypothesized that extended exposure to AgNPs causes a change in mitochondrial membrane potential (MMP), which is enhanced upon CQ treatment; further, the mitochondrial fragmentation induced is positively correlated to the extent of mitochondrial depolarization. We hence analyzed MMP by JC-1 staining and further analysis through a flow cytometer. As evident from the figure given below, there was an alteration in MMP after AgNP exposure, which was further perturbed after CQ exposure; however, Rapa resulted in a contrasting effect [**Fig 7.2.5 a (i) & (ii)**]. This also suggests that AgNPs cause a depolarization of mitochondria, which is enhanced by autophagy inhibition but rescued by autophagy enhancement. Our results thus corroborate well with what we observed in the morphological pattern of mitochondria after AgNP exposure**.** Now a depolarization of the mitochondrial membrane or deterioration of cellular mitochondrial health is often associated with cell death or apoptosis. We hence analyzed the same through AnnexinV and PI staining. As expected, inhibition of autophagy showed enhanced cell death compared to only AgNP treatment, whereas, Rapa rescued the cytotoxic effect [**Fig 7.2.5 b (i) & (ii)**]. Overall, through the above experiments, we prove that AgNPs cause inhibition of flux, resulting in depolarization or perturbation of mitochondrial health, triggering their fission. These fragmented mitochondria accumulate overtime due to inhibition of autophagic flux, eventually resulting in apoptotic cell death. On the contrary, activation of autophagy can salvage this AgNP induced effect, thus reducing cell death.

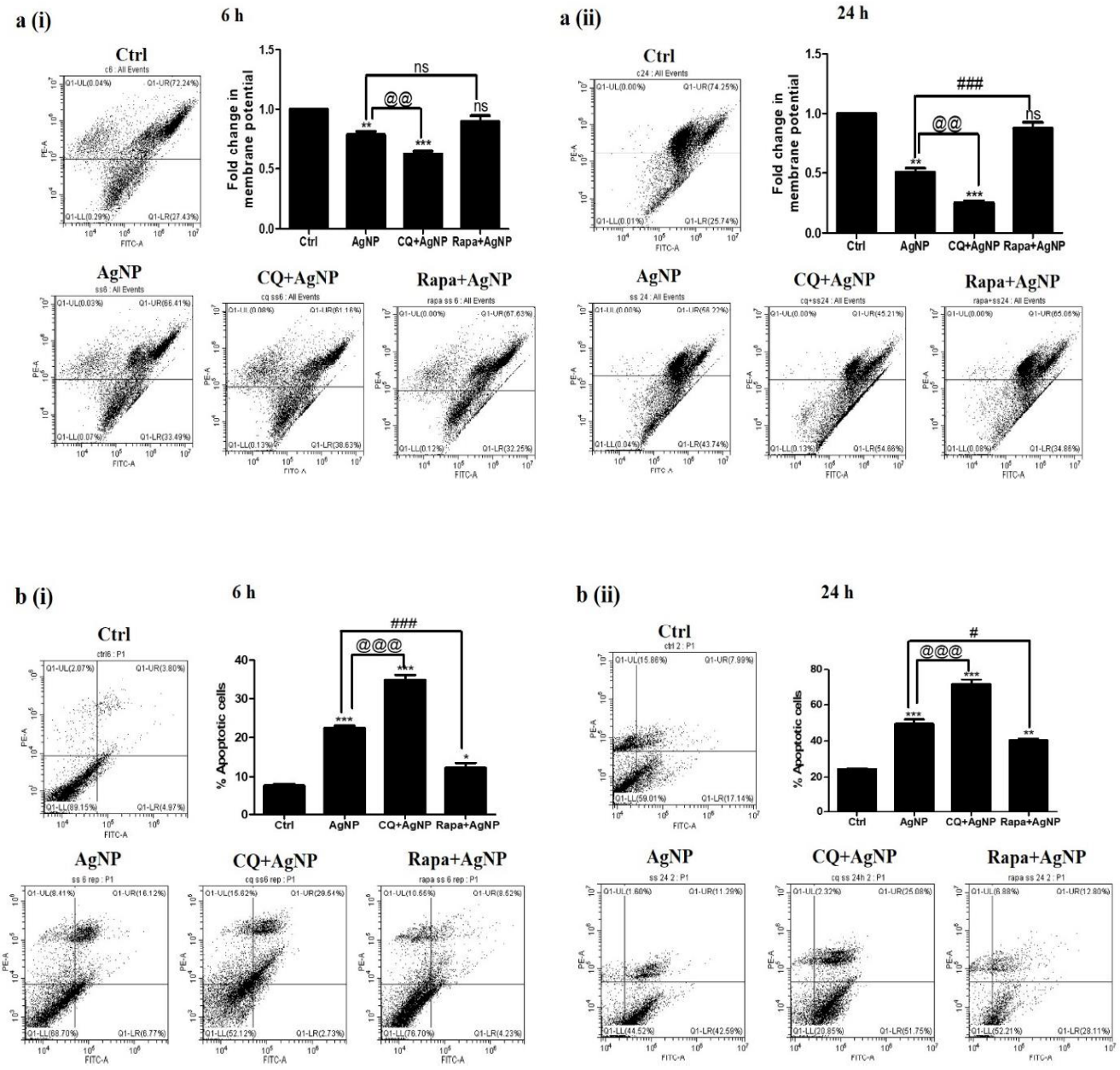

Figure 7.2.5. Analysis of MMP and cytotoxicity upon autophagy modulation in presence of AgNPs. **[a (i) & (ii)].** Flow cytometric analysis of MMP with JC-1 dye in cells treated with 25 µM dose of AgNPs for 6 and 24 h. **[b (i) & (ii)]** Dot plots of AnnexinV/PI staining post exposure to AgNPs (25 µM) for 6 h and 24 h, respectively, as analyzed through flow cytometry. The symbol (*) represents significance difference levels with respect to untreated cells, (@) and (#) represents the significance levels between AgNP as compared to CQ+AgNP and Rapa+AgNP treated cells, respectively.

7.2.6 AgNPs cause induction of ER stress

The endoplasmic reticulum (ER) is known to regulate intracellular protein folding, and a disturbance in cellular homeostasis can often lead to protein misfolding or accumulation of proteins, resulting in ER stress. To circumvent such a situation, cells activate homeostatic signaling cumulatively called the unfolded protein response (UPR), which orchestrates the recuperation of the ER function [3]. Autophagy is also required for eliminating worn-out proteins and protein aggregates, thus essentially linking itself as a protective mechanism during ER stress. These 2 systems are dynamically interconnected, and recent investigations have further revealed the intense crosstalk between ER and mitochondria as well. Considering the links, we further analyzed the induction of ER stress after AgNP exposure. ER chaperons like Bip, Calnexin are involved in promoting degradation or proper folding during UPR and hence, helps in reducing the ER stress. IRE1 is one of the transmembrane proteins which is responsible for execution of ER stress. This IRE1 along with PERK and ATF6 binds to Bip making it inactive in absence of ER stress. We observed that prolonged exposure to the AgNPs caused upregulation of proteins involved with ER stress like, Bip, IRE1α, and Calnexin, more significantly ($^{###}$) after 24 h of NP exposure [**Fig 7.2.6 a (i) & (ii)**]. We were therefore interested to understand whether the induced ER stress is associated with AgNP cell death or not. To prove the same, we treated the cells with Tunicamycin (Tuni), known to induce ER stress by inhibiting the biosynthesis of N-linked polysaccharides in proteins [15]. Importantly, a significant increase in the expression of proteins like Bip and Calnexin was observed at an early time point compared to only AgNP treatment (**Fig 7.2.6 b**), associated with a significant decrease in cell viability at 6 and 24 h in cells treated with both Tuni and AgNPs [**Fig 7.2.6 c (i) & (ii)**], confirming that ER stress can be associated with cytotoxicity.

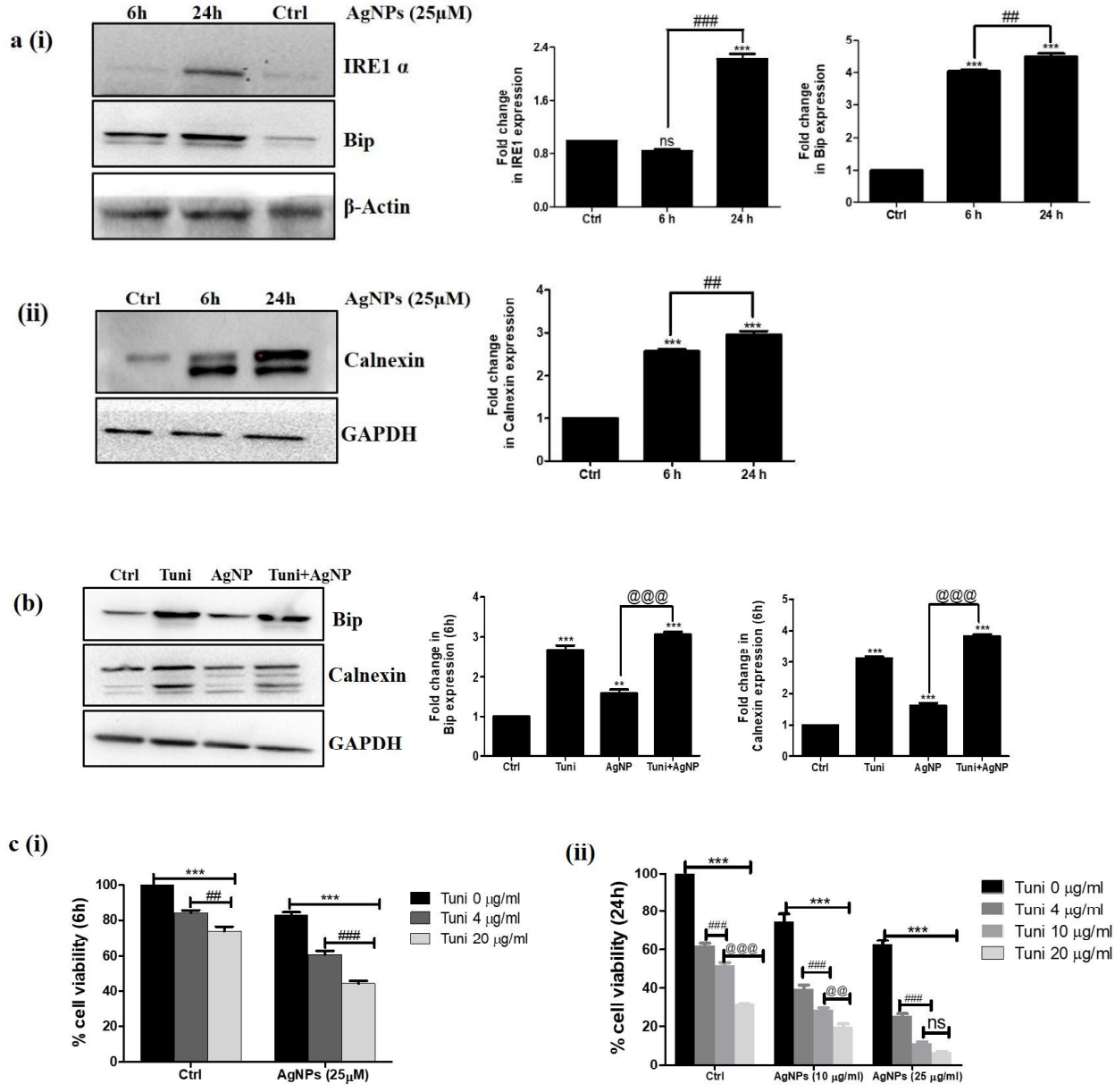

Figure.7.2.6. Analysis of ER stress induced by AgNPs. **[a (i) & (ii)].** Immunoblots representing the expression of ER stress marker proteins after treatment with AgNPs (25 µM) for 6 and 24 h. β-actin and GAPDH were used as control. **(b).** Immunoblots showing the change in expression of Bip and Calnexin upon addition of Tuni (4 µg/mL) with and without AgNPs (25 µM) for 6 h. The symbol (*) represents the significance of difference as compared to control cells. (#) denotes significance levels between 6 and 24 h AgNP treated

cells, (@) represents the significant differences between AgNP and Tuni+AgNP treated cells. **[c (i) & (ii)]** Cell viability assay after exposure to different doses of Tuni with or without AgNPs for 6 and 24 h, respectively. The symbol (*) represents the significance of difference as compared to cells treated with or without Tuni. (# and @) denotes significance levels between cells treated with different dose of Tuni with or without AgNPs.

7.3 Discussion

In the earlier chapters we analyzed the effect of AgNP exposure on autophagy, especially macroautophagy. However, autophagy is intricately linked with organelle homeostasis. Therefore, in this chapter, we have explored the response of mitochondria and ER to AgNP exposure. We observed a significant (***) increase in protein expression of the outer mitochondrial membrane protein TOM20, providing indications towards alteration of mitochondrial health. Also, TOM20 showed perinuclear distribution indicating altered localization of mitochondria as well with AgNP treatment. However, to delve deep, we further analyzed mitochondrial morphology and dimensions by Mitotracker staining. It further showed elongated mitochondrial networks in untreated control or at early hours post-AgNP exposure; however, in contrast, at 24 h fragmented mitochondria were pretty much predominant. Also, as observed with immunostaining of TOM20, Mitotracker staining also showed that the connection between the mitochondrial networks gradually diminishes with an increase in time of exposure. We were therefore interested to know whether the differential localization and the fragmented morphology of mitochondria apparent after prolonged exposure were accompanied by a loss of mitochondrial function as well. A significantly (***) increased depolarization of the mitochondrial membrane was observed after extended exposure to NPs. Therefore, we hypothesize that extended exposure to AgNPs impacts mitochondrial health negatively, resulting in depolarization and fragmentation of

mitochondria. To confirm the fragmentation, we performed further experiments. Mitochondrial fission is often accompanied by recruitment of Parkin, the ubiquitin ligase, to damaged mitochondria, which usually marks it for probable degradation in the lysosomes through a process of selective autophagy called mitophagy. Interestingly, at 24 h, we observed an increased accumulation of Parkin. The question that we asked here was- if mitochondria are tagged for disposal then why Parkin fluorescence increases? Importantly, at 24 h we have earlier shown that there is an inhibition of autophagic flux. Therefore, we postulated that after prolonged exposure to AgNPs, although the mitochondria are tagged with Parkin for degradation, however, due to inhibition of flux and lysosomal damage, their degradation is not accomplished resulting in the accumulation of Parkin signal. This was further confirmed when we observed a decrease in AO fluorescence at 24 h indicating reduced acidic vesicles, like lysosomes. Therefore, it is apparent that an impairment of the final step of autophagic process resulted in the accumulation of Parkin, more predominantly at 24 h. To further confirm that this inhibition of flux contributes towards fragmented morphology of mitochondria, we exposed the cells to CQ. Interestingly CQ led to increased fragmented morphology of mitochondria even at 6 h of AgNP exposure. Furthermore, we observed a decrease in the protein expression level of OPA1 (optic atrophy 1), a protein involved in fusion of mitochondria, in AgNP plus CQ treated cells compared to only AgNP at 6 h of exposure; in contrast, the protein MFF, involved in fission, showed increased expression with AgNP plus CQ treatment confirming our hypothesis. Thereafter, we wanted to check whether the increased fragmentation of mitochondria after AgNP exposure was associated with cell death? Interestingly, upon inhibition of flux with CQ, we found that there was extensive depolarization of mitochondria and increased apoptosis, when compared to only AgNP treatment. This supports the fact that a flux inhibition is accompanied by depolarization of MMP, fragmentation and associated increased cell death. These AgNP

induced effect could be partially rescued upon addition of Rapa that enhances autophagic flux. There are existing reports that establish the crosstalk between ER and mitochondria. We therefore investigated the same as well. AgNPs caused an upregulation of ER stress proteins like, Bip and Calnexin indicating that AgNPs parallely induce an ER stress as well. This was expected, as we earlier observed an accumulation of ubiquitinated proteins upon AgNP exposure suggesting a disruption protein homeostasis. The latter is very much linked to ER stress. To confirm the role of induced ER stress in AgNP induced cytotoxic effect, we increased ER stress by a well-known ER stress inducer- Tunicamycin. We found a significant (***) reduction in cell viability with Tuni plus NP treatment when compared to only AgNP exposure, indicating that ER stress is involved in enhancing the cytoxicity of the AgNPs. **Figure 7.3** represents the effect of AgNPs on organelle homeostasis in a schematic manner. Though we have observed that both ER stress and mitochondrial homeostasis is perturbed by AgNPs, yet, the crosstalk between the two organelles remains to be further investigated. However, in this chapter we provide evidences for temporal modification of these two organelles coupled to intracellular autophagy status in breast cancer cells after AgNP exposure. Further, we also provide hints towards enhancing AgNP mediated cytotoxicity by use of autophagy modulators like, CQ, or ER stress inducers like, Tuni thus complementing AgNPs.

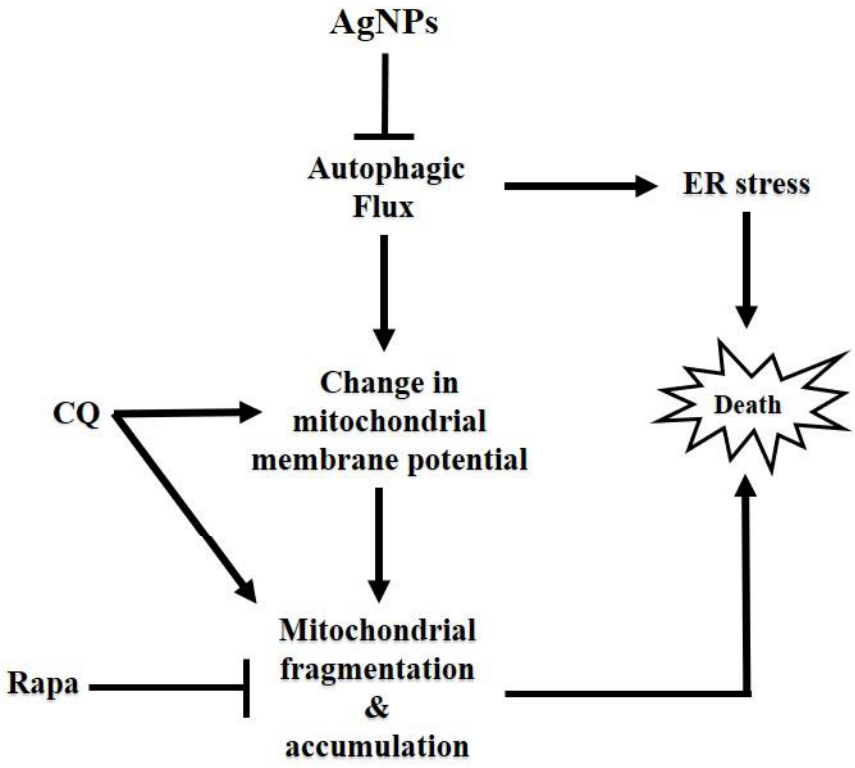

Figure 7.3. Schematic representation of effect of AgNPs on organelle homeostasis.

7.4 References

1 Anderson, G.R. et al. (2018) Dysregulation of mitochondrial dynamics proteins are a targetable feature of human tumors. *Nature communications* 9 (1), 1-13

2 Ni, H.-M. et al. (2015) Mitochondrial dynamics and mitochondrial quality control. *Redox biology* 4, 6-13

3 Bhat, T.A. et al. (2017) Endoplasmic reticulum-mediated unfolded protein response and mitochondrial apoptosis in cancer. *Biochimica et biophysica acta (BBA)-Reviews on cancer* 1867 (1), 58-66

4 Senft, D. and Ze'ev, A.R. (2015) UPR, autophagy, and mitochondria crosstalk underlies the ER stress response. *Trends in biochemical sciences* 40 (3), 141-148

5 Panigrahi, R. et al. (2015) The Design and Structure of Outer Membrane Receptors from Peroxisomes, Mitochondria, and Chloroplasts. *Structure* 23 (10), 1783-1800

6 Gomes, L.C. and Scorrano, L. (2013) Mitochondrial morphology in mitophagy and macroautophagy. *Biochimica et biophysica acta (BBA)-Molecular cell research* 1833 (1), 205-212

7 Cottet-Rousselle, C. et al. (2011) Cytometric assessment of mitochondria using fluorescent probes. *Cytometry part A* 79 (6), 405-425

8 Gomes, L.C. et al. (2011) During autophagy mitochondria elongate, are spared from degradation and sustain cell viability. *Nature cell biology* 13 (5), 589-598

9 Xiong, W. et al. (2019) Mitofusin 2 participates in mitophagy and mitochondrial fusion against angiotensin II-induced cardiomyocyte injury. *Frontiers in physiology* 10, 411

10 Benischke, A.-S. et al. (2017) Activation of mitophagy leads to decline in Mfn2 and loss of mitochondrial mass in Fuchs endothelial corneal dystrophy. *Scientific reports* 7 (1), 1-11

11 Narendra, D.P. and Youle, R.J. (2011) Targeting mitochondrial dysfunction: role for PINK1 and Parkin in mitochondrial quality control. *Antioxidants & redox signaling* 14 (10), 1929-1938

12 Thomé, M.P. et al. (2016) Ratiometric analysis of Acridine Orange staining in the study of acidic organelles and autophagy. *Journal of cell science* 129 (24), 4622-4632

13 Lebeau, J. et al. (2018) Coordinating mitochondrial biology through the stress-responsive regulation of mitochondrial proteases. In *International review of cell and molecular biology* (Vol. 340), pp. 79-128, Elsevier

14 Liu, R. and Chan, D.C. (2015) The mitochondrial fission receptor Mff selectively recruits oligomerized Drp1. *Molecular biology of the cell* 26 (24), 4466-4477

15 Guha, P. et al. (2017) Tunicamycin induced endoplasmic reticulum stress promotes apoptosis of prostate cancer cells by activating mTORC1. *Oncotarget* 8 (40), 68191

Chapter-8

Conclusion, limitations and future prospects

Chapter-8

Conclusion, limitations and future prospects

8.1 Conclusion:

Nanotechnology has emerged as a novel approach against conventional therapies for cancer treatment. In this regard, metal NPs are reported to offer diverse opportunities, owing to their suitable physicochemical and biological properties. Noble metal NPs like Ag, Au, or their combination, therefore, hold immense therapeutic prospects. However, a better understanding of their mechanism of ease of cell penetration and intracellular mechanism of action can further accelerate their probable use in the field of therapeutics. In this context, the physicochemical properties of NPs, like the size, shape, composition, surface charge, surface functionalization, etc. are known to play a crucial role in their interaction with the cell and dictating the intracellular fate of the NPs. Various reports suggest that small-sized NPs have a low binding affinity. In contrast, larger NPs, because of their multivalent receptor binding is easily membrane wrapped, facilitating their subsequent endocytosis. However, contradictory reports also suggest that the smaller sized NPs are easily internalized, attributable to their minute size, promoting intracellular entry.

Before embarking on this study, we hypothesized that the intracellular entry and the subsequent effect of the NPs are not only dictated by variation of size but also depend on the type of NPs and their physic-chemical state, i.e., mono-metallic or bi-metallic. We prepared β-CD capped AgNPs with minute variation in size. Interestingly, with a small variation in the size of AgNPs (~10 nm), there was a significant difference in the internalization potential of the NPs with the ss-AgNPs being more penetrative than the ls-AgNPs. So, we conclude that in the cell type studied, here the breast cancer cells, a small size variation can have a deep impact on the internalization potential of the AgNPs. However, further studies are required to

delineate whether the same phenomenon is observed across various cell types or not. An ICP-OES analysis proved that the intracellular release of Ag ions was considerably slower in bi-metallic NPs, thus resulting in reduced cytotoxicity at identical time points. Therefore, from this part of the study, we concluded that the AgNPs, by virtue of their size and release of Ag ions, are more toxic than the bi-metallic NPs, and a modification of the NP composition does alter their cytotoxic potential. Furthermore, upon pharmacological inhibition of the different endocytic routes, we observed that the endocytic route of ss-AgNPs was predominantly different than ls-AgNPs. Following the analysis of the internalization process, we focused on the intracellular mechanism of action of the NPs, especially the AgNPs. Silver metal is known for its various medicinal properties since ancient times; we, therefore, analyzed its anti-cancerous efficiency. The AgNPs were found to increase the ROS levels along with the simultaneous induction of JNK signaling and autophagy. We henceforth characterized the dynamic crosstalk that existed between internalized AgNPs and the cellular homeostatic process- autophagy.

Interestingly, we observed that inhibition of autophagic flux (fusion of autophagic vesicles with lysosomes) by the drug chloroquine (CQ) significantly reduced the internalization of the AgNPs, irrespective of their route of entry; functional autophagy thus augmented successful internalization of the NPs. Also, autophagy induction after AgNP exposure was mediated through an upstream activation of Janus Kinase (JNK) signaling. Importantly, the cellular homeostatic process autophagy significantly contributed to the regulation of intracellular ROS levels after AgNP exposure, thus playing a protective role in the tumor cells. However, prolonged exposure to AgNPs resulted in lysosomal dysfunction leading to inhibition of autophagic flux. Therefore, inhibition of flux after extended exposure to AgNPs resulted in increased ROS, ubiquitinated protein accumulation, and pronounced cytotoxicity. Hence, from this part of the study, we conclude that AgNPs exert a temporal effect on autophagy,

which dynamically changes over time in the tumor cells; functional autophagy initially imparts a protective function through regulation of ROS, but its eventual impairment leads to irreversible cytotoxic damage.

Since autophagy was found to be involved in regulating intracellular ROS and mitochondrial function is intricately linked to cellular ROS levels, we hence explored changes in mitochondrial dynamicity coupled to autophagy after AgNP exposure. Strikingly, a loss of autophagic function after prolonged exposure to AgNPs was associated with massive mitochondrial depolarization, enhanced fragmentation or fission of mitochondria, and recruitment of Parkin that triggers mitochondrial clearance. An autophagy inducer, rapamycin, partially rescued the fragmentation effect, while CQ was found to promote it. Therefore, we concluded that AgNPs significantly impact cellular mitochondrial health, which can be a contributing factor resulting in the cytotoxic effect of the AgNPs. Furthermore, we observed that disruption of mitochondrial homeostasis was also associated with ER stress. An UPR response was triggered upon AgNP exposure. A further induction of ER stress enhanced the AgNP mediated cytotoxic effect. It remains to be observed whether there is probable crosstalk between ER and mitochondria determining cell fate. Overall, this study provides key information on how alteration in the physicochemical property of NPs impacts its biological function; furthermore, it also provides insights into how the internalized NPs temporally modulate key intracellular events like autophagy and organelle dynamics. Our study thus helps in the basic understanding of the molecular mechanisms induced by AgNPs, which can be used as a plausible approach for breast cancer therapy. **Figure 8.1** shows the series of cellular events caused by AgNP exposure**.**

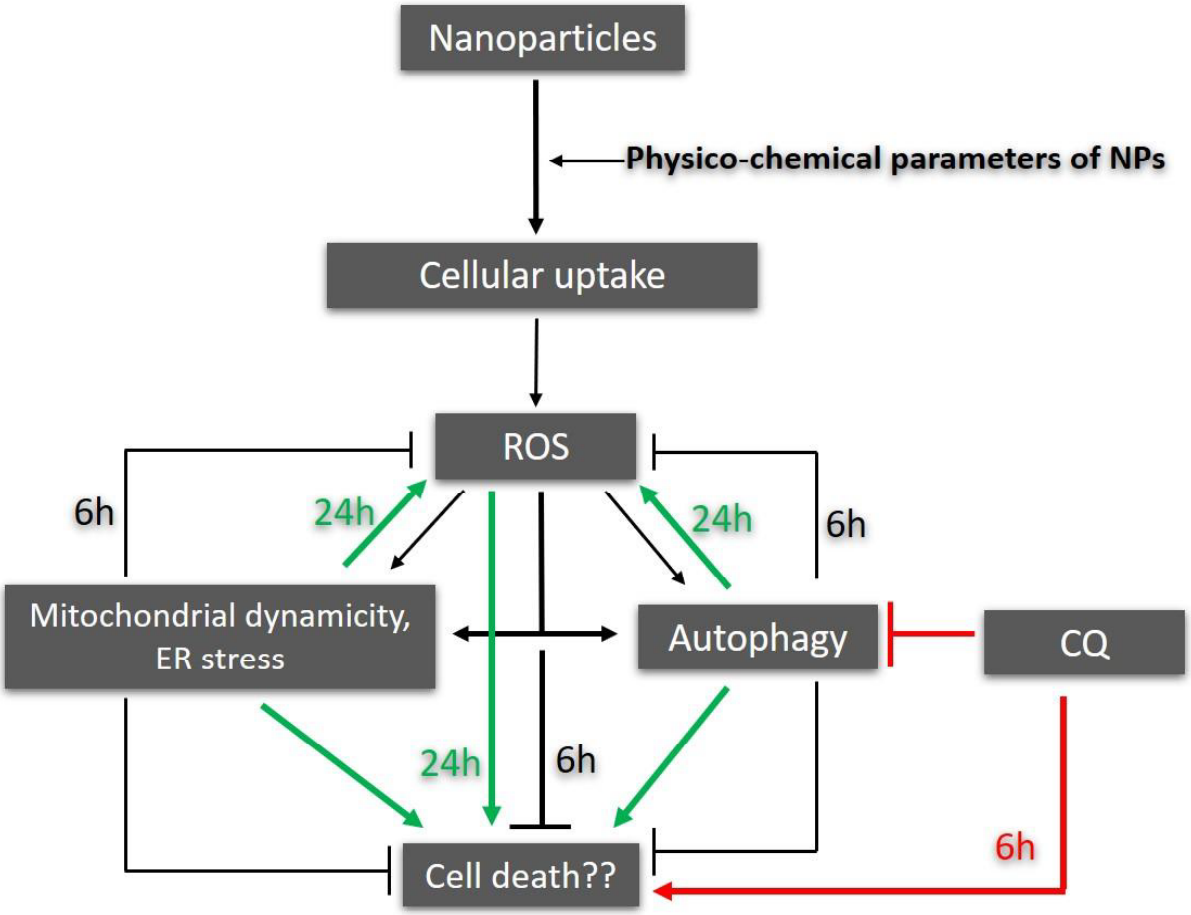

Figure 8.1 Representation of events occurring after AgNP exposure in MCF-7 cells.

8.2 Limitations and future prospects:

- The present study is mainly focused on AgNPs with smaller size variations in the range from 9 to 19 nm only. However, the effect with larger size variation would be interesting to explore through future studies. Also, this study is restricted to breast cancer cells only; whether the observed effect of the NPs, described in this study, is universal to tumor cells of different origin or varies with cell type remains to be further elucidated.

- This study is focussed to primarily understand how minute variation in size of NPs impacts their internalization and intracellular signalling inclusive of their cytotoxicity. However, the effect of alteration in other physical parameters of the NPs like, shape would be interesting to investigate further.

- Here we have analyzed the temporal effect of AgNP exposure on the cellular homeostatic process autophagy. Autophagy has a paradoxical role in carcinogenesis. However, recent studies predominantly highlight its pro-survival role under stress, say chemotherapy. Herein, we also observed the protective function of autophagy upon AgNP stress. This provides an avenue to further enhance the cytotoxic effect of NPs through coupled inhibition of the autophagic process alongside NP treatment. Therefore, synthesis and conjugation of NPs with drug or chemical that has autophagy inhibitory function can be considered for future treatment.

- From a fundamental perspective, this study is restricted mostly to the macroautophagy process. It would be interesting to understand the effect of AgNPs on the selective autophagic processes like chaperone-mediated autophagy (CMA), ER phagy, etc.

- We have shown that AgNPs induce a significant dysregulation of mitochondrial dynamicity and simultaneous induction of ER stress. Fundamentally, it would be exciting to observe whether ER stress mediates a change in mitochondrial dynamics or vice versa. The molecular links connecting the crosstalk between ER and mitochondria under AgNP stress can provide critical information on how tumor cells communicate at the organelle level post-NP exposure. The understanding might be essential to future therapy design.

APPENDIX

A.1. List of publications

From the thesis

i. **Leena Fageria,** Vishakha Bambroo, Angel Mathew, Sudeshna Mukherjee, Rajdeep Chowdhury, and Surojit Pande, Functional autophagic flux regulates AgNP uptake, and the internalized nanoparticles determine tumor cell fate by temporally regulating flux. International Journal of Nanomedicine 2019:14 9063-9076. (Published)

ii. **Leena Fageria,** Sudeshna Mukherjee, Rajdeep Chowdhury, and Surojit Pande, Impairment of autophagy after AgNP exposure is associated with disruption of organelle homeostasis. (In process)

iii. **Leena Fageria,** B. Srinidhi**,** Sudeshna Mukherjee, Rajdeep Chowdhury, and Surojit Pande, Dual metal nanoparticles enters through a mechanism different from their mono-metallic forms. (In process)

iv. **Leena Fageria,** 'Silver is the New Gold.' selected as the best science story for the AWSAR Award 2019 by the Department of Science and Technology (DST).

Other Publications

i. Sengottuvelu Dineshkumar, Abhishek Raj, Abhilasha Srivastava, Sudeshna Mukherjee, Sheik Saleem Pasha, Vishal Kachwal, **Leena Fageria,** Rajdeep Chowdhury, Inamur Rahman Laskar. Facile Incorporation of "Aggregation-Induced Emission"-Active Conjugated Polymer into Mesoporous Silica Hollow Nanospheres: Synthesis, Characterization, Photophysical Studies, and Application in Bioimaging. ACS Applied Materials & Interfaces 2019, 11, 31270-31282.

ii. Paritosh Shukla, Ashok Sharma, **Leena Fageria,** and Rajdeep Chowdhury, "Novel Spiro/non-Spiro Pyranopyrazoles: Eco-Friendly Synthesis, In-vitro Anticancer

Activity, DNA Binding, and In-silico Docking Studies," Current Bioactive Compounds 2019, 15: 257.

iii. Sheik Saleem Pasha, **Leena Fageria**, Clàudia Climent, Nigam P. Rath, Pere Alemany, Rajdeep Chowdhury, Aniruddha Roy, and Inamur Rahaman Laskar. Evaluation of novel platinum (II) based AIE compound-encapsulated mesoporous silica nanoparticles for cancer theranostic application. Dalton Transactions, 2018, 47, 4613.

iv. Vishal Kachwal, I. S. Vamsi Krishna, **Leena Fageria** Jagrity Chaudhary, Ram Kinkar Roy, Rajdeep Chowdhury, and Inamur Rahaman Laskar. Exploring the hidden potential of a benzothiazole based Schiff-base exhibiting AIE and ESIPT and its activity in pH sensing, intracellular imaging and ultrasensitive & selective detection of aluminium (Al3+). Analyst, 2018, 143, 3741.

v. **Leena Fageria**, Vikram Pareek, R. Venkataramana Dilip, Arpit Bhargava, Sheik Saleem Pasha, Inamur Rahaman Laskar, Heena Saini, Subhra Dash, Rajdeep Chowdhury, and Jitendra Panwar, Biosynthesized protein-capped silver nanoparticles induce ROS-dependent pro-apoptotic signals and pro-survival autophagy in cancer cells. ACS Omega 2017, 2 (4): 1489-1504.

A.2. List of conferences

Presented posters in the following conferences:

i. Elucidation of temporal crosstalk between nanoparticles and autophagy in cancer cells. **Leena Fageria**, Sudeshna Mukherjee, Rajdeep Chowdhury, and Surojit Pande. EMBO workshop entitled: Autophagy from molecular principles to human diseases held in **Crieff, United Kingdom** from 26-30 August 2019.

ii. Change in the physicochemical property of nanoparticles decide their mode of internalization and induces pro-survival autophagy in breast cancer cells.

Leena Fageria, Sudeshna Mukherjee, Rajdeep Chowdhury, and Surojit Pande.1st National Biomedical Research Competition-2018. **AIIMS, Rishikesh, Uttarakhand,** 15th October 2018.

iii. Fungal derived silver nanoparticles induces ROS, apoptotic and autophagic signaling in cancer cells.

Leena Fageria, R. Venkataramana Dilip, Arpit Bhargava, Vikram Pareek, Salim Pasha, Inamur R Laskar, Rajdeep Chowdhury, and Jitendra Panwar. National Symposium on Current Research in Cancer Biology and Therapy, University and Institute of Advanced Research, **Gandhinagar, Gujarat,** 7-8 October 2016.

iv. The anti-cancerous effects of biologically synthesized silver nanoparticles in human hepatoma cells.

Leena Fageria, R. Venkataramana Dilip, Jitendra Panwar, and Rajdeep Chowdhury. BITS conference on Gene and Genome regulation (BCGGR). **BITS-Pilani, Rajasthan.** 18-20 February 2016.

v. Molecular Alterations Involved in Cisplatin-induced Chemo-resistance and Epigenetic Alterations in Hepatocellular Carcinoma Cells.

Leena Fageria, Nagraj J, Mathur A, Goru S, Gaikwad A, Mukherjee S, and Chowdhury R. Global Cancer Summit, Indian Institute of Sciences, J.N.TATA Auditorium Bengaluru, **Bengaluru, Karnataka**, India. 18-20 November 2015.

A.3. Biographies

A brief biography of the Supervisor

Dr. Rajdeep Chowdhury is currently working as an Associate Professor, Department of Biological Sciences, BITS Pilani, Pilani Campus, Rajasthan. He earned his Bachelors and Masters degrees from Calcutta University and his PhD degree (CSIR-NET) from Jadavpur University. He has made contributions in the field of Cancer Biology. He was awarded DBT Post-Doctoral Research Fellowship in 2008. In 2009, he joined Massachusetts Institute of Technology (MIT), USA, Department of Bioengineering, as a post-doctoral researcher. At MIT he studied the myriad set of genetic events following Nitric Oxide (NO) exposure. His project extended from understanding the effects of NO-induced post translational modifications to its cancer promoting effects and also its role in cell death mechanisms like, autophagy. In Oct 2012 he joined BITS-Pilani as an Assistant Professor in Dept of Bio-Sciences. He is currently investigating the molecular causes leading to cancer drug tolerance and subsequent resistance, with special emphasis on the role of the cellular homeostatic process, autophagy. He is also interested in understanding the epigenetic marks of drug tolerant cells. He has received research grants from various government funding authorities like (i) Department of Science and Technology (DST) under fast track scheme of Young Scientist; (ii) Science and Engineering Research Board (SERB) under Extra-Mural Research Funding; (iii) University Grants Commission (UGC) under Minor Research Project; (iv) Life Sciences Research Board (LSRB, DRDO) and (v) Department of Biotechnology under Pilot Project and (vi) projects from SERB and ICMR as co-PI as well. The findings from his works have been published in more than 30 international scientific journals. At present he is guiding four Ph.D. students for the fulfilment of their dissertation.

A brief biography of the Co-supervisor

Dr. SUROJIT PANDE

Associate Professor,

Department of Chemistry,

BITS Pilani, Pilani campus, Rajasthan, 333031

Email: surojitpande@gmail.com, spande@pilani.bits-pilani.ac.in

Dr. Pande did his M.Sc. in Inorganic Chemistry, Kalyani University, Kalyani, West Bengal and Ph. D. from Indian Institute of Technology, Kharagpur. During Ph. D., he worked on metal and metal oxide nanoparticles and their application in catalysis and surface enhanced Raman spectroscopy. He worked on application of metal and metal oxide nanoparticles in catalysis, analytical and environmental chemistry, and surface enhance Raman scattering (SERS) studies using DOPAMINE, 1,10 Phenanthroline, and various dyes as a SERS probe. Before joining BITS on March 2012, Dr. Pande was a postdoctoral fellow in the Richard M. Crooks research group at The University of Texas at Austin, Texas, USA with research interests in homogeneous catalysis using dendrimer-encapsulated nanoparticles. He was experienced on spectroscopic study of sixth and fourth generation of hydroxy-terminated poly(amidoamine) (PAMAM) dendrimer. Synthesis of mono- (Au, Pd, and Pt) and bi-metallic (Au@Pd and Pd@Au) dendrimer-encapsulated nanoparticles of definite cluster size and atoms (magic no cluster) and their application in electrocatalyst. Dr. Pande has joined BITS Pilani as an Assistant Professor in March, 2012. Since then he has developed various mono- and bi-metallic, oxide, sulphide, and heterostructure nanomaterials for catalysis, photocatalysis, and electrocatalysis reactions. He has handled projects from DST, UGC, BITS agencies and his two students defended their thesis successfully in the field of catalysis, electrocatalysis, and photocatalysis.

A brief biography of the candidate

Ms. Leena Fageria has graduated in Biotechnology from Kurukshetra University, Kurukshetra, Haryana, India, in 2011. She has completed her Masters in Biochemistry as a major and Molecular Biology & Biotechnology as a minor subject, from Chaudhary Charan Singh Haryana Agricultural University (CCSHAU), Hisar, Haryana in the year 2014. She joined BITS-Pilani, Pilani campus as a Ph.D. student in the year 2015, under the supervision of Prof. Rajdeep Chowdhury and Co-supervision of Prof. Surojit Pande. Her doctoral research is in the field of cancer biology and nanotechnology. She has presented her research work as posters in three international conferences and two national conferences. She has been awarded an international travel grant from CSIR for poster presentation in an EMBO conference on autophagy and human diseases, held in Crieff, United Kingdom. She has been selected for the AWSAR Award by DST for writing her research work as the best scientific story. She has published 6 research articles in peer-reviewed journals. During her Ph.D., she was also involved in the teaching activities of the Department by taking courses for first and higher degree students of BITS Pilani campus.

An analysis of the uptake mechanism of nanoparticles, its temporal effect on autophagy and organelle dynamics in breast cancer cells

THESIS

Submitted in partial fulfillment

of the requirements for the degree of

DOCTOR OF PHILOSOPHY
by

Ms. Leena Fageria

2014PHXF0425P

Under the Supervision of

Prof. Rajdeep Chowdhury

&

Co-Supervision of

Prof. Surojit Pande

BITS Pilani
Pilani | Dubai | Goa | Hyderabad
BIRLA INSTITUTE OF TECHNOLOGY AND SCIENCE

PILANI

2020

Chapter-8

Conclusion, limitations and future prospects

Chapter-8

Conclusion, limitations and future prospects

8.1 Conclusion:

Nanotechnology has emerged as a novel approach against conventional therapies for cancer treatment. In this regard, metal NPs are reported to offer diverse opportunities, owing to their suitable physicochemical and biological properties. Noble metal NPs like Ag, Au, or their combination, therefore, hold immense therapeutic prospects. However, a better understanding of their mechanism of ease of cell penetration and intracellular mechanism of action can further accelerate their probable use in the field of therapeutics. In this context, the physicochemical properties of NPs, like the size, shape, composition, surface charge, surface functionalization, etc. are known to play a crucial role in their interaction with the cell and dictating the intracellular fate of the NPs. Various reports suggest that small-sized NPs have a low binding affinity. In contrast, larger NPs, because of their multivalent receptor binding is easily membrane wrapped, facilitating their subsequent endocytosis. However, contradictory reports also suggest that the smaller sized NPs are easily internalized, attributable to their minute size, promoting intracellular entry.

Before embarking on this study, we hypothesized that the intracellular entry and the subsequent effect of the NPs are not only dictated by variation of size but also depend on the type of NPs and their physic-chemical state, i.e., mono-metallic or bi-metallic. We prepared β-CD capped AgNPs with minute variation in size. Interestingly, with a small variation in the size of AgNPs (~10 nm), there was a significant difference in the internalization potential of the NPs with the ss-AgNPs being more penetrative than the ls-AgNPs. So, we conclude that in the cell type studied, here the breast cancer cells, a small size variation can have a deep impact on the internalization potential of the AgNPs. However, further studies are required to

delineate whether the same phenomenon is observed across various cell types or not. An ICP-OES analysis proved that the intracellular release of Ag ions was considerably slower in bi-metallic NPs, thus resulting in reduced cytotoxicity at identical time points. Therefore, from this part of the study, we concluded that the AgNPs, by virtue of their size and release of Ag ions, are more toxic than the bi-metallic NPs, and a modification of the NP composition does alter their cytotoxic potential. Furthermore, upon pharmacological inhibition of the different endocytic routes, we observed that the endocytic route of ss-AgNPs was predominantly different than ls-AgNPs. Following the analysis of the internalization process, we focused on the intracellular mechanism of action of the NPs, especially the AgNPs. Silver metal is known for its various medicinal properties since ancient times; we, therefore, analyzed its anti-cancerous efficiency. The AgNPs were found to increase the ROS levels along with the simultaneous induction of JNK signaling and autophagy. We henceforth characterized the dynamic crosstalk that existed between internalized AgNPs and the cellular homeostatic process- autophagy.

Interestingly, we observed that inhibition of autophagic flux (fusion of autophagic vesicles with lysosomes) by the drug chloroquine (CQ) significantly reduced the internalization of the AgNPs, irrespective of their route of entry; functional autophagy thus augmented successful internalization of the NPs. Also, autophagy induction after AgNP exposure was mediated through an upstream activation of Janus Kinase (JNK) signaling. Importantly, the cellular homeostatic process autophagy significantly contributed to the regulation of intracellular ROS levels after AgNP exposure, thus playing a protective role in the tumor cells. However, prolonged exposure to AgNPs resulted in lysosomal dysfunction leading to inhibition of autophagic flux. Therefore, inhibition of flux after extended exposure to AgNPs resulted in increased ROS, ubiquitinated protein accumulation, and pronounced cytotoxicity. Hence, from this part of the study, we conclude that AgNPs exert a temporal effect on autophagy,

which dynamically changes over time in the tumor cells; functional autophagy initially imparts a protective function through regulation of ROS, but its eventual impairment leads to irreversible cytotoxic damage.

Since autophagy was found to be involved in regulating intracellular ROS and mitochondrial function is intricately linked to cellular ROS levels, we hence explored changes in mitochondrial dynamicity coupled to autophagy after AgNP exposure. Strikingly, a loss of autophagic function after prolonged exposure to AgNPs was associated with massive mitochondrial depolarization, enhanced fragmentation or fission of mitochondria, and recruitment of Parkin that triggers mitochondrial clearance. An autophagy inducer, rapamycin, partially rescued the fragmentation effect, while CQ was found to promote it. Therefore, we concluded that AgNPs significantly impact cellular mitochondrial health, which can be a contributing factor resulting in the cytotoxic effect of the AgNPs. Furthermore, we observed that disruption of mitochondrial homeostasis was also associated with ER stress. An UPR response was triggered upon AgNP exposure. A further induction of ER stress enhanced the AgNP mediated cytotoxic effect. It remains to be observed whether there is probable crosstalk between ER and mitochondria determining cell fate. Overall, this study provides key information on how alteration in the physicochemical property of NPs impacts its biological function; furthermore, it also provides insights into how the internalized NPs temporally modulate key intracellular events like autophagy and organelle dynamics. Our study thus helps in the basic understanding of the molecular mechanisms induced by AgNPs, which can be used as a plausible approach for breast cancer therapy. **Figure 8.1** shows the series of cellular events caused by AgNP exposure**.**

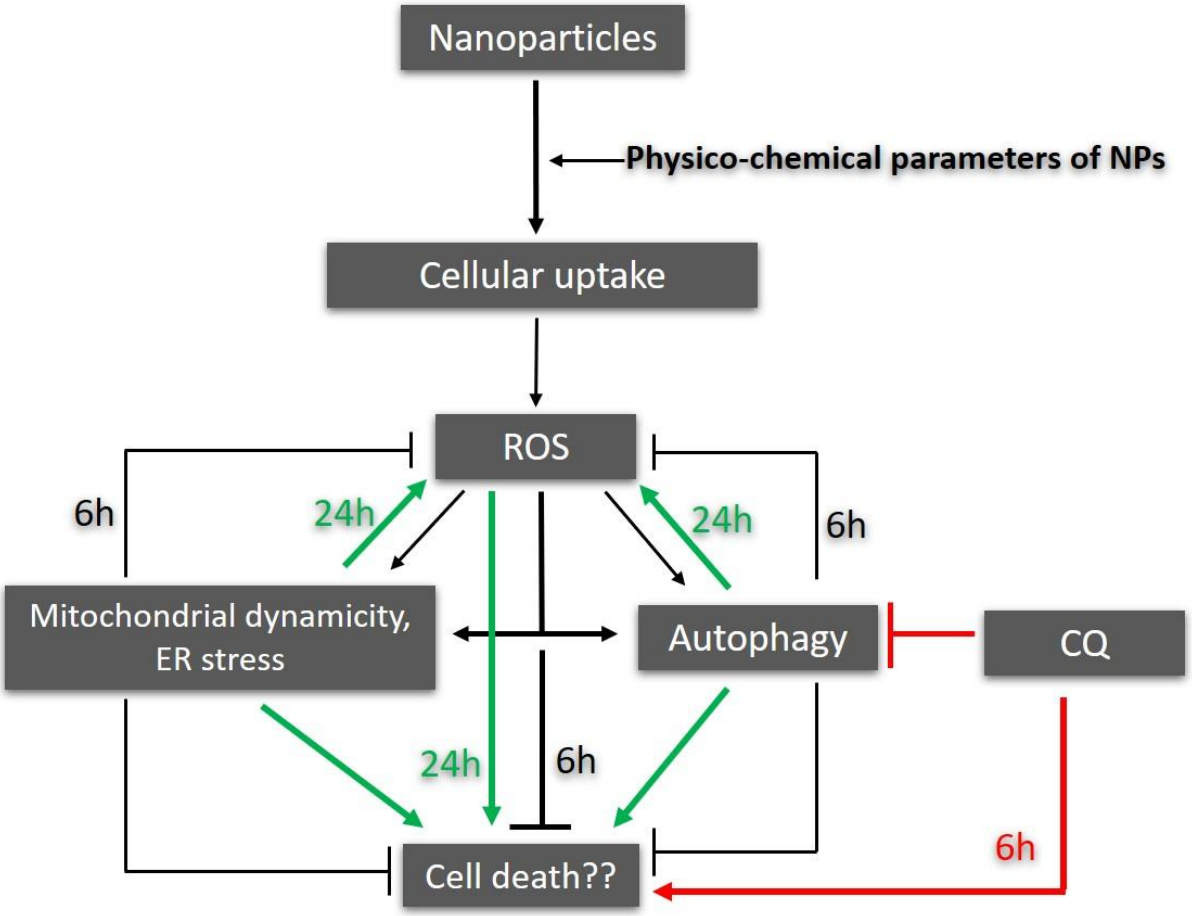

Figure 8.1 Representation of events occurring after AgNP exposure in MCF-7 cells.

8.2 Limitations and future prospects:

- The present study is mainly focused on AgNPs with smaller size variations in the range from 9 to 19 nm only. However, the effect with larger size variation would be interesting to explore through future studies. Also, this study is restricted to breast cancer cells only; whether the observed effect of the NPs, described in this study, is universal to tumor cells of different origin or varies with cell type remains to be further elucidated.

- This study is focussed to primarily understand how minute variation in size of NPs impacts their internalization and intracellular signalling inclusive of their cytotoxicity. However, the effect of alteration in other physical parameters of the NPs like, shape would be interesting to investigate further.

- Here we have analyzed the temporal effect of AgNP exposure on the cellular homeostatic process autophagy. Autophagy has a paradoxical role in carcinogenesis. However, recent studies predominantly highlight its pro-survival role under stress, say chemotherapy. Herein, we also observed the protective function of autophagy upon AgNP stress. This provides an avenue to further enhance the cytotoxic effect of NPs through coupled inhibition of the autophagic process alongside NP treatment. Therefore, synthesis and conjugation of NPs with drug or chemical that has autophagy inhibitory function can be considered for future treatment.

- From a fundamental perspective, this study is restricted mostly to the macroautophagy process. It would be interesting to understand the effect of AgNPs on the selective autophagic processes like chaperone-mediated autophagy (CMA), ER phagy, etc.

- We have shown that AgNPs induce a significant dysregulation of mitochondrial dynamicity and simultaneous induction of ER stress. Fundamentally, it would be exciting to observe whether ER stress mediates a change in mitochondrial dynamics or vice versa. The molecular links connecting the crosstalk between ER and mitochondria under AgNP stress can provide critical information on how tumor cells communicate at the organelle level post-NP exposure. The understanding might be essential to future therapy design.